STUDY OF DEGENERATE MAGNETIC SEMICONDUCTORS

Toshiaki TATSUKAWA

1982

Abstract

It is well known that degenerate semiconductors such as PbTe, SnTe and GeTe exist in the middle state between a metal and a usual II - VI semiconductors with regard to the electric conduction and the chemical binding. Therefore, it is very interesting to study the magnetic properties of these semiconductors diluted with magnetic impurity atoms. These materials are so-called degenerate magnetic semiconductors.

We prepared sigle crystals of $Pb_{1-x}Mn_xTe$, $Ge_{1-x}Mn_xTe$ and $Sn_{1-x}(Me)_xTe$ (Me; magnetic elements such as Mn, Fe, Cr, Ni, and Co) with various x-values 0.03 $\sim$ 20 at.%, and with carrier concentrations of $\simeq 10^{18}$ cm^{-3} for PbTe, $\simeq 10^{20}$ cm^{-3} for SnTe and $\simeq 10^{21}$ cm^{-3} for GeTe by a Bridgman method. Then we measured the ESR for all the samples and resistivity, anomalous Hall effect (AHE), Hall mobility and magnetic susceptibility for $Sn_{1-x}Mn_xTe$ and $Sn_{1-x}Cr_xTe$ samples in the temperature range of 2 $\sim$ 350 K.

At first, in the case of Mn as a magnetic impurity, the g-values are known to be nearly equal to 2 from the ESR measurements for all the samples and the ESR linewidth at x = 0.5 $\sim$ 1.5 at.% is affected by an exchange narrowing effect. In addition, we observe a bottleneck effect from the detailed linewidth measurements for $Pb_{1-x}Mn_xTe$. While, on the transport measurements for $Sn_{1-x}Mn_xTe$, we observe the scattering effect due to mixed spin-orbit interaction and the fact that the critical temperatures for yielding the spin ordering are independent of x or a little dependent on x.

The above experimental results can be well explained in terms of a s-d interaction in the system which both magnetic spins and carrier spins couple together because of nearly equal g-values of both the spins. Then, it is shown that there are s-state carriers with no orbital angular momentum in the vicinity of a Mn ion. While, the g-values of the carriers in the IV - Te compounds are generally known to be large according to the spin-orbit interactions.

On the other hand, for $x \geq 2$ at.%, the linewidth increases with increasing x. For $Sn_{1-x}Mn_xTe$, there are anomalous variations observable around boundary range of x = 2 at.% for all the measurements; especially the x dependences of ESR and AHE reverse themselves around x = 2 at.%.

Such a reverse effect of x-dependence is known to also appear in other materials and has been attributed to short range direct interactions between two spins in spite of existence of predominant RKKY interaction at lower Mn content crystals. Thus, it is found that in these magnetic semiconductors, the clusters originated from the direct exchange are formed anisotropically and distributed non-uniformly. Such a phenomenon is one of the problems characteristic of the magnetism in random spin systems.

In the analyses of the experimental results for $Sn_{1-x}Cr_xTe$, we can estimate that CrTe molecules in a SnTe crystal form clusters more easily than MnTe molecules in the crystals according to a strong direct interaction between CrTe molecules. In the study of the x dependences of these magnetic materials, we observe the ferromagnetism due to CrTe at room temperatre. Moreover we found that the Cr ions can be used as a sensitive probe in the study of the lattice instabilities such as a structural phase transition of the host SnTe crystal.

Finally, we discussed qualitatively the magnetism of degenerate magnetic semiconductors with a model of composite magnetism in a single sample with strongly dependence on x, as a new type magnetic materials.

Acknowledgements

This work has been made at the Faculty of Engineering, Fukui University.

The author would like to express his sincere thanks to Professor S. Narita of Faculty of Engineering Science, Osaka University, for his constant guidance and encouragement. He also wishes to thank Professor M. Inoue of Faculty of Science, Hiroshima University, and Professor H. Yagi of Faculty of Engineering, Fukui University, for many helpful discussions.

Thanks are extended to Professors A. Yoshimori, T. Haseda, and E. Fujita of Faculty of Engineering Science, Osaka University, and Professor K. Murase of Faculty of Science, Osaka University, for their useful discussions and their giving helpful suggestions.

Contents

I. Introduction

1. Summary of the Knowledges on PbTe, SnTe and GeTe

The IV-VI compounds, such as lead telluride, tin telluride and germanium telluride, are extremely interesting semiconductors. For more than twenty years, these materials have been the subjects of considerable research efforts, due in part to the technological importance of these materials as detectors of infrared radiation. However, many interesting problems in the basic physics of these semiconductors have stimulated the many investigations. Indeed, IV-Te compounds group exhibits unusual, and possibly unique properties compared with other semiconductors.

Together with the experimental study, the calculation of the band structures of these materials has been an especially important part of the study[1-5] of these semiconductors and especially, a number of calculations of the band structures of the lead salts have been done recently using various calculation techniques. These band structure calculations cited here indicate that the Bloch functions for the conduction and valence band edges can be written by the representations L_6^- and L_6^+ of the small (double) group at the L point. The minimum energy gap $E_0 = E(L_6^-)-E(L_6^+)$ is thus a direct gap, from the results of these theoretical calculations, and is an order of $0.1 \sim 0.3$ eV for these salts. In addition, there is a considerable amount of experimental evidence indicating the existence of a second valence band maximum at an energy slightly below the L_6 edge of the highest valence band; therefore, the valence band is composed of the light-mass and heavy-mass hole bands[6] (the two-valence-band model).

These crystals are p or n type materials with usually high concentrations of carriers ($\simeq 10^{18}$ for PbTe, $\simeq 10^{20}$ for SnTe and $\simeq 10^{21}$ for GeTe); then, they are so-called degenerate semiconductors.

In the tight-binding approximation[1] the Bloch functions are chosen as

linear combinations of atomic orbitals centered on the lattice sites of the crystal. A natural choice for the tight-binding origin of these six bands is the three spin-degenerate p orbitals associated with the anion sites (Te) and the three p orbitals associated with the cation sites (Pb, Sn, or Ge). Therefore, large spin-orbit mixing of these levels is expected since the spin-orbit splitting of the np levels in atomic lead, tin and germanium is quite large (more than 1.4 eV), and thus, it is known that the g-value of a carrier is different from that of free electron. However the band caculation by the augmented-plane-wave approximation[2] shows existence of charge-density distributions of plane wave, s type and p type for the valence- and coduction- band edges.

Next, PbTe and SnTe crystallize in the rock salt crystal structure, while GeTe has a face-centered rhombohedral structure which represents only a small distortion from the rock salt structure. The SnTe and GeTe have known to take place a structural phase transition (rock salt $\leftrightarrow$ rhombohedral) at a well-defined critical temperature T_s. The sixfold coordinated rock-salt crystal structure of the IV- Te compounds is indicative of the high degree of ionicity as well as covalency in their interatomic bonding. It is known that the static dielectric constant ε_0 of these crystals must be relatively large as a consequence of their ionic character. While it has proven difficult to make direct electrical measurements of ε_0 for the IV-tellurides group because of their high carrier concentrations. Various measurements[7,8] have been made to determine the dielectric constant using experimental values of the frequencies ω_{LO} and ω_{TO} of longitudinal and transverse optical phonons and of the high frequency dielectric constant ε_∞ based on the Lyddane-Sacks-Teller relation.

On the other hand, it is known that the temperature dependences of ε_0 and ω_{TO} are mainly due to the softening of the optical phonon mode. For PbTe,

Kawamura et al. and Shimizu et al. observed them at a low temperature.

Moreover, it has been shown that these tellurides are nearly ferroelectric materials because of their large dielectric constant. From this point, the structural phase transition[11] is a ferroelectric transition[12] associated with a softening of the TO phonon. Because of this unusual characteristic of lattice instability[11], SnTe and GeTe were studied both theoretically and experimentally by Kobayashi et al.[11] and Kawamura.[13]

Finally, $Pb_{1-x}Sn_xTe$ mixed crystal has been known to have a band gap whose width is varied by the composition x; a band inversion between the conduction and valence bands (L_6^+, L_6^- bands) occurs at a certain x[11,14,15]. The narrow gap states of the mixed crystals have been studied by far-infrared,[16] transport and de-Hass Shubinikov measurements.[17,18]

2. Summary of Degenerate Magnetic Semiconductors such as $Pb_{1-x}Mn_xTe$, $Sn_{1-x}Mn_xTe$ and $Ge_{1-x}Mn_xTe$

In a material system consisting of magnetic impurities dissolved in these characteristic IV-VI semiconductors, or degenerate magnetic semiconductors, a number of interesting phenomena which can not be found in usual semiconductors, are revealed, because the magnetic properties are closely related to the electronic states in the conduction and valence bands. Since early 1970's, these material systems have been extensively investigated by several investigator.[19] According to their experimental and theoretical studies, the magnetisms of these systems have been attributed to (i) s-d interaction between the localized spin system and carrier spin system, (ii) Rudderman-Kittel-Kasuya-Yosida (RKKY) interaction, (iii) direct exchange interaction between impurity spins, or (iv) other various spin-order states.

As is well known, the s-d interactions are classified into two different types as found in dilute alloys; one is an s-d mixing type in which the carrier

spins couple with the impurity spins as in Cu;Mn,[20] and the other type is the case where both the spins do not couple each other because the g-value of each spin is different from each other as in Pd;Fe alloys.[21] By considering a large g-value of carrier spins as found by de Haas-Shubnikov measurements and their ESR experiments, Toth et al.[22] have pointed out that in $Pb_{1-x}Mn_xTe$ the latter type is dominant. However, it is shown later that magnitudes of the s-d interaction are different among various measurements; magnetic susceptibility and transport experiments on $Sn_{1-x}Mn_xTe$ or $Ge_{1-x}Mn_xTe$. The magnitude J_{sd} is of the order of 0.8-0.9 eV[24], whereas from ESR linewidth and other transport measurements it is of the order of 0.05-0.09 eV,[22,25] an order of magnitude smaller than the former.

On the other hand, since there are simultaneously s-like and p-like carriers in these narrow-gap semiconductors, there may exist both s-d and p-d interactions. In fact, these two types of interactions are found in semimagnetic semiconductors.[26,27]. Thus it is expected that similarly in degenerate magnetic semiconductors there may possibly exist such two types of interactions; but no definite evidence have been reported for this prediction.

Theoretically and experimentally Cochrane et al.[24,25] have shown that the RKKY interaction in the $Sn_{1-x}Mn_xTe$ system becomes predominant in the impurity concentration range x=0.5-20 at.%. In their theory, both the RKKY type interaction and the direct antiferromagnetic interaction between nearest neighbors have been taken into account, giving a Curie temperature that depends linearly on x, in agreement with their results of magnetic susceptibilities.

Our concentration dependence of the Curie temperature, determained by electrical resistivity and anomalous Hall effect measurements, is different from their theoretical predictions, but rather is similar to the Kondo theory

on s-d interactions.[28] While, studies of semimagnetic semiconductors such as $Hg_{1-x}Mn_xTe$ and $Cd_{1-x}Mn_xTe$ have revealed the same behabiors as predicted by Cochrane et al., in which experimental results for $x \geq 2$ at.% are satisfactorily explained by considering the antiferromagnetic interaction between Mn spins.[29,30] The critical impurity concentration of about 2 at.% is also seen in our degenerate magnetic semiconductors, and various properties of the degenerate magnetic semiconductors are different between the concentrations below and above $\simeq$ 2 at.%. Such a problem is still of current interest.

The Cochrane theory on the existence of antiferromagnetic interactions between nearest neighbors has predicted that in these materials the spin ordering at low temperature may be complicated states, in which an overall arrangement is ferromagnetic but local alignment is antiferromagnetic. Recently Inoue et al.[31] have shown that in degenerate magnetic semiconductors there are two magnetic transitions, one from paramagnetic to antiferromagnetic and the other antiferromagnetic to ferromagnetic phases. However, there still remains questions as for the detailed mechanism of low temperature magnetic orderings in these material systems.

3. Summary of the Present Work

In the present work we have performed ESR, transport, and magnetic measurements on Bridgman-grown $Pb_{1-x}Mn_xTe$, $Sn_{1-x}Mn_xTe$, $Ge_{1-x}Mn_xTe$ and $Sn_{1-x}Cr_xTe$ crystals in a wide range of temperature. As a result, it is found that for $x < 0.5$ at.% the interaction between magnetic impurities is small and the impurities serve as a good probe to detect the surrounding crystalline environment of the probe, which provide us with information about a bonding state of tellurides or magnetic and structural phase transition; these results are in good agreements with those reported by other investigators.

ESR and Hall effect measurements on the crystals with $x < 1$ at.% show that conduction carriers near the magnetic impurities have a strong exchange interaction with the impurity spins and thus they in a sense localize around the impurities. In this case the effect of ℓ-s coupling of the carrier is weak and s-state carriers play an important role.

Moreover, for crystals with $x > 2$ at.% some sort of local clusters are produced through direct exchange interactions between the magnetic spins. In practice, the formation of these clusters is not specially uniform, giving rise to an anisotropic interaction.

II. Sample Preparation and Measurement Techniques

The single crystals of $Sn_{1-x}Mn_xTe$, $Sn_{1-x}Cr_xTe$, $Ge_{1-x}Mn_xTe$, $Pb_{1-x}Mn_xTe$ and $Sn_{1-x}Pb_xTe$;Mn were grown by the Bridgman method at a lowering rate of 2 mm/hr; the furnace temperature was fixed in the range of 870-960 °C. Except for SnTe crystal, these crystals were all grown with a stoichiometric metal-to-tellurium ratio, and for SnTe with a non-stoichiometric ratio Sn/Te = 0.495/0.505, which is modified from 0.49/0.51 done by Butler et al.[32]. For $Sn_{1-x}Cr_xTe$ crystals, at first the CrTe were synthesized at 1000 °C in a vaccum-sealed quartz ampoule taking a few hours, and then the mixed crystals $Sn_{1-x}Cr_xTe$ were grown by the Bridgman method. Some of these as-grown crystals were anealed in a metal vapor such as Zn and Pb for 2 days at 500-600 °C and quenched by dropping into water.

Typical carrier concentrations of these as-grown crystals are listed in Table I together with those of annealed samples, and in the case of the mixed crystals of $Sn_{1-x}Pb_xTe$;Mn the carrier concentration varies with x as shown in Fig. 1. In these degenerate magnetic semiconductors the carrier concentration is usually insensitive to the amount of magnetic impurities but it depends strongly on the isothermal annealing.

The grown crystal was cut by a spark cutting machine into a rectangular shape (typically 1×1×8 mm) for electrical measurements or a disk shape (4-5 mm thick and 8 mm diameter) for magnetization measurements. For ESR experiments the crystals were usually crushed into powder to minimize the skin effect. The ESR measurement was usually done by using annealed crystals because the crystals have less carrier concentration. Transport measurement (specific heat, Hall effect, resistivity) were measured over a wide range of temperature 2 ∿ 300 K in a conventional method using home made cryostat.[33]

Table I. Typical carrier concentrations in the IV- Te compounds.

	as-grown (cm^{-3})	annealed (cm^{-3})	x (at.%)
$Pb_{1-x}Mn_xTe$	$n = 5\text{-}7\times10^{18}$	n or $p = 2\text{-}5\times10^{18}$	0.06-3
$Sn_{1-x}Mn_xTe$	$p = 7\text{-}10\times10^{20}$	$p = 1.2\text{-}2\times10^{20}$	0.02-4
$Ge_{1-x}Mn_xTe$	$p \simeq 10^{21}$	$p \simeq 10^{21}$	0.03-7
$Sn_{1-x}Cr_xTe$	$p = 6\text{-}10\times10^{20}$	$p = 1\text{-}4\times10^{20}$	0.2-5

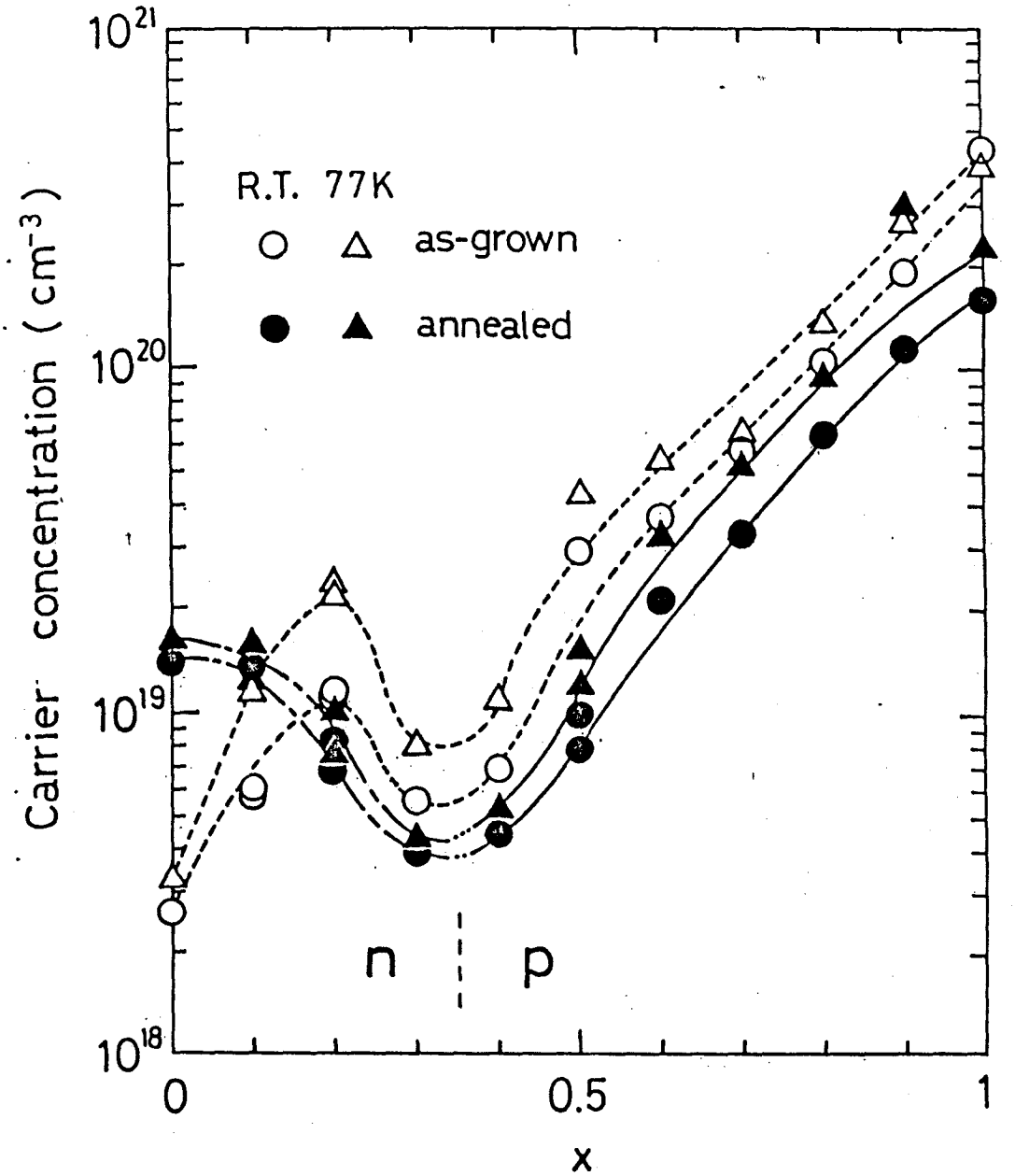

Fig. 1. The composition dependence of the nominal carrier concentration of $Pb_{1-x}Sn_xTe$ crystals. In the case of the annealed crystals, the conduction type (n or p) is marked in the figure.

The cryostat used for the electrical measurements was a conventional type as shown in Fig. 2. The sample was placed on the bottom of a copper holder and an Allen-Bradley carbon resistor was attached in a hole drilled close to the sample. A manganin heater was wound around the upper part of the copper block and the lead wires were all in contact with a thermal anchor. The cavity was put in the center of the superconducting solenoid. Above 4.2 K the cavity was kept at 10^{-5} Torr vacuum when the heater was switched on, and its current was controlled in order to keep a constant temperature better than ± 0.01 K by a home-made current controller (Fig. 3). Below 4.2 K the entire liquid helium bath was evacuated by a mechanical pump and the vapor pressure was regulated by a manostat.

In the magnetoresistance and the Hall effect experiment, the magnetic field was produced by a commercial superconducting magnet (bore 30 mm, length 21 cm, maximum field 40 kG, manufactured by Vacuum Metallurgical Co.) equipped with a regulated current source; the exciting current can be changed manually or automatically at a rate of 5 A/min so that the sample voltages against the field strength could be recorded on a X-Y recorder. The magnet was immersed in liquid helium contained in a home-made metal dewar. A typical field distribution along the axis of the solenoid has a fairly good homogeneity (0.01% / ± 15 mm) around the central part.

The ESR measurements were made using X- and V-band spectrmeters which were operated in the temperature range 2-480 K. The X-band spectrometer used in this experiments was a conventional commercial type (JES-3BX, Japan Electon Optics Laboratory Co., Ltd.) which can be operated over the temperature range 120-480 K. Our V-band spectrometer was a home-made type[34] as shown in the block diagram of Fig. 4. The klystron power supply (OKI-50V10 or 45V10, maximum power about 80 mW in the frequency range 45-50 GHz) was stabilized by a reflector modulation (10 kHz or 100 kHz) technique

through A.F.C. circuit, and the klystron was immersed in an oil bath cooled by water. A.F.C. signals were fed from either a reference cavity or a sample cavity depending on the measurement of real part or imaginary part of the magnetic susceptibility, respectively. The total detector system was a simple autodyne in which the power controlled by a 10 dB coupler is divided into the two ways of microwave circuits. The main power of microwave was lead to the sample cavity through a triangular circulator and to a one of arms of magic tee, and the other backing power was gain- and phase-controlled by the attenuator and phase-shifter, respectively and followed another arm of magic tee. The output mixed with these two signals was detected by a silicon crystal (1N53C), which was displayed on a synchroscope or an X-Y recorder after phase sensitive detector. The modulation signal frequency is in the range of 20 Hz ∿ 10 kHz which is the detection frequency of lock-in-amp.

For low temperature ESR measurement, a metal dewar was used, and liquid refrigerant was contained in a copper container which is nonmagnetic. Figure 5 shows the low temperature apparatus. The tail part of the dewar is the sample cavity which made of copper with a cylindrical TE_{014} mode. The unloaded Q-value of the sample cavity was about 10000 at 4.2 K.[35] The temperature control below 4.2 K was made by a reduction of the vapor pressure of the liquid helium. The temperature was measured by a thermocouple (chromel-gold cobalt) or precise manometer, and a few carbon resistors were fixed in the cryostat as a level indicator of liquid helium. In addition, the all systems of microwave circuits and cryostat parts were tightly fixed on the mechanical supports to reduce any microphonic noise. As a result, the overall apparatus was sufficient for the ESR studies of the degenerate semiconductors.

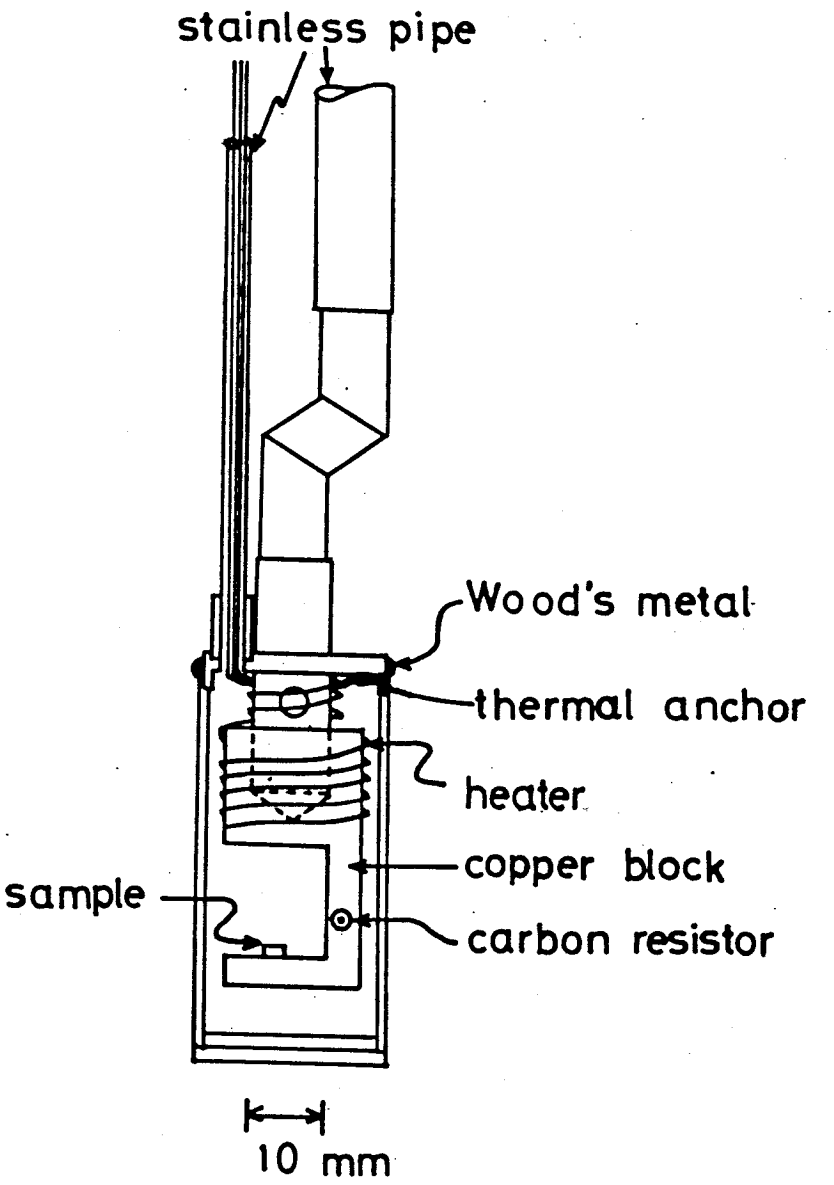

Fig. 2. A cryostat for the electrical measurements.

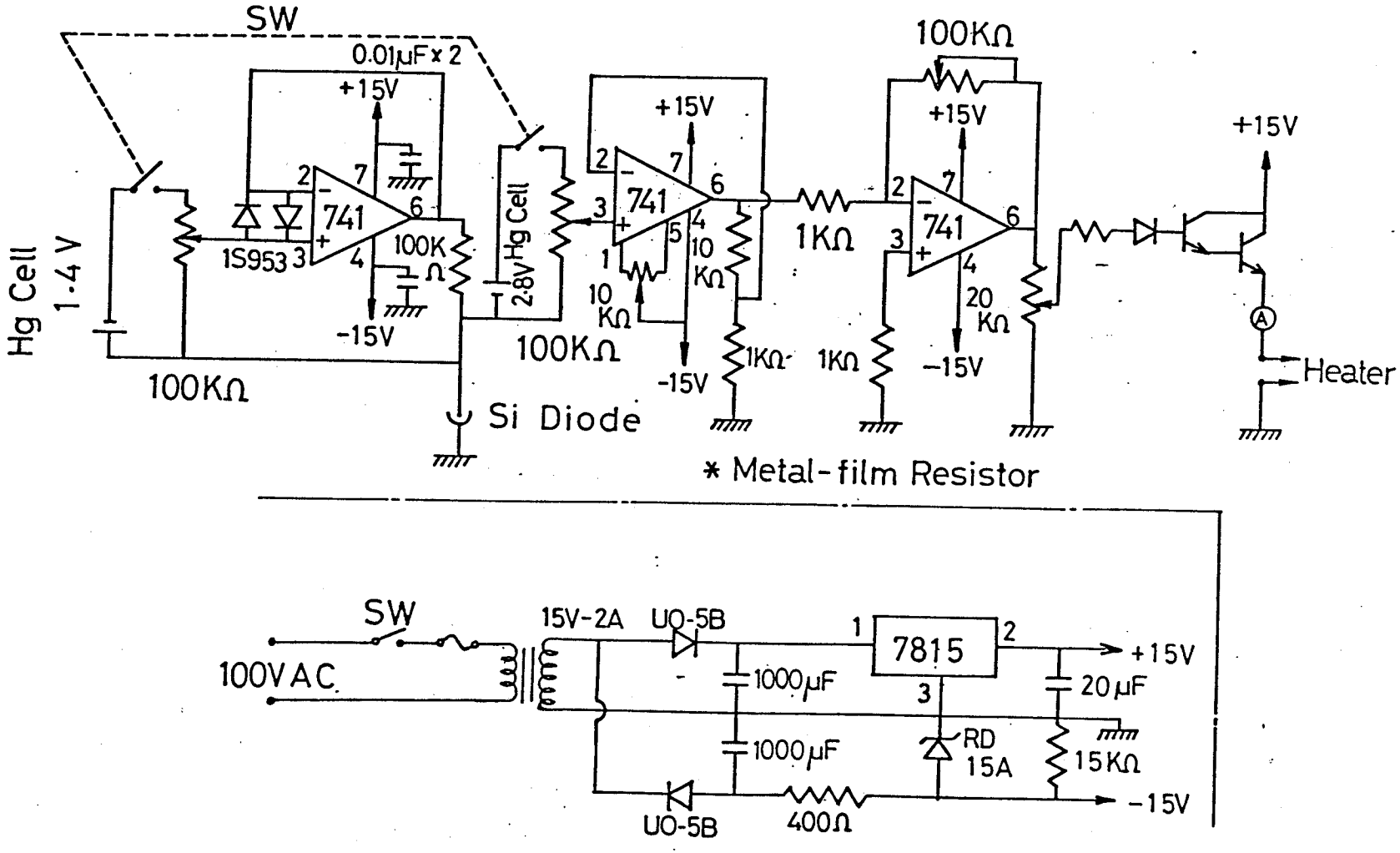

Fig. 3. An automatic current controller for desired temperatures.

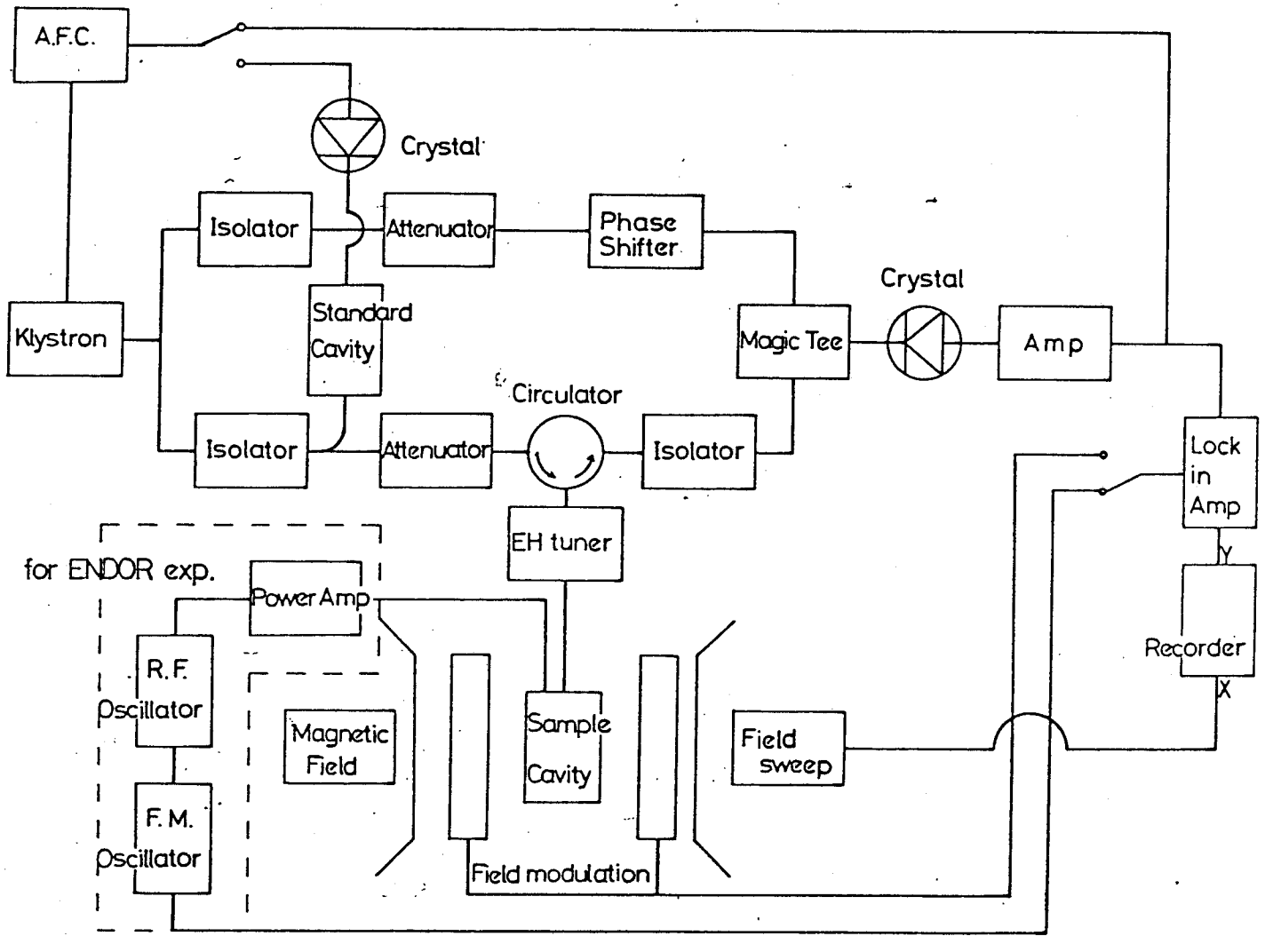

Fig. 4. Block diagram of V-band ESR spectrometer.

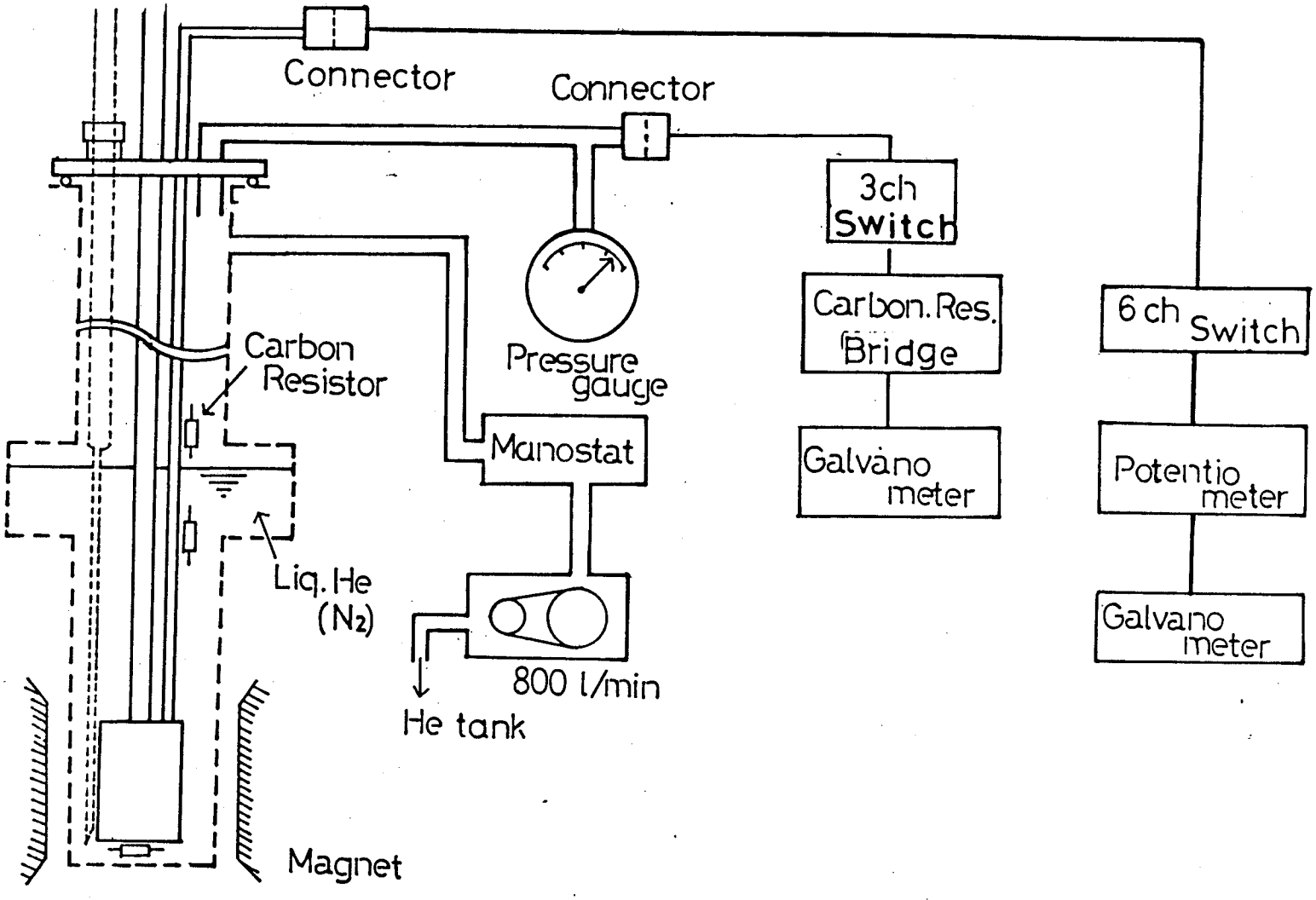

Fig. 5. Experimental set-up for low temperatures.

III. Results and Discussions

1. Transport Measurements

For degenerate magnetic semiconductors, conduction carriers are scatterd by usual phonons, ionized magnetic impurities, and spin-dependent scatterings through the s-d interactions between free carriers and localized magnetic ions. Our interest is concerned with the effect of magnetic impurity on the electrical properties of conduction carriers in degenerate magnetic semiconductors. For this purpose, we studied $Sn_{1-x}Mn_xTe$ crystals by the measurements of the anomalous Hall effect and electrical resistivity. In the crystals with small x-value ($x \leq 5$ at.%), Mn ions normally exist in the 2+ cation state whose electron configuration is the ^6S ($3d^5$) configuration and thus has no orbital angular momentum (as shown later).

The host crystal of SnTe at room temperature usually crystallize in a NaCl structure, where crystal field around the cation is cubic symmetry (A_{1g}). Therefore, the crystal structure changes to the rhombohedral structure under a structural phase transition associated with a small distortion along the <111> direction.

a) Resistivity and Hall mobility

We shall first show the effect of magnetic impurities as scattering centers on the carrier transport in $Sn_{1-x}Mn_xTe$. As one of the spin dependent transport properties, figure 6 shows the temperature dependence of the resistivity for some of annealed samples with different Mn content. As shown in the figure, starting from a higher temperature the resistivity decreases almost linearly with decreasing temperature. The resistivity shows a small maximum or a sharp drop at a characteristic temperature denoted by T_m. The dependence of T_m on x will be shown later in Fig. 14. Ghazali et al[36] attributed such a resistivity maximum to the critical scattering of carriers by spin fluctuation.

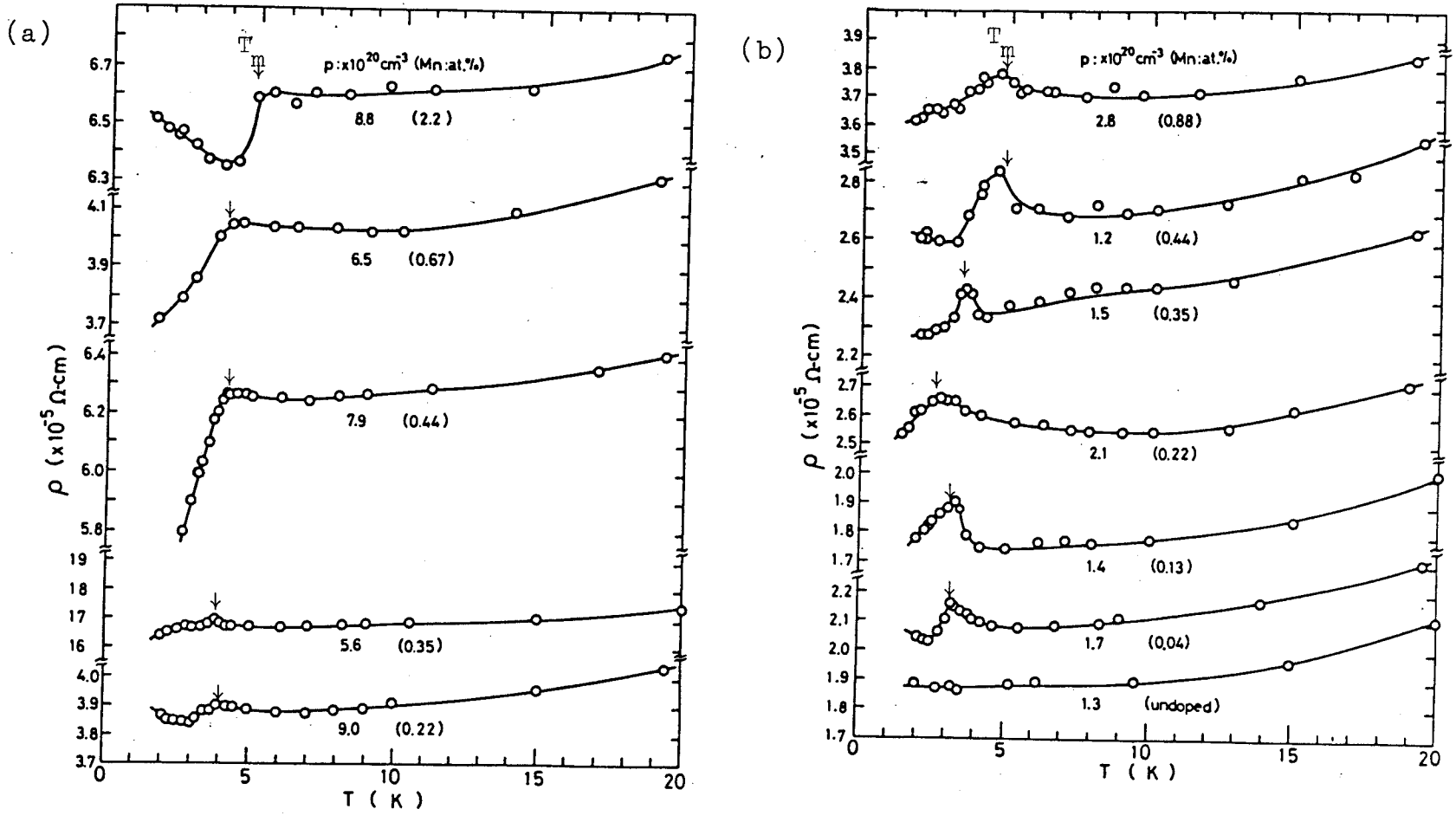

Fig. 6. Temperature dependence of resistivity for Mn-doped SnTe crystals (a) with high carrier concentration p = (5.6–9)×10^{20} cm^{-3} (as-grown crystals) and (b) with low carrier concentration p = (1.2–2.8)×10^{20} cm^{-3} (annealed crystals). The Mn content in at.% for each sample is indicated in parentheses.

In Fig. 7 the residual resistivities at 4.2 K, $\rho_{4.2}$, are plotted against x for the samples studied thus far. The dotted lines indicate the general trend of the behavior. It should be emphasized that the residual resistivity is also dependent on the amount of magnetic impurities, and that the increase in the resistivity is gradual up to $x \simeq 2$ at.% and rather abrupt for $x > 2$ at.%. Similar Mn content-dependences are seen in the Hall mobility. Such differences in the transport properties depending on Mn content are attributed to the differences in the scattering mechanisms (as shown later). It can be seen that the resistivity for low carrier density (annealed crystals) is smaller than that for high carrier density (as-grown crystals); this means that native defects (mostly Sn vacancies), together with Mn atoms, are responsible for the resistivity. This fact is also proved by the fact that the ratio of resistivity at 300 K to that at 4.2 K, $\rho_{300}/\rho_{4.2}$, decreases linearly with increasing carrier density; the ratio was found to be 8 for $p = 1.2 \times 10^{20}$ cm^{-3} and 3 for $p = 8 \times 10^{20}$ cm^{-3}.

In Fig. 8(a) is shown the Hall mobility μ_{77} at 77 K as a function of the carrier concentration for several Mn contents x's. It decreases linearly with carrier concentration as has been found by many workers and the absolute value becomes smaller with increasing the impurity content. To make the latter fact more clearly we plot the Hall mobilities as a function x in Fig. 8(b); the annealed samples are indicated by open symbols and the as-grown samples by solid symbols. Again the dotted lines in Fig. 8(b) indicate the general trend of the μ_{77} vs x relation covering all samples with different carrier concentrations $p = (1 \sim 10) \times 10^{20}$ cm^{-3} and the upper part in the bound region by the two dotted curves correponds approximately to the lower carrier concentration. It is to be noted that the decrease in the Hall mobility with increasing x is gradual up to $x \simeq 2$ at.% and rather abrupt for $x > 2$ at.%.

In Fig. 9 the Hall mobilities μ are plotted against temperature; the data of undoped crystal (x=0) are also shown for comparison. With increasing Mn content, the temperature dependence and the absolute value of μ decrease. The temperarure dependence of the observed Hall mobility μ in the range 77-300 K can be approximated empirically by the form :

$$\mu \propto T^{-n} , \qquad (1)$$

where n depends on x as shown in Fig. 10. Also in this case, the value n begins to decrease abruptly for x > 2 at.%. As is well known in ordinary nondegenerate semiconductor physics, a different scattering mechanism leads to a different temperature dependence of the Hall mobility; roughly speaking for electrons (n-type material), n = 1.5 corresponds to the acoustic and nonpolar phonon scattering,[37] n = -1.5 to the ionized impurity scattering[38] at high temperature, n = 0 to the neutral impurity scattering[39] and s-d scattering[40] except for the vicinity of Kondo temperature. In practice, these mechanisms are cooperated and for As-doped Ge by Debye et al.[41] and for As-doped Si by Morin[42], it was shown that mobility and its temperature dependence are decreased with increasing impurity contents.

However, the informations about the values n, for the degenerate semiconductors are little, in particular for $Sn_{1-x}Mn_xTe$ in which the transport mechanisms are attributed to the two factors; the spin-dependent scattering and the existence of the carriers in the two valence bands (light and heavy holes). The small values of n for $Sn_{1-x}Mn_xTe$ suggest that there occur the relatively large spin-dependent scattering and the phonon scattering compensated by the ionized-impurity scattering. From the data for x > 2 at.% we conclude that magnetic impurity scattering centers and potential scattering centers of impurity cluster.

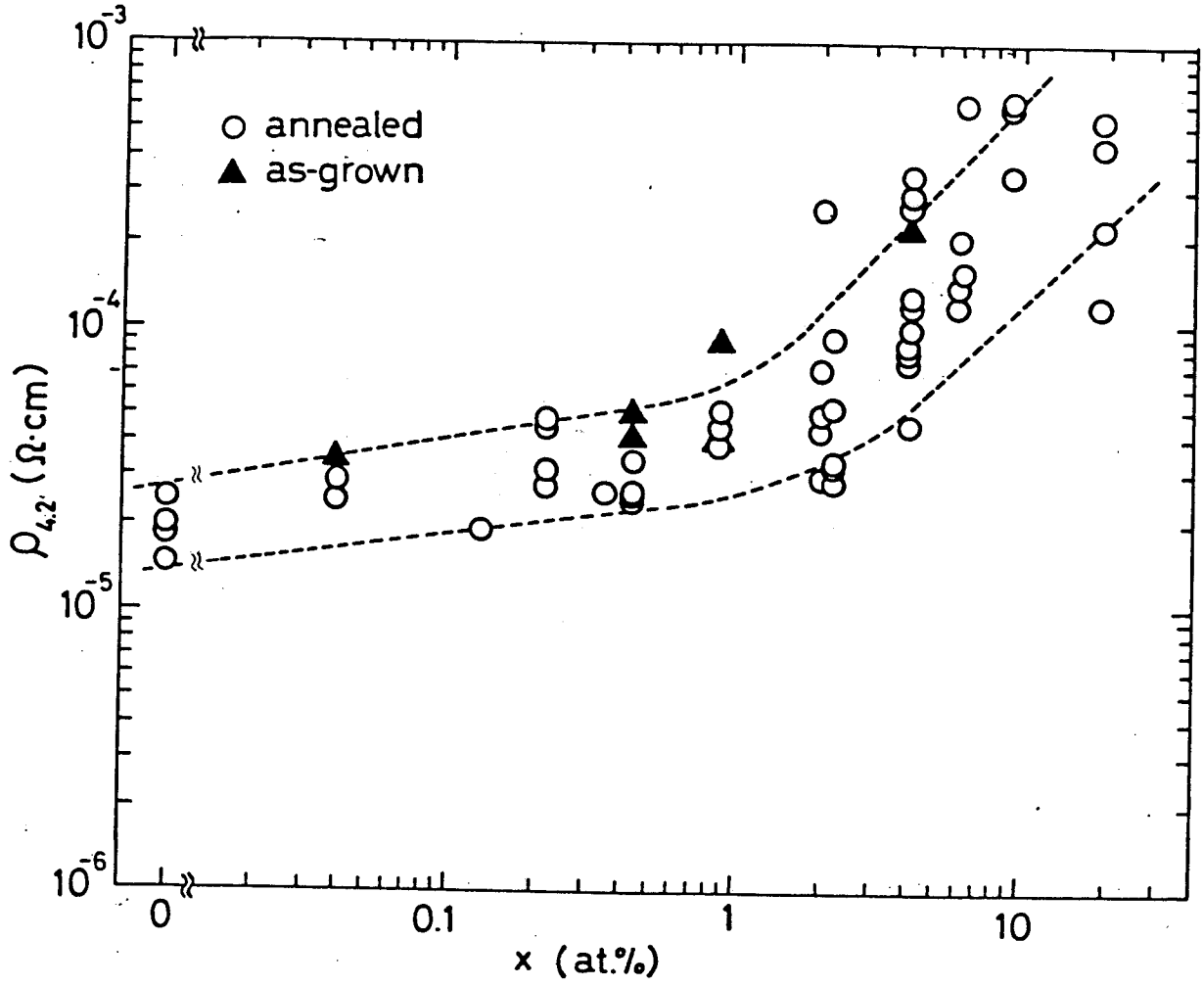

Fig. 7. Dependence of residual resistivity for $Sn_{1-x}Mn_xTe$ at 4.2 K against Mn content. The points on the left side are the data for the undoped samples (x=0).

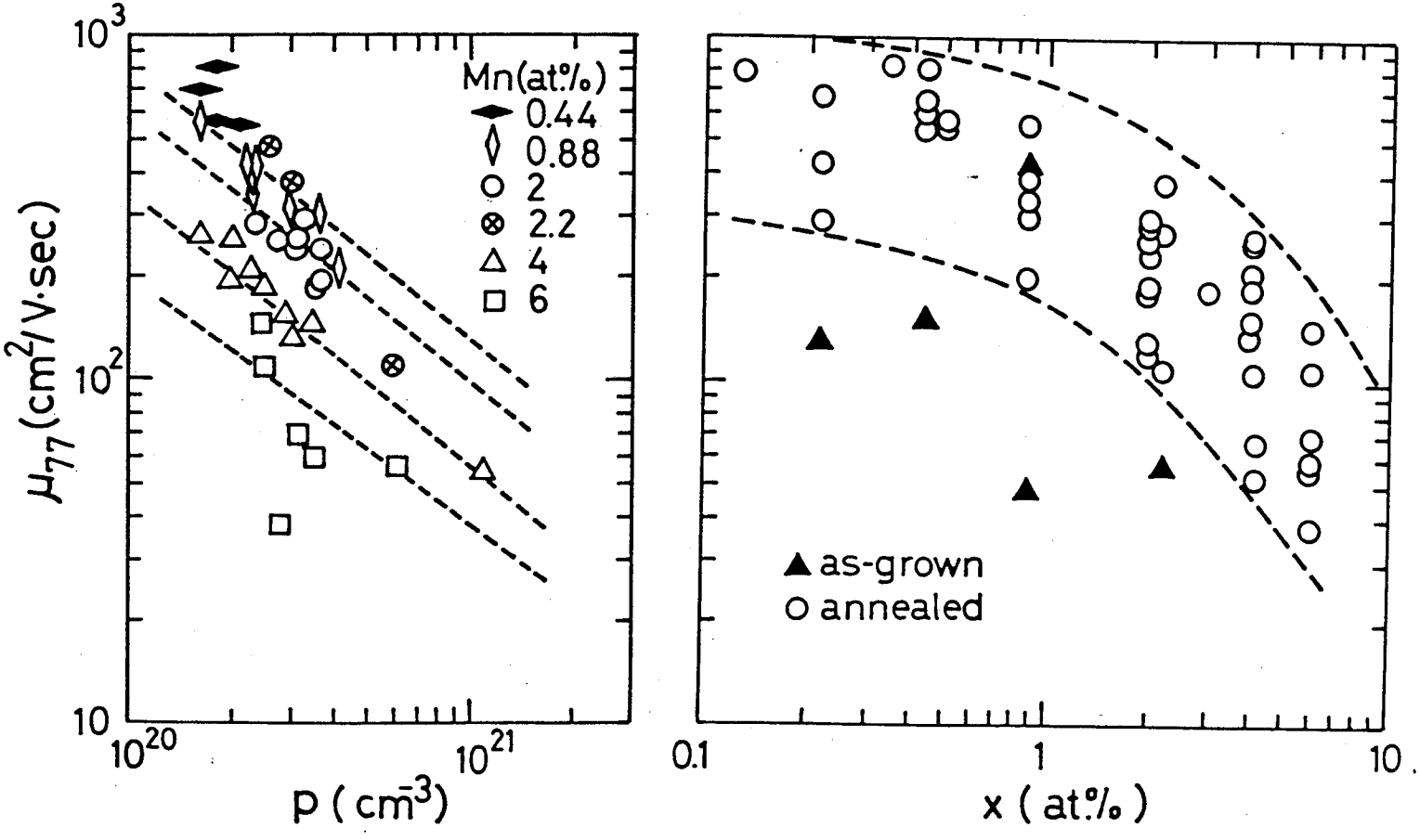

Fig. 8. Hall mobility of $Sn_{1-x}Mn_xTe$ at 77 K plotted against (a) carrier concentration p at 300 K and (b) against Mn content x.

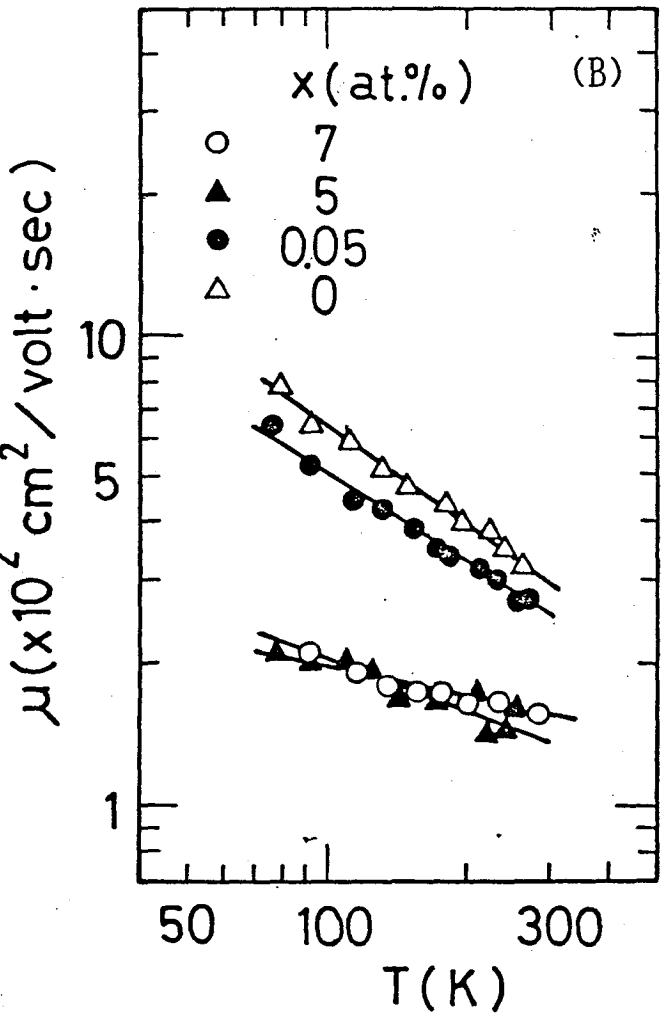

Fig. 9. Teperature dependence of the Hall mobility for $Sn_{1-x}Mn_xTe$ in the temperature range 300–77 K. Carrier cocentration at 300 K p = 1.35–1.75 × 10^{20} cm^{-3} .

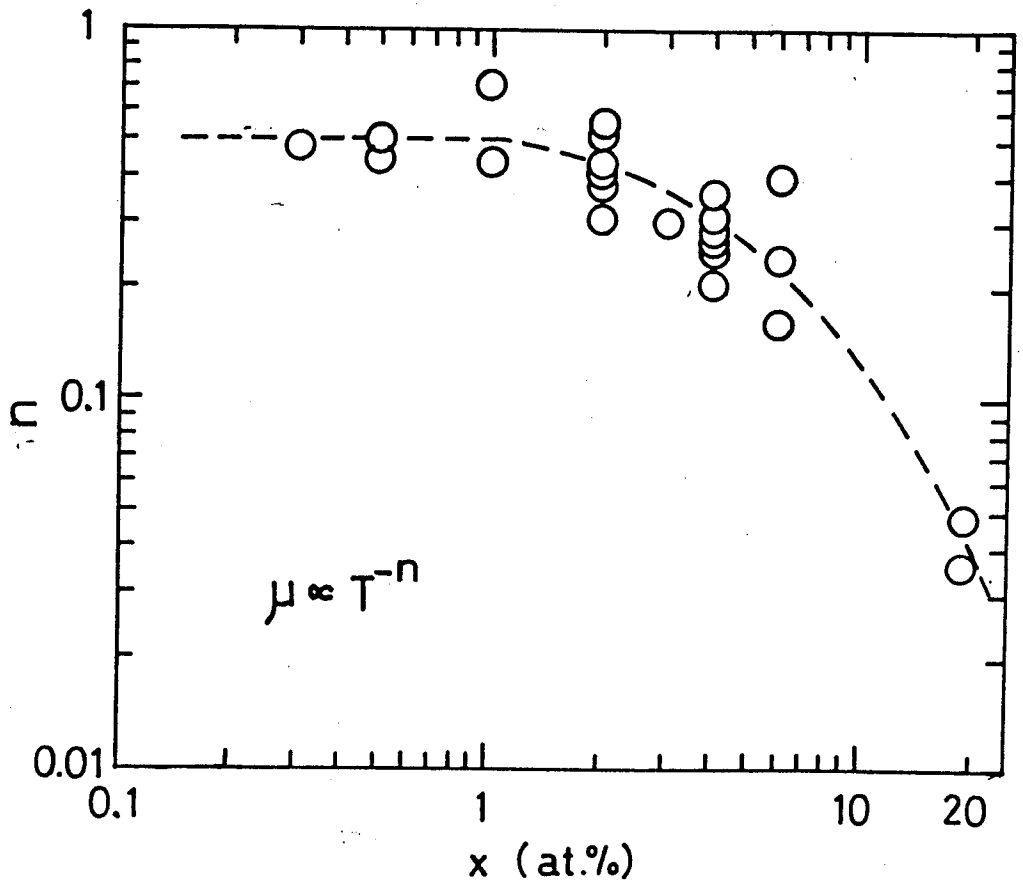

Fig. 10. The index n of T plotted against Mn content x in the temperature dependence of the Hall mobility, $\mu \propto T^{-n}$, for the annealed $Sn_{1-x}Mn_xTe$ samples with $p = (1\text{-}4)\times10^{20}$ cm^{-3}.

b) Anomalous Hall effect

Our main interest is concerned with the magnetization dependent Hall effect in the degenerate magnetic semiconductors. The recorder traces of the Hall voltages against the magnetic field strength at various temperature are shown in Fig. 11 for the samples with (a) x = 0.22 at.% and (b) x = 2.0 at.%. The pairings of the curves in the figures mean that the measurements were performed at a fixed temperature by reversing the magnetic field direction at each step as usually employed in the Hall effect measurement. The absolute Hall voltages were checked by a dc potentiometer. At high enough temperatures the Hall voltage varies linearly with the applied field, showing a normal Hall effect. Once the temperature is lowered down to a critical temperature, or to a magnetic ordering temperature T_c, an initial increment in the Hall voltage at weak field is observed in spite of the linear and normal region at higher field. Such behavior are quite similar to those found in ferromagnetic materials and some magnetic alloys, in which there is a contribution of the internal field to the Hall field depending on the state of magnetization of the sample. For a sample with high Mn content, however, the behavior observed at weak field becomes complicated as the temperature is lowered, as shown in Fig. 11(b). Presumably this may be due to the presence of a spin ordering whicn is not the same as in usual ferromagnetic materials. Here we will deal with the Hall resistivity ρ_H for ferromagnetic samples. For ferromagnetic materials and some magnetic alloys, ρ_H is expressed empirically by

$$\rho_H = R_0 B + 4\pi \cdot R_s M = R_0 \cdot [\, H_a + 4\pi\, M \cdot (1-N)\,] + 4\pi\, R_s M \qquad (2)$$

$$= R_0 H_i + R_1 M \ ,$$

$$\text{with} \qquad H_a = H_i + 4\pi\, M, \quad R_1 = 4\pi \cdot (R_0 + R_s) \ ,$$

where R_0 is the ordinary Hall coefficient, R_1 the anomalous Hall coefficient (often R_s is called the spontaneous Hall coefficient),[43] M the macroscopic magnetization, N the demagnetization factor, H_i the internal magnetic field

and H_a the applied magnetic field. Since in practice $|R_0| \ll |R_s|$ is usually true, R_s or R_1 can be determined experimentally from the $\rho_H - H_a$ curve. In general, there is initially a rapid, linear rise of the Hall voltage with increasing H_a followed by a second linear portion having a relatively smaller gradient (see Fig. 11). The first and second portions give R_1 and R_0, respectively, and the magnetic field H_a ($= 4\pi N M_s$) at saturation is determined from the crossing point of the two linear portions.

For $Sn_{1-x}Mn_xTe$, the ordinary Hall coefficient R_0 of the order of $(2\text{-}4) \times 10^{-2}$ cm^3/C was found to be independent of x and temperature over the temperature ranges studied. On the contrary, the anomalous component R_1 was strongly temperature-dependent. The experimental results are illustrated in Fig. 12 for various samples. The absolute value of R_1 and the slope of the $R_1 - T$ curves differ slightly from each other, but it is found that there is a systematic variation of R_1 with magnetic impurity content for less or more than 2 at.%, as often described. Since the Hall field measured is very sensitive to the various crystalline imperfections such as lattice defects and inhomogeneous distribution of magnetic impurities over a grown ingot, the detailed discussion of the R_1 vs x relation requires the data on the samples with good crystalline homogeneity.

Now, it can be seen that the temperature dependence of R_1 for $Sn_{1-x}Mn_xTe$ system at $T < T_c$ (ferromagnetic state) is expressed roughly as $R_1 \propto T^2$, in agreement with the Voloshinskii model which is based on theories with localized magnetic electrons and takes account of the mixed spin-orbit interaction, together with spin disorder as scattering mechanism. The concept of the mixed spin-orbit interaction was introduced by Voloshinskii[44] and Maranzana[45] with particular reference to the anomalous Hall effect and we can get some physical picture of the interaction if, in a tight-binding scheme, the itinerant charge carrier can be imagined to have

an orbit around the ion during the scattering process. Then the magnetic field produced by this circulating current will interact directly with that due to the localized moment, and will produce a coupling between the d spin and the orbit of the itinerant s electron. In the non-s state with angular orbital momentum, there occurs a intrinsic spin-orbit interaction in which the temperature dependence of R_s is proportional to T^3, as given by Irkhin's calculation.[46)]

For degenerate magnetic semiconductors there occurs both the mixed spin-orbit interaction and the intrinsic spin-orbit interaction because the carrier state exist in both s-state and non-s-state (mainly p-state). There is an analogy between degenerate magnetic semiconductors and the well-known semimagnetic semiconductor such as $Hg_{1-x}Mn_xTe$. For both these systems, since the band gap is relatively smaller than usual II-VI semiconductors, the carrier state is formed by the mixed s-state and p-state. Then the interaction between the carriers and magnetic impurity consists of a s-d interaction and a p-d exchange. However, since the anomalous Hall coefficient of the $Sn_{1-x}Mn_xTe$ systems follows the T^2 behavior, it is shown that the mixed spin-orbit interaction is predominant and that the s-d exchange interaction plays more important role than those of p-d exchange. This result is also in agreements with the ESR results as shown later.

We return to the observed Hall field shown in Fig. 11, from which according to eq. (2) we can estimate the spontaneous magnetization $4\pi \cdot NMs$ at temperature T of the samples. The well-known Bloch spin-wave theory for ferromagnetic materials predicts that the temperature dependence of the magnetization varies as, at low temperature $T < T_c$

$$M_s(T) = M_s(0) \cdot \{ 1 - (T/T_c)^{3/2} \} \quad , \tag{3}$$

where $M_s(0)$ is the saturation of the magnetization at absolute zero temper-

ature, T_c the Curie temperature which has linear dependence on exchange energy between two spins. We attemped to plot the normalized magnetization against $T^{3/2}$ as shown in Fig. 13. The experimental results obey well the $T^{3/2}$ law. The slope for x = 0.2 at.% is different from the others observed because of the different T_c. From the best-fit theoretical curve of eq. (3) for each sample we estimate the values of $4\pi \cdot NM_s(0)$ and T_c, where the demagnetization factor N is actually unknown for our sample of a rectangular bar. But we assume that N is approximately the same for all the samples with nearly identical dimensions.

Furthermore, figure 14 shows the Curie temperature determined from Fig. 13 with eq. (3) as a function of x. For comparison, in Fig. 14 also are shown those obtained from magnetic measurements by Cohen et al.[47] and Escorne et al.[48] and our characteristic temperature T_m determined by the resistivity anomaly in its temperature dependence (dotted line). It is interesting to see a remarkable difference in the Mn content dependence of these characteristic temperatures, depending on whether it is determined by magnetic measurements or by transport ones. In their analysis of the magnetic measurements on $Ge_{1-x}Mn_xTe$ system, Cochrane et al.[24] took into account the Mn atoms having a well defined local moment and assumed the simple RKKY interaction $\{ J_1(i,j)\}$ as well as a nearest-neighbor antiferromagnetic exchange $\{ J_2(i,j),\ J_2 < 0\}$ between the Mn ions. Treating the Hamiltonian by the random-phase approximation for spins, they found that both the ferromagnetic Curie temperature T_c and paramagnetic Curie-Weiss temperature θ are

$$T_c = \frac{S(S+1)}{3k} \times \left(\frac{1}{N} \sum_k \frac{1}{J(0) - J(k)} \right)^{-1}, \tag{4}$$

$$\theta = \frac{S(S+1)}{3k} \times J(0), \tag{5}$$

$$\text{with} \quad J(k) = \sum_{R_{ij}} J(R_{ij})\, e^{-kR_{ij}},$$

where $J(R_{ij})$ is the exchange energy between i th- and j th-spins (included J_1 and J_2), R_{ij} their distance and x the Mn content. From eqs. (4) and (5), both the T_c and θ are proportional to x and thus the difference between these temperature is attributed to the frequency component of the exchange energy. Equation (4) agrees with the magnetic measurements by Cohen et al., Escorne et al. (as shown in Fig. 14) and Sondermann[49], and also is in a good agreement with the measurements of specific heat by Mathur et al.[50]

The small x dependence of T_c was also obtained from thermopower measurements by Inoue et al.[51] There have been little knowledge about mechanisms of the small x dependence of T_c for $Sn_{1-x}Mn_xTe$. There may be different mechanisms between the transport and the magnetic phenomena; in the transport measurements we meet at first with the interaction between carrier spins and Mn ones, but in the magnetic measurements a interaction of two spins (RKKY interaction) plays more important role. Thus the result in eq. (4) is seen to be due to a RKKY interaction which increases with increasing x. While the s-d interaction rather depends on the symmetries of the impurity and the carrier spin states than impurity content. Thus in transport phenomena, it is important to note what kind of cooperative phenomena of carrier and d electron occur.

According to the Kondo effect in dilute alloy system, it is well known that the temperature T_{min} at which the resistance is a minimum depends on the one-fifth power of x, while the temperature T_{max} at the resistance maximum depends linearly on x. Also, for the case of $Sn_{1-x}Mn_xTe$, the transition temperature T_m obtained from the resistivity measurements is proportional to $x^{1/5}$. However, the magnetic state of our $Sn_{1-x}Mn_xTe$ can not be a Kondo state but rather exists in the RKKY region, because of the high Mn content of used samples. Nevertheless, it is evident that the observed anomalies in our samples are caused by the magnetic scattering of carriers through the s-d interaction, although the T_m - x relationship remains unexplained.

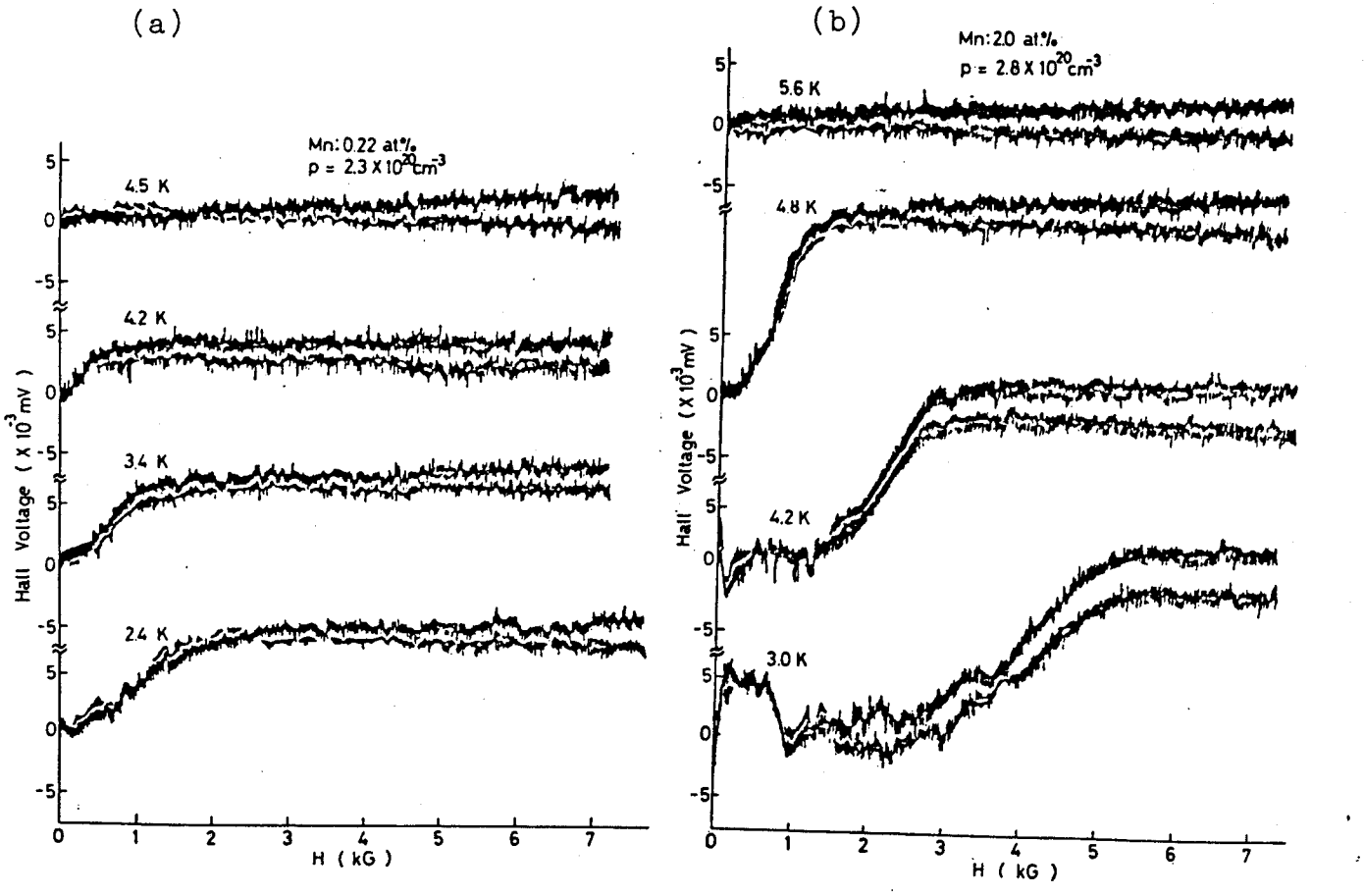

Fig. 11. The recorded traces of the Hall voltages against the applied magnetic field at various temperatures for $Sn_{1-x}Mn_xTe$ (a) x=0.22 at.% and $p=2.3\times10^{20}$ cm^{-3}, and (b) x= 2.0 at.% and $p=2.8\times10^{20}$ cm^{-3}. A pair of the curves at a fixed temperature were obtained by reversing the field.

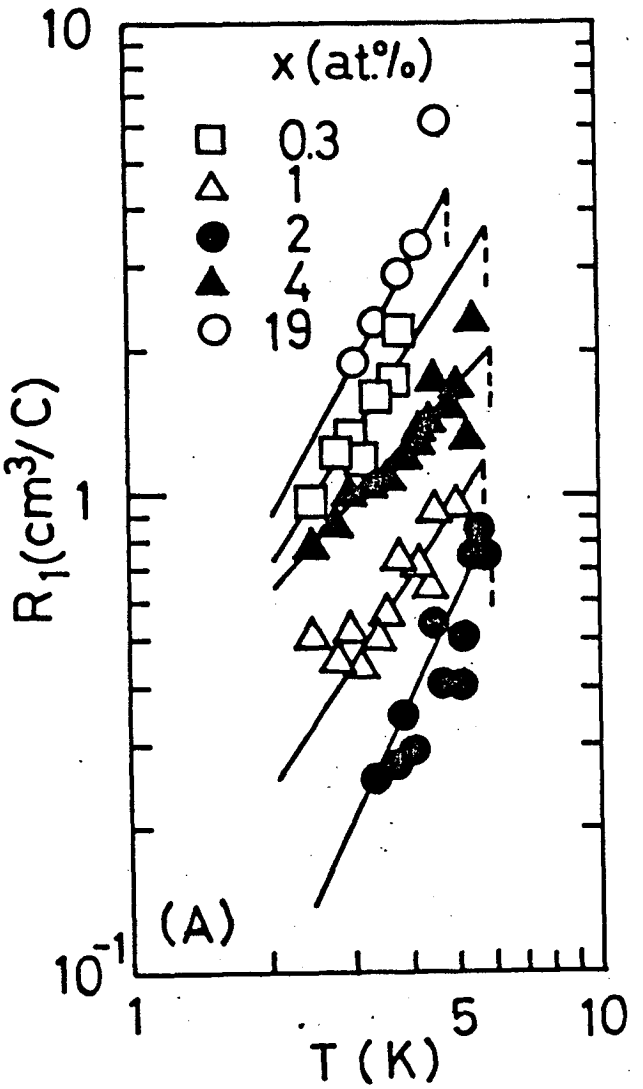

Fig. 12. Temperature dependence of the anomalous Hall coefficient R_1 for $Sn_{1-x}Mn_xTe$ samples with various Mn contents. A vertical dotted line for each sample indicates the Curie temperature T_c at which the anomalous component vanishes.

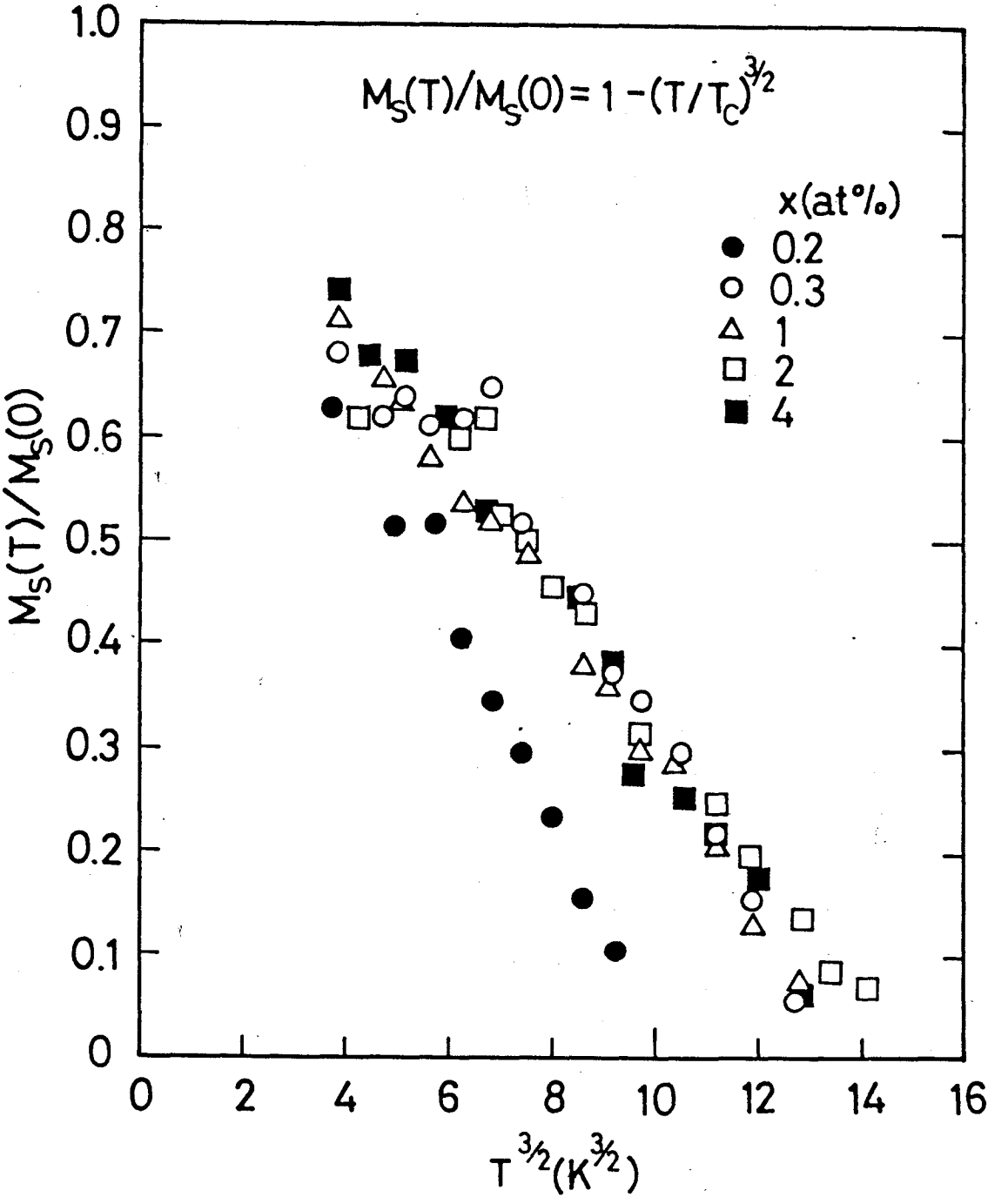

Fig. 13. Temperature dependence of the normalized spontaneous magnetization for $Sn_{1-x}Mn_xTe$ crystals with various Mn contents.

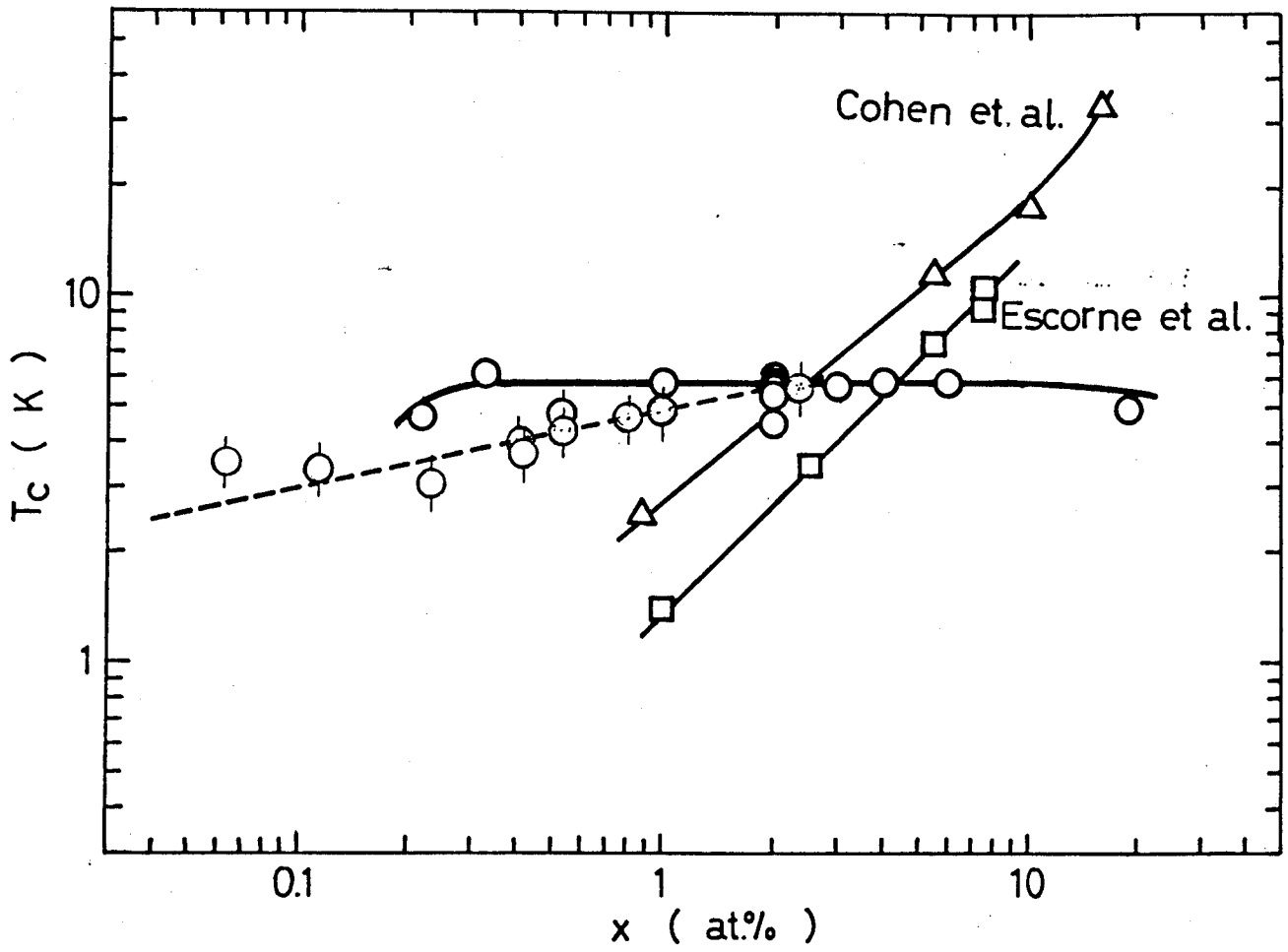

Fig. 14. Dependence of magnetic ordering (Curie) temperature on Mn content in $Sn_{1-x}Mn_xTe$ Open circles: Present work. Dotted line: Ordering temperature T_c determined earlier from the resistivity anomaly. Open triangles and squares are obtained from the magnetic measurements by Cohen et al.and Escorne et al., respectively.

2. Magnetic Measurements

Figure 15 shows the temperature dependence of the magnetization σ for the various as-grown crystals $Sn_{1-x}(Me)_xTe$ (Me = Cr, Mn, Fe, Co and Ni), all with x = 1 at.%. It is interesting to note that there exist different types of magnetism among these systems. The magnetization curves of Cr- and Fe-doped crystals show ferromagnetic behavior whereas those of the Co- and Ni-doped ones are diamagnetic. Only Mn-doped crystals are paramagnetic.

In Fig. 16 the reciprocal susceptibilities of the annealed $Sn_{1-x}Mn_xTe$ crystals with various impurity concentrations are plotted as a function of temperature. Since SnTe itself has a small temperature-dependent diamagnetic contribution ($\simeq -4 \times 10^{-7}$ emu/Oe•g at 77 K), the magnetic susceptibility χ follows well the Curie-Weiss law with the Curie constant C and the paramagnetic Curie temperature θ. The susceptibility and the Curie constant are represented by

$$\chi = C / (T-\theta), \quad C = N \cdot S(S+1)\, g^2\beta^2/3k \ , \qquad (6)$$

where N is the number of spins per gram, β the Bohr magneton, S the spin quantum number, g the g-value nearly equal to 2 obtained from ESR results (shown in later) and k the Boltzman constant. Nearly the same results were obtained for the as-grown crystals too.

In Table II are summarized the values of χ at 77 K, the Curie constant C obtained from the slopes of the $1/\chi$ - T curves, and the spin quantum number S caculated from C using eq. (6) for both the as-grown and annealed samples. Let us note two characteristic features: First, the experimentally obtained spin quantum numbers of the magnetic ions are very close to the free ion value S = 5/2, regardless of the impurity concentration, indicating that the Mn ions are in the paramagnetic S-state (Mn^{2+}, $3d^5$) in the crystal lattices. Second, more interesting and important feature is that

there are no appreciable differences, within experimental errors, in the magnetic data (χ, C, and S) between the as-grown and annealed crystals.

Moreover, magnetic studies on $Sn_{1-x}Mn_xTe$ by other workers[49] have also shown that for the samples with high contents of x = 10 ∿ 40 at.%, the magnetic susceptibilities obey the Curie-Weiss law in the temperature range above 50 K. Thus, in conclusion, the $Sn_{1-x}Mn_xTe$ is a well diluted sample of the Mn content in a host crystal.

On the other hand, the Cr-doped crystal is ferromagnetic at low temperature and becomes diamagnetic at high temperatures due to a strong diamagnetic background of the host crystal as shown in Fig. 15. The magnetizations at weak field of 30 Oe, σ_r (residual magnetization) as a function of temperature are shown in Fig. 17 for the as-grown and the annealed $Sn_{1-x}Cr_xTe$ crystals with various x's. The ferromagnetic Curie temperatures obtained from these magnetization-temperature curves are seen strongly dependent on both the impurity concentration and the heat-treatment, as shown in Fig. 18. The presence of the similar ferromagnetic phase in this system is also confirmed by the anomalies in the ESR signals as shown later.

In Fig. 19 are shown the temperature dependence of low field (about 30 Oe) magnetization σ for the crystal with x = 0.5 at.% annealed in Zn vapor for various times ranging from 5 min through 2 hrs to 7 days; the as-grown sample were quenched by dropping in to water after annealing. It is worthy to note that as the annealing time is increased the magnetic transition occurs gradually and shifts to a high temperature side, ultimately near 300 K.

These results show that after the annealing in Zn-vapor the rearrangements of Cr ions must take place in the lattices and thus some of the magnetic ions will migrate to form some sort of "clusters". For these results, the followings can be supposed; 1) Cr ionic radius is smaller than those of the constitutent ions, 2) the configuration function of Cr ions can not exist stably in the A_{1g} crystal field formed by Te ions.

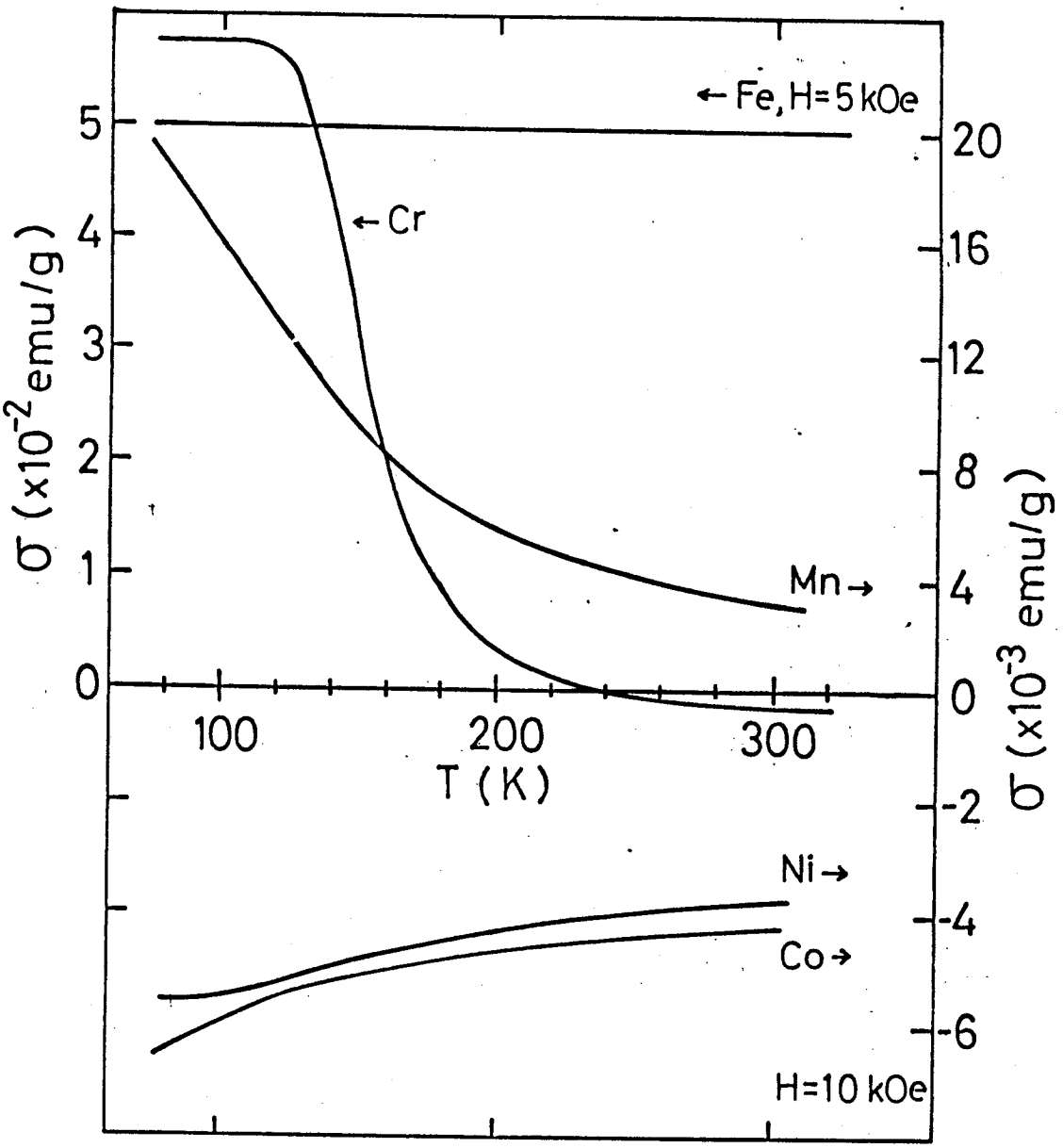

Fig. 15. Temperature dependence of the magnetization for as-grown $Sn_{1-x}(Me)_xTe$ crystals with Me = Cr, Mn, Fe, Co and Ni (all x = 1 at.%); the applied magnetic field is 5 kOe for Fe and 10 kOe for the others.

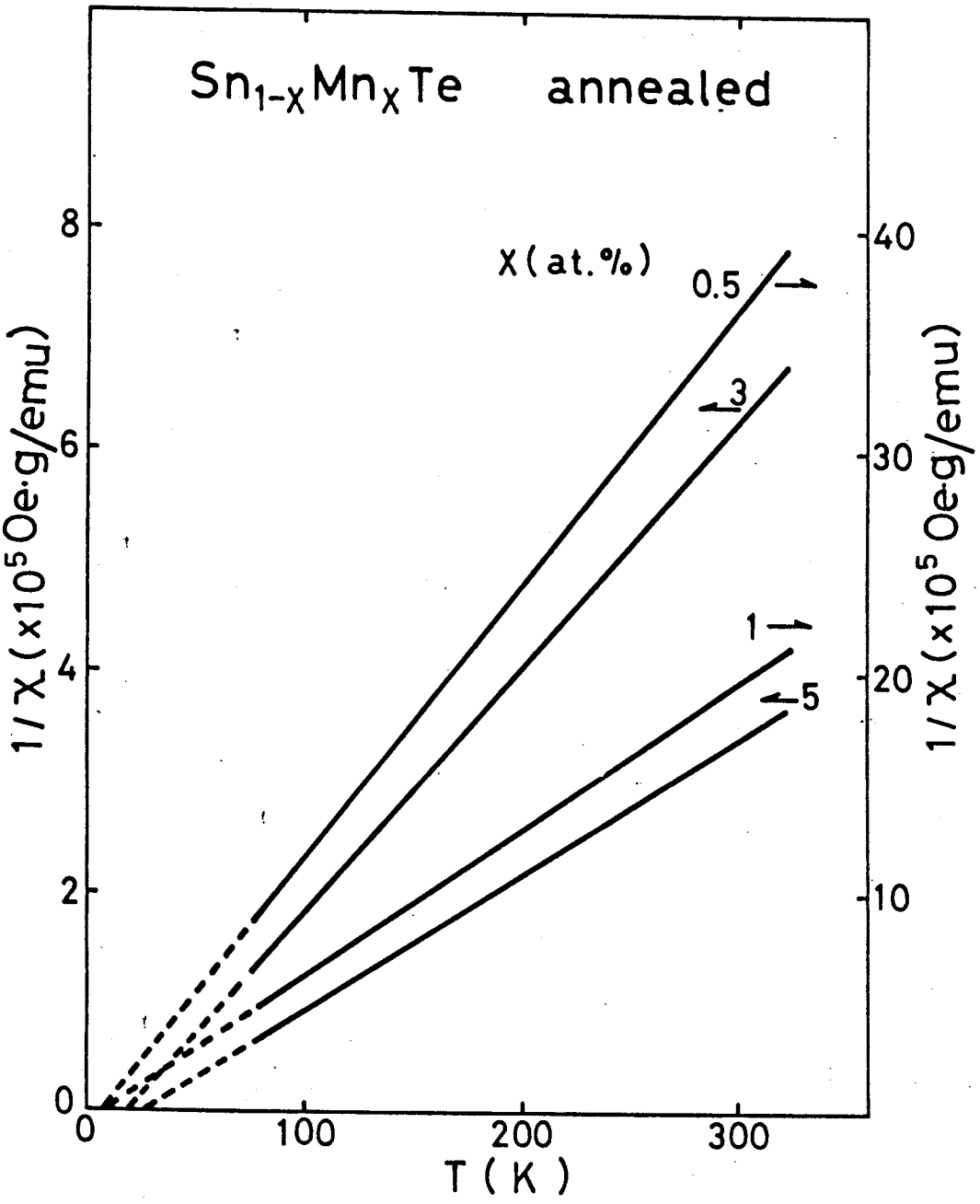

Fig. 16. Temperature dependence of the reciprocal magnetic susceptibility for the annealed $Sn_{1-x}Mn_xTe$ crystals with different impurity contents. The arrows indicate the right or left scale. Here the diamagnetic contribution from the host SnTe crystal is subtracted.

Table II. Magnetic susceptibility χ ($\times 10^{-6}$ emu/Oe·g) at 77 K, Curie constant C ($\times 10^{-4}$ emu·K/Oe·g), and spin quantum number S for the as-grown and annealed $Sn_{1-x}Mn_xTe$ crystals.

x (at.%)		χ	C	S
0.5	A	0.61	0.68	2.2
	B	0.58	0.81	2.4
1	A	1.6	1.2	2.0
	B	1.6	1.5	2.3
3	A	7.0	4.2	2.2
	B	6.8	4.2	2.2
5	A	14	8.9	2.5
	B	13	8.8	2.5

A: as-grown, B: annealed.

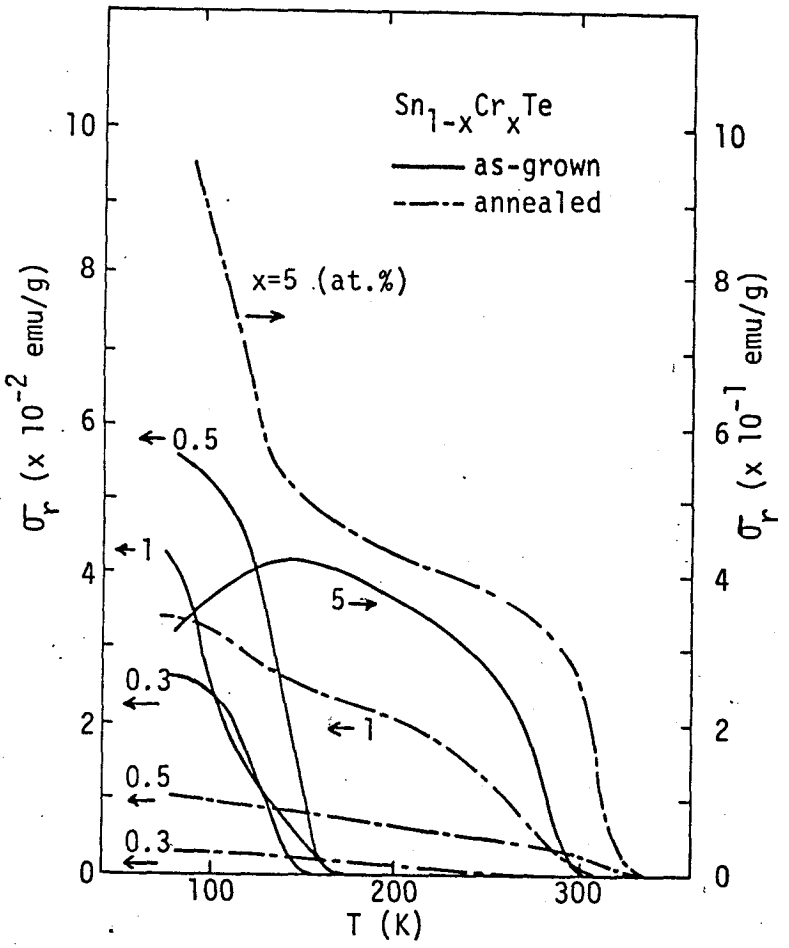

Fig. 17. Temperature dependence of the magnetization at 30 Oe for as-grown and Zn-annealed $Sn_{1-x}Cr_xTe$ crystals with different x.

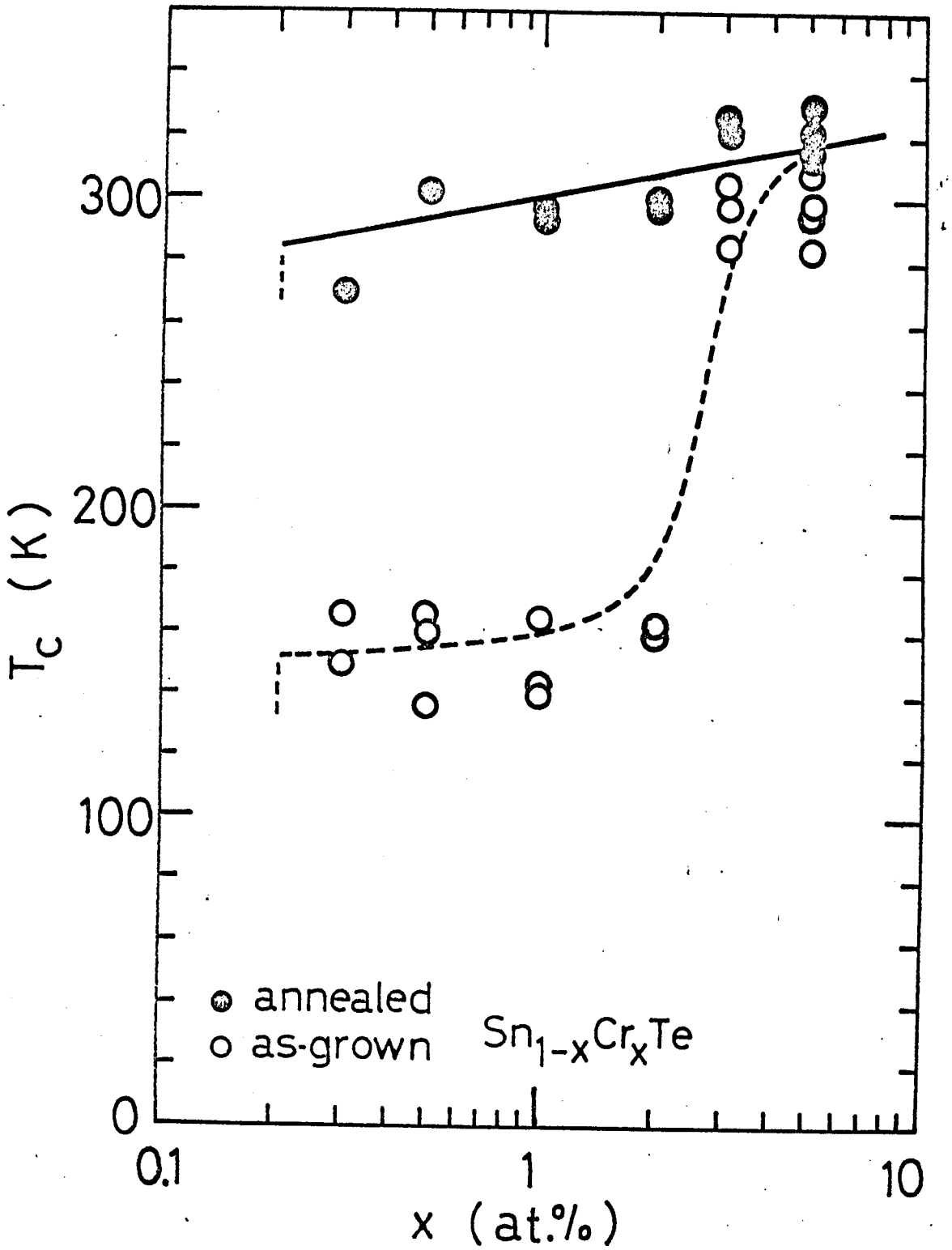

Fig. 18. Ferromagnetic Curie temperatures obtained from σ-T curves for as-grown and annealed $Sn_{1-x}Cr_xTe$ plotted against x.

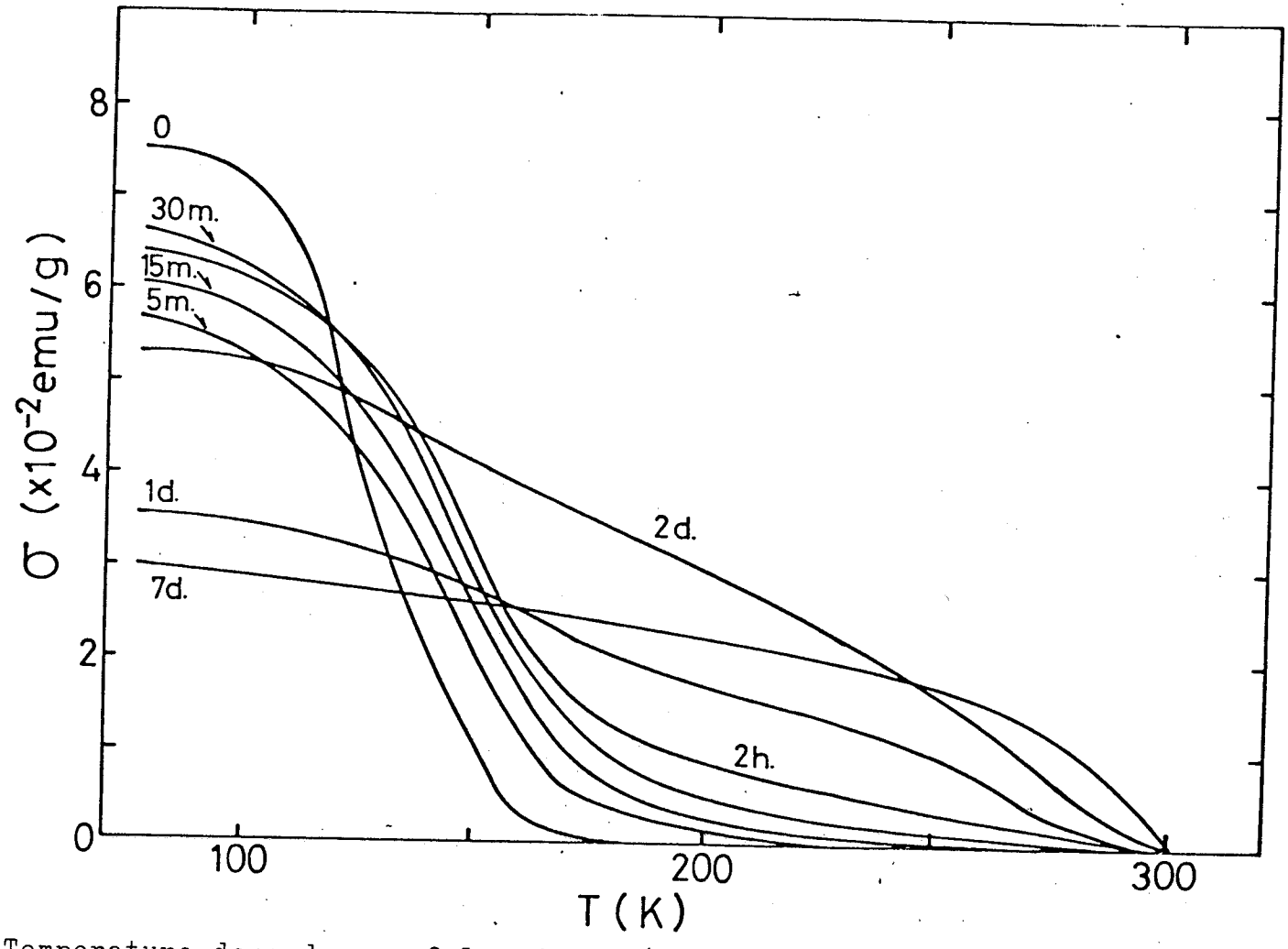

Fig. 19. Temperature dependence of low field (about 30 Oe) magnetzation for $Sn_{1-x}Cr_xTe$ (x = 0.5 at.%) crystals, which are annealed in Zn vapor for various times ranging from 5 min through 2 hrs to 7 days; the as-grown sample indicated by 0.

3. ESR Measurements

a) Hyperfine structure of localized Mn^{2+} spins

The state of a magnetic impurity in degenerate magnetic semiconductors is a localized spin state for lower concentration of impurities in which the spin-spin interaction is small. The magnetic impurity ion is the Mn^{2+} state and the ground state is ^6S ($3d^5$) configuration which has no orbital angular momentum and is exposed to the surrounding of a cubic symmetry. Therefore, the spin Hamiltonian of localized Mn^{2+} in these surrounding is well-known a simple form at the first order as follows

$$\mathcal{H} = g\beta\, \mathbf{S}\, \mathbf{H} + A\, \mathbf{S}\, \mathbf{I} \quad , \tag{7}$$

where $\mathbf{S}$ is the electron spin operator, $\mathbf{I}$ the nuclear spin operator, g the g-values of magnetic spin and A the hyperfine constant (HFC). The first and second terms in eq.(7) are a Zeeman and a hyperfine term, respectively. As ^{53}Mn nucleus has nuclear spin I = 5/2, the observed hyperfine lines are resolved into six structure lines as suggested in eq. (7).

The typical signals at 120 K are shown in Fig. 20 for $Sn_{1-x}Mn_xTe$ (0.04 at.% Mn) and $Pb_{1-x}Mn_xTe$ (0.06 at.% Mn). The value A of these crystals obtained from the ESR measurement are given in Table III together with lattice constant a[53-55], the Debye temperature Θ_D,[56,57] and the Phillips ionicity parameter f_i[8] which are concerned with the value A as shown later.

It is well known that the hyperfine splitting of Mn^{2+} ions stems from a core-polarization of s-electrons at the nucleus. The mechanisms responsible for the modification of A due to covalency can be classified as follows: First, we have an indirect effect of the covalent modified 3d electrons in the core polarization field H_{cp}. Second, the 1s, 2s, 3s, and 4s orbitals can contribute directly when they are admixed by overlap (1s, 2s, 3s) and transfer (4s) from the ligand orbitals. The decrease of A is

calculated by Simanek et al.[58] as follows

$$A = -(8\pi\gamma_n\beta / 3S)\cdot\{ \rho_\uparrow(0) - \rho_\downarrow(0)\}$$

$$\rho_\uparrow(0) - \rho_\downarrow(0) = \{ \sum_{n=2}^{3}[\phi_{ns}^2(0) - \phi_{ns}'^2(0)]\} + \{\sum_{n=2}^{3}<1_i|\phi_{ns}>^2[\phi_{ns}^2(0) - \phi_{ns}'^2(0)]$$
$$+ 2\sum_{n=2}^{3}<1_i|\phi_{ns}><1_i|\phi_{ms}>[\phi_{ns}(0)\phi_{ms}(0) - \phi_{ns}'(0)\phi_{ms}'(0)]\} + \{\gamma_a^2\cdot\phi_{4s}^2(0)$$
$$- \gamma_b^2\cdot\phi_{4s}'^2(0) - 2\sum_{n=2}^{3}<1_i|\phi_{ns}>[\gamma_a\phi_{ns}(0)\phi_{4s}(0) - \gamma_b\phi_{ns}'(0)\phi_{4s}'(0)]\}. \quad (8)$$

where $\phi_{ns}(0)$ and $\phi_{ns}'(0)$ are the wave functions of up- and down-ns-state at R =0 (ie, at Mn nucleus) respectively, $\rho_\uparrow(0)$ and $\rho_\downarrow(0)$ the their total electron density at R = 0, respectively. $<1_i|\phi_{ns}>$ is the overlap integral between a symmetric combination (A_{1g}) of the ligand ionic orbitals and s-state function ϕ_{ns} (neglecting small 1s contribution), and γ_a or γ_b the probabilities of the excitation to $3d4s_\uparrow$ or $3d4s_\downarrow$ involved in the transfer process from ligands. In eq. (8) the last terms involving the 4s admixture is caused by the 3d-4s exchange interaction, which pulls the 4s orbital (with spin parallel to the 3d spin) inward, increasing $\phi_{4s}(0)$; the hyperfine field reduction occurs by the covalent bonding.

The ionicity (in turn, covalency) dependence of A in Table III agrees with the consideration of eq. (8): The covalency between Mn and Te depends linearly on the covalency or chemical binding nature of the host crystals in which the magnetic ions are dissolved.

Now, the values of A for PbS;Mn^{2+} and PbSe;Mn^{2+} determined by Pifer,[59] are 71.8 ± 0.4 and 67.6 ± 0.3 cm^{-1}, respectively. Comparing these values with the A value for $Pb_{1-x}Mn_xTe$, we can find a systematic variation of A with the degree of covalency for Mn^{2+} among the various salts. The same effect was found generally in hyperfine field of Mn^{2+} at the octahedrally arranged ligands by Watson et al.[60] and Van Wieringen[61]; the hyperfine field H_{cp} decreases in the order of H_2O, F^-, O^{2-}, S^{2-}, Se^{2-} and Te^{2-} ligands. While,

in different cations, the A value seems to vary with the spread of the outer wave functions at free ions $4p(Ge^{2+})$, $5p(Sn^{2+})$ and $6p(Pb^{2+})$. In practice, however, there is no such systematic variation because of the binding force independent of this variation. Rather, only a hyperfine constant of $Pb_{1-x}Mn_xTe$ is a large one as shown in the Table.

In addition, the excitation mechanism such as the last term in eq. (8) also involves the admixture of excited configuration states $3d^4ns$ into the ground $3d^5$ configuration by a dynamic phonon-induced noncubic field, as was first proposed by Šimánek and Orbach.[62] The admixed s-state will result in a net decrease of hyperfine field which is produced primarily by a temperture dependent core polarization.

In Fig. 21 is plotted the HFS constant A of Mn^{2+} in degenerate semiconductors against temperature. The value of A for GeTe is seen to be approximately equal to that for SnTe, which suggests that both crystals have the same degree of ionicity. This result agrees with the fact that the Phillips ionicity parameters f_i for both the crystals are nearly equal to each other as given in Table III. On the contrary, the temperature dependence of the HFS constant A in GeTe is negligibly small, whereas those in SnTe and PbTe increase and then tend to level off as the temperature is lowered, as the same way as in many ionic crystals. Here we attempted to use the Huang's theoretical expression[63] of temperature-dependent A(T) for Mn^{2+} in octahedral symmetry, applicable to ionic crystal, where the model is based on the Van Vleck orbit-lattice interaction: It can be expressed by

$$A(T) = A_0 - B \cdot T, \tag{9}$$

where $$B \propto (e \cdot e_{eff})^2 / \rho R^8 \Theta_D^3.$$

Here A_o is the temperature independent term, e the charge of the bound electron at the magnetic impurity, e_{eff} the effective charge of an anion,

ρ the density, R the nearest-neighbor distance, and Θ_D the Debye temperature.

From our data of $Pb_{1-x}Mn_xTe$ and $Sn_{1-x}Mn_xTe$, the values of B in eq.(9) are found to be about 7.5×10^{-3} and 1.5×10^{-2}, respectively, and these values are larger than $1\sim5\times10^{-3}$ Gauss/K for typical ionic crystals: $MgO:Mn^{2+}$ and $ZnO;Mn^{2+}$.[64] The difference of temperature-dependent A is arised from the phonon induced ligand-4s transfer as well as excitation. The transfer mechanism exsists in degenerate semiconductors with rather chemical covalency bonding, but this effect is very small in ionic crystals.

The fact of the irrelevance of A in GeTe with temperature means that the factor B in eq.(9) is vanishingly small. However, the variations of the parameters R, Θ_D, in eq.(9) among these IV-VI crystals seem to be too small to account for the small value of B in GeTe; one might expect that B for GeTe becomes smaller because it has the highest Debye temperature in the three crystals listed in Table III. It is rather inferred that the temperature independence of A in GeTe is attributed to the crystal structure with a lattice vibration mode which has no cubic but orthorhombic symmetry.

Now, there is another information obtained from the hyperfine constant in $Pb_{1-x}Sn_xTe;Mn^{2+}$ (Mn, 0.01 wt.%). Our primary concern is the variation of the HFS constant A with x, whose result at 140 K is shown in Fig. 22. In general, $Pb_{1-x}Sn_xTe$ has been well known to have a band gap whose width is varied with composition x; at $x = 0.3\sim0.4$, a band inversion between L_+^6 and L_-^6 bands (conduction and valence bands) occurs.[65] In contrast to a linear dependence, as one might expect, the constant A decreases sharply until $x = 0.3\sim0.4$, corresponding to the band inversion point, and becomes almost constant at higher SnTe compositions. Since the magnitude of A is attributed to the core-polarization of s-electrons existing near the Mn ions as indicated in eq. (8), this behavior evidently shows that the probability of s-like electron in the valence band is suddenly diminished at

the higher SnTe compositions, corresponding to the change of the inversion of the band symmetry at the L point; namely L_6^+ band is s-like around cations but L_6^- band is p-like (as the s-like electrons of the valence band changes into those of the conduction band, the reduction of A results from core-polarization of both bands). In addition, it is of interest to note that its boundary agrees nearly with the SnTe composition where the conduction type of the carrier is varied from n type to p type as shown before.

Then, the typical ESR spectra of Mn^{2+} in $Pb_{1-x}Sn_xTe$ for Pb-rich side ($0 \leq x \leq 0.4$) at 140 K are shown in Fig. 23. The observed signals consist of not only main six HFS lines, but also additional small lines which do not appear in pure PbTe and the samples with $x > 0.4$. Though it is not clear in these spectra in Fig. 23, the enlarged ESR spectra show that these additional lines are further separated by $\delta H = 10 \sim 15$ G, which corresponds to the forbidden hyperfine transitions of the type $\Delta M = \pm 1$ and $\Delta m = \pm 1$, where M and m are the electronic and nuclear magnetic quantum numbers, respectively.

These additional lines are known to arise from the combination of higher-order effects of two kinds;[66] shifts of order $D^2/g\beta H$, which can be found from the effects of off-diagnal terms on the electronic quadrupole interaction (fine structure) and shifts of order $D^2A/(g\beta H)^2$, which arise from the second order admixtures due to cross product terms in the spin Hamiltonian between the fine structure splitting and hyperfine structure splitting.

Speaking from the results in our $Pb_{1-x}Sn_xTe$ crystals, because of the different lattice constants between PbTe and SnTe host crystals, the mixed crystal has locally non-cubic symmetry from which the above orbital effect (fine structure effect) arises. However, the relation between the band inversion and the higher order signals is not clear.

In conclusion, the ESR measurements of mixed crystals suggest that at the

SnTe composition of the band invertion, the band structure changes from a PbTe-like structure to a SnTe-like one. Similar chemical affinity around the Mn^{2+} ions has been observed in $CdS_{1-x}Se_x$[67;68] and $ZnS_{1-x}Se_x$,[69] for which the anions are alternated. In the case of replacing the cations, on the contrary, the A-x curve is found to be linear as observed in $Cd_{1-x}Mg_xTe$[69] and $Cd_{1-x}Zn_xS$.[70] As is well known, these II - VI semiconductors with a zincblende or wurtzite structure have a wide and direct band gap at the Γ-point in the Brillouin zone and there shows no band inversion accompanied with the alloying of the two components, which is a remarkable contrast to the case of IV-VI semiconductors.

At last, in Fig. 24 and Fig. 25 is shown the g-values of Mn^{2+} spins as a function of the Mn content and the temperature respectively for $Sn_{1-x}Mn_xTe$. In Fig. 24, for comparison, the g-values of Mn^{2+} in PbTe ($Mn \leq 0.06$ at.%) is also shown by the arrows. Within the experimental errors, the g-values for SnTe are almost constant ($g = 2$) over the temperature and Mn content ranges studied. To a good approximation the g-value would be the same as for the free ion. In this view point, Watanabe[71] have suggested that the spin-orbit coupling produces a slight breakdown of LS-coupling, introducing a small admixture of excited state $^4P_{5/2}$ into the ground state $^6S_{5/2}$, but the expected deviation $\Delta g = g - g_s$ is only about -0.0004 for Mn^{2+}. From the same reason as valid for $Sn_{1-x}Mn_xTe$ and $Pb_{1-x}Mn_xTe$ with NaCl structure, a small g-shift may be expected for $Ge_{1-x}Mn_xTe$ with nearly NaCl structure.

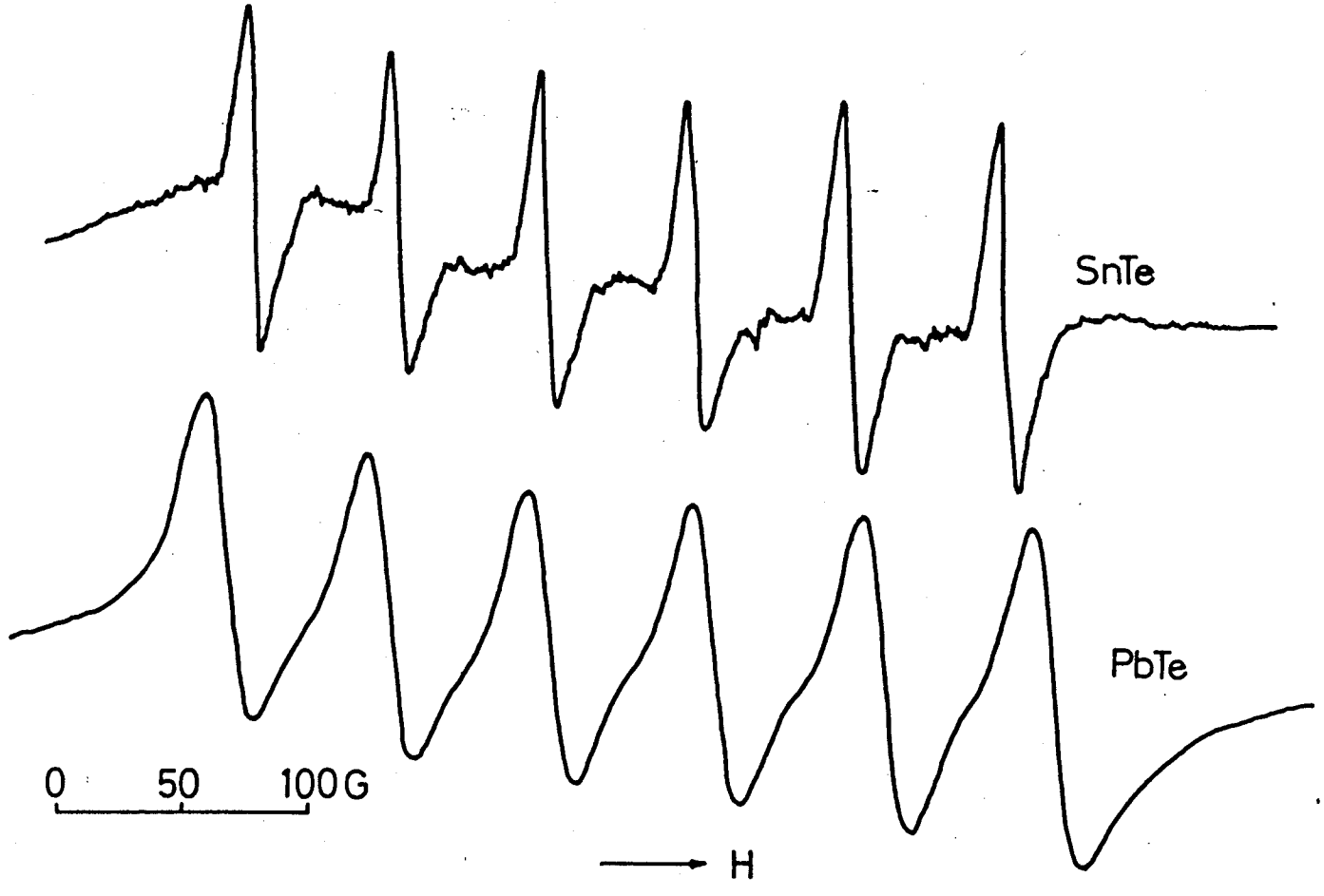

Fig. 20. Hyperfine structure lines at 120 K for p-SnTe (0.04 at.% Mn) and n-PbTe (0.06 at.% Mn).

Table III. Some parameters of the group IV- tellurides: lattice constant a, Phillips ionicity f_i,[8] Debye temperature Θ_D,[57] and hyperfine structure constant A of Mn^{2+}[).]

	a (Å)	f_i	Θ_D (K)	A ($\times 10^{-4}$ cm^{-1})
PbTe	6.462[53]	0.74	135	61.2**
SnTe	6.313[54]	0.61	152	56.0**
GeTe*	5.986[55]	0.62	200	56.2**

* fcc rhombohedral. ** This work

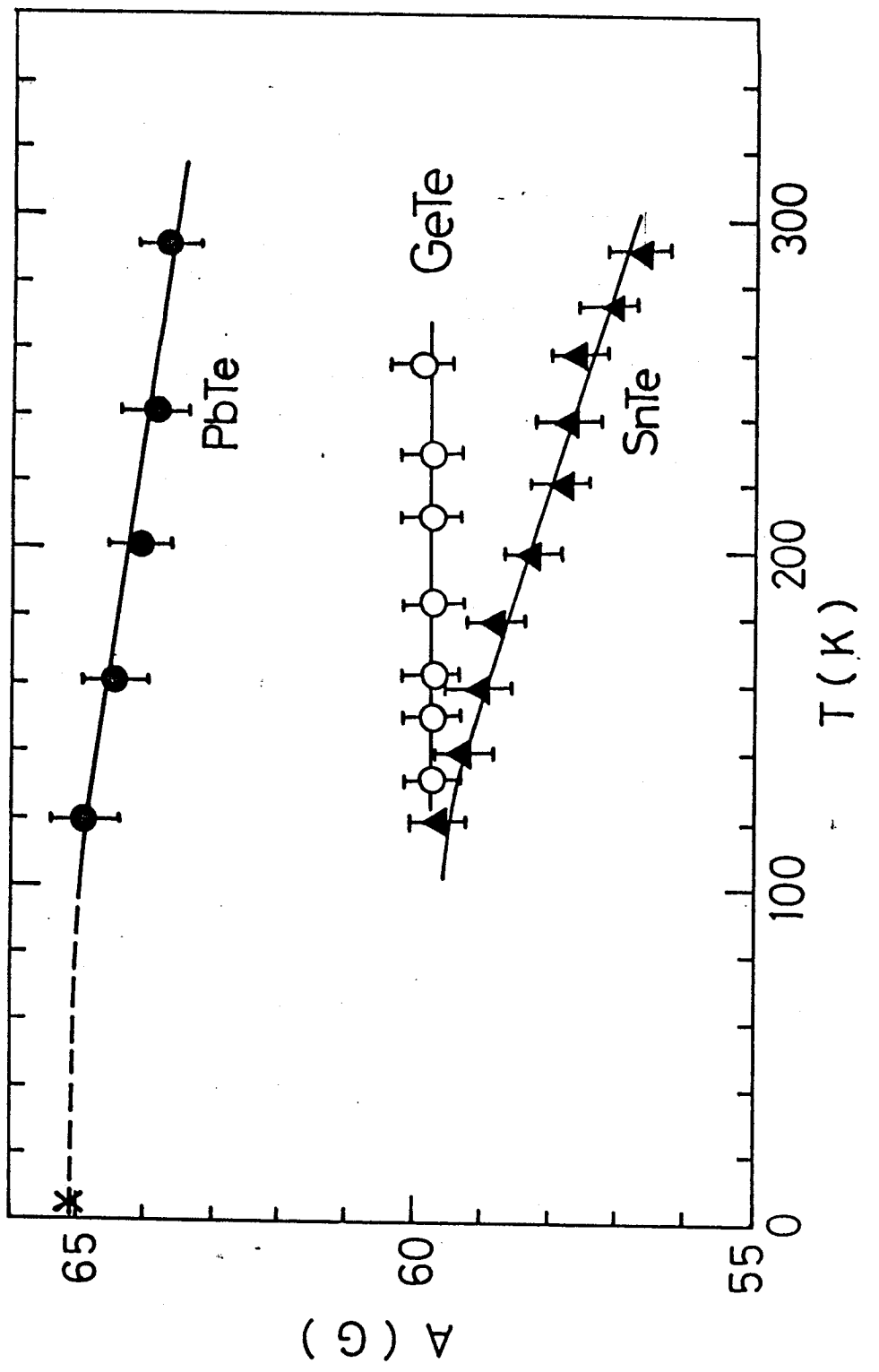

Fig. 21. Temperature dependence of the HFS constant A of Mn^{2+} in GeTe, PbTe and SnTe.

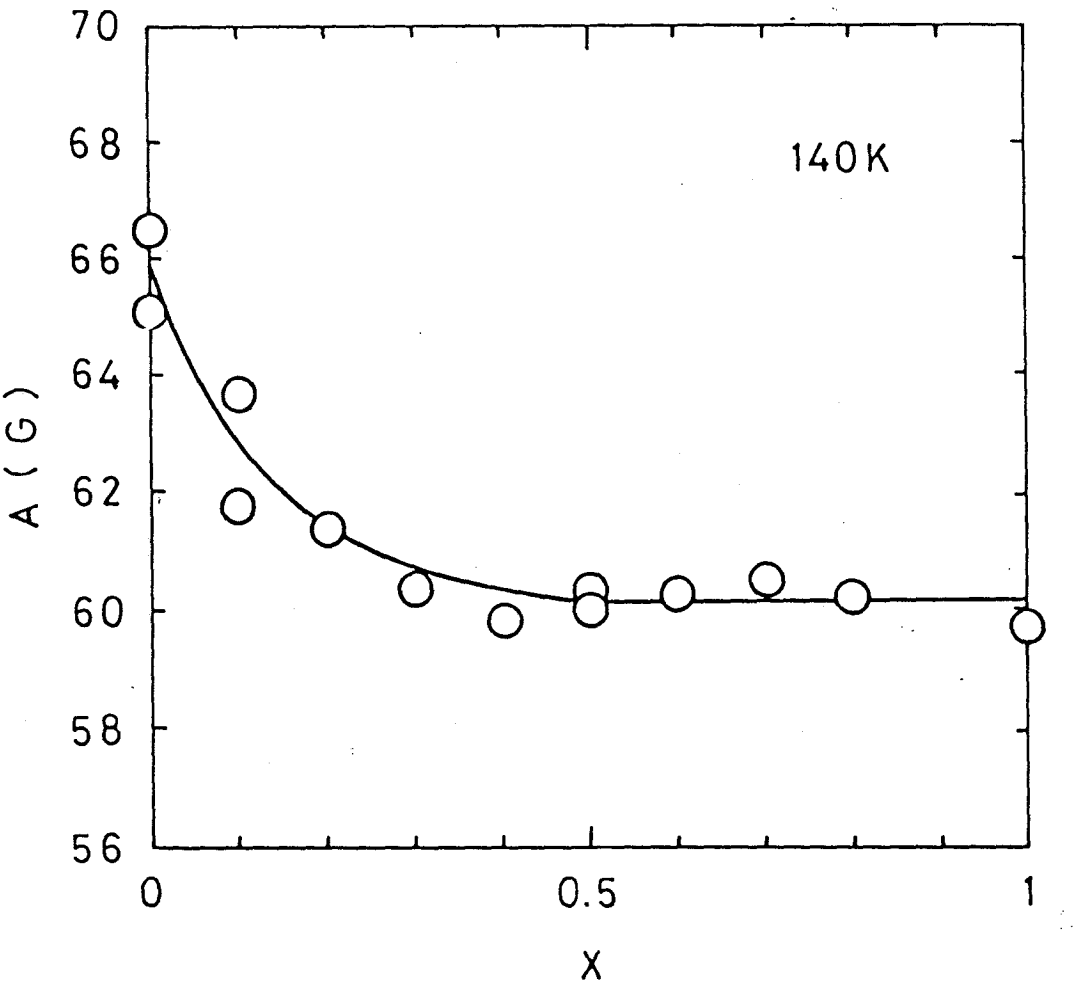

Fig. 22. The composition dependence of the HFS constant A of Mn^{2+} at 140 K in $Pb_{1-x}Sn_xTe$.

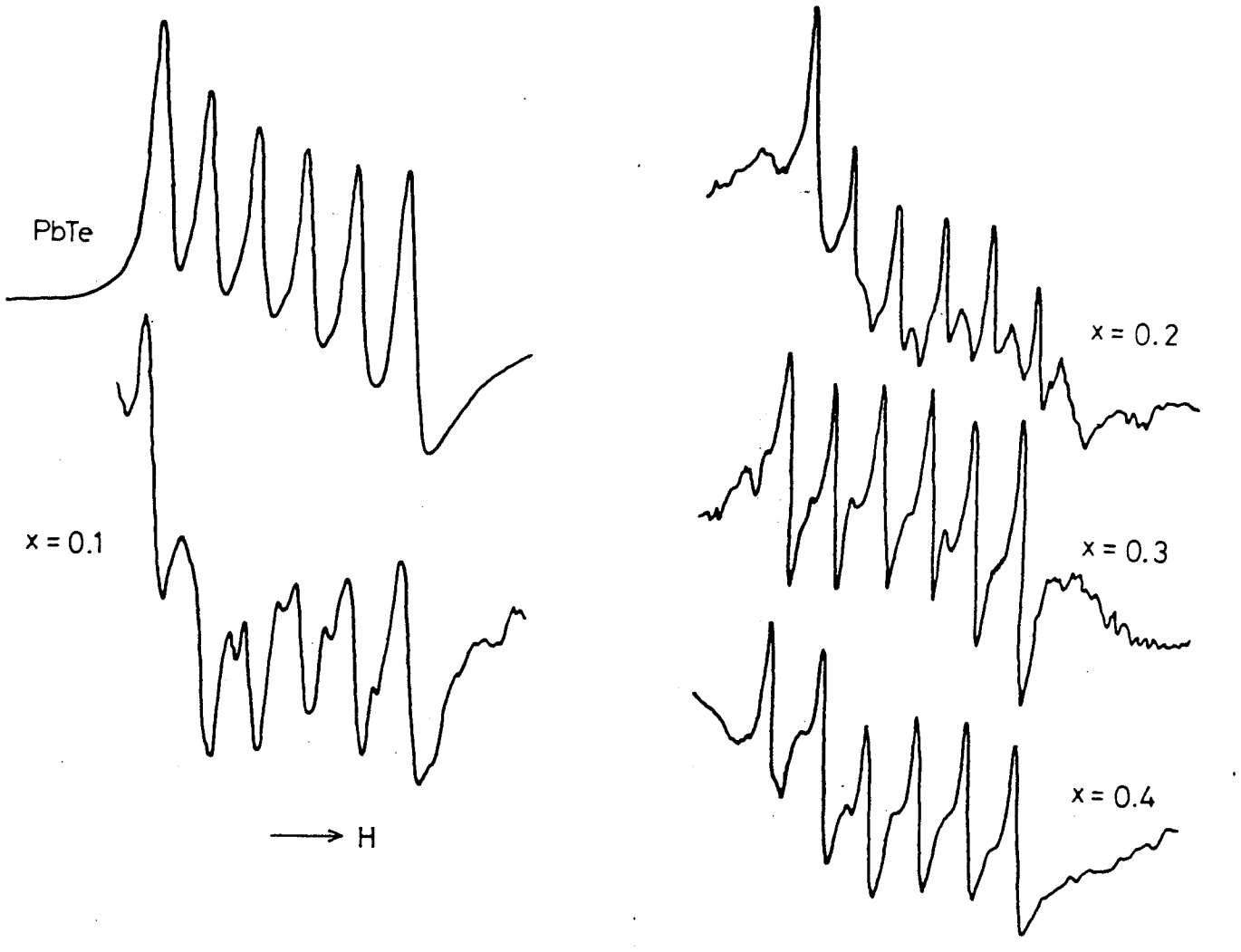

Fig. 23. The ESR spectra of Mn^{2+} at 140 K for $Pb_{1-x}Sn_xTe$ crystals in the Pb-rich side ($x<0.4$).

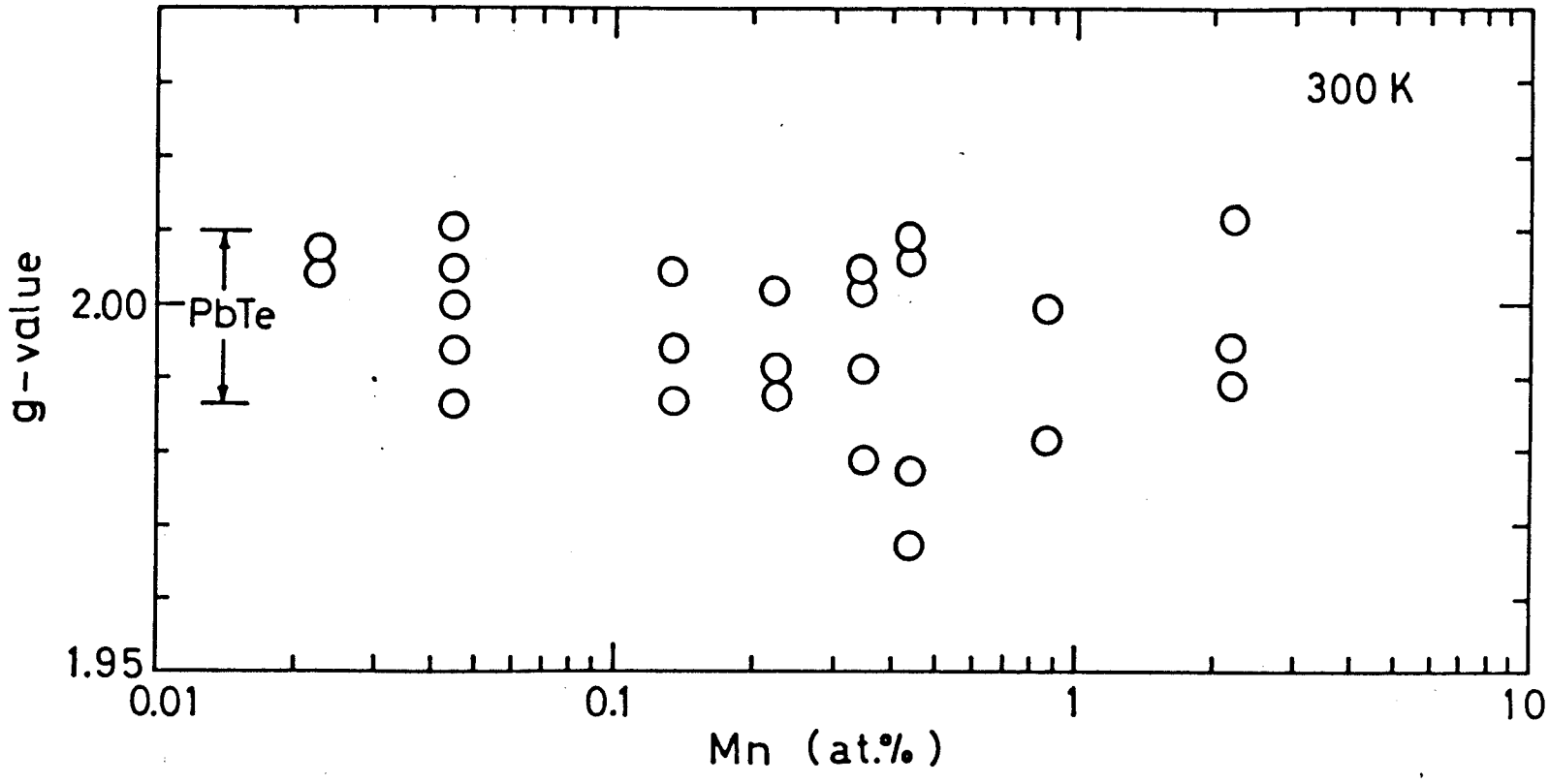

Fig. 24. The g-value of $Sn_{1-x}Mn_xTe$ at room temperature against the Mn content; the values of PbTe are obtained from the HFS-resolved lines of $Pb_{1-x}Mn_xTe$.

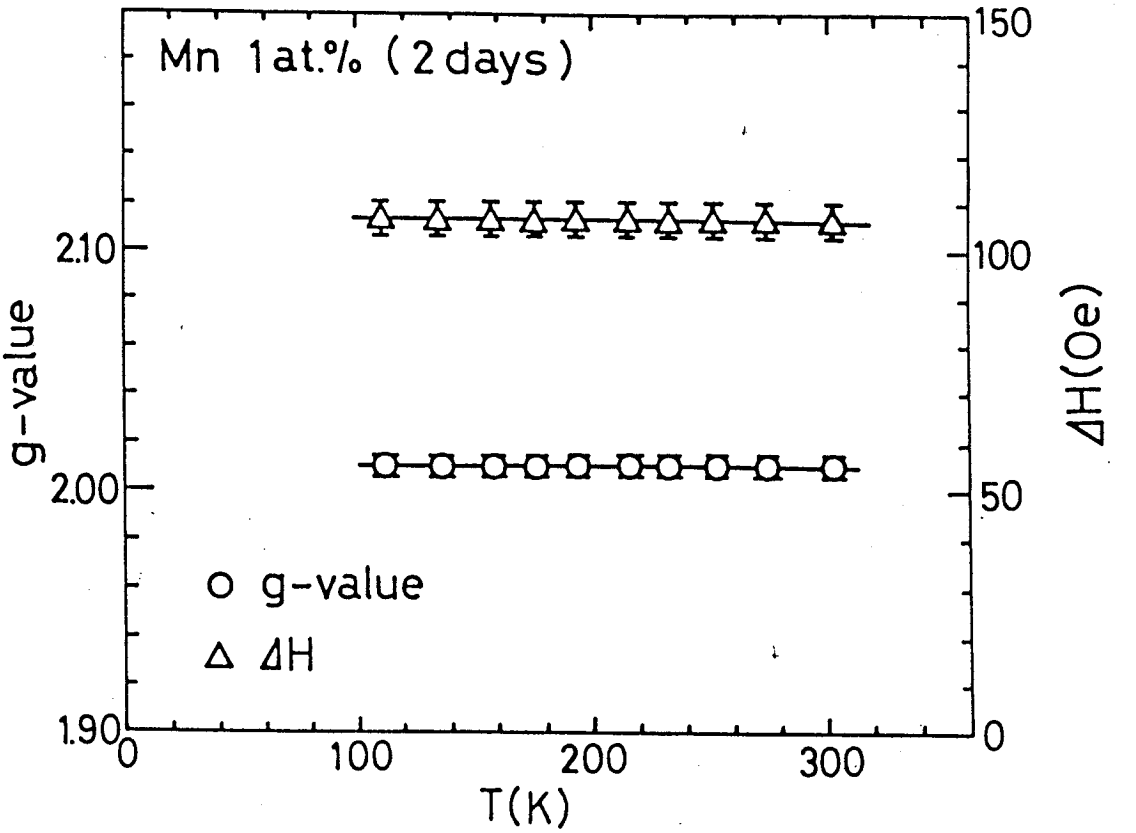

Fig. 25. Temperature dependence of the linewidth and g-value for the annealed $Sn_{1-x}Mn_xTe$ crystal with x=1 at.%.

b) Linewidth of ESR spectrum

(b-i) Mn content dependence

Linewidth of ESR in degenerate semiconductors is mainly caused by the following factors; 1) hyperfine interaction 2) exchange interaction between two spins (included RKKY interaction) 3) relaxation by s-d interaction and 4) dipolar or any other anisotropic interaction of pair spins. Each factor is going to predominant with varying Mn content, and thus ESR measurements are useful method to clarify the magnetic properties of these semiconductors.

Figure 26, 27 and 28 show the ESR linewidths against the Mn contents for $Pb_{1-x}Mn_xTe$, $Ge_{1-x}Mn_xTe$ and $Sn_{1-x}Mn_xTe$, respectively, whose linewidths have similar characteristics. For lower Mn contents less than about 0.4 at.%, the ESR signals of these samples are resolved into six hyperfine structure lines. For Mn contents ranging from 0.6 to 1 at.%, the hyperfine-resolved lines converge to almost a single broad lines whose widths decrease with increasing the Mn contents. For Mn contents higher than 1.2 at.%, the ESR signal merges completely into a single broad line whose width increases with increasing the Mn content.

(b-i)$_{\cdot}$1 Mn content < 0.4 at.%

In this region, the average distance between two spins is more than 20 Å, there is no predominant effect arising from the interaction between two spins. However so-called Kondo state exists in the range of magnetic spin less than about 0.05 at.%, in which ESR signal is small. In Fig. 29 is shown ESR signals of $Ge_{1-x}Mn_xTe$ at various lower Mn contents. The figure suggests that ESR signals less than 0.036 have much less S/N ratio.

On the other hand, ESR linewidth of each hyperfine resolved line itself seems to be independent of Mn content in appearance in this region, but x = 0.36 at.% these lines are assembled on a small base line broadened around g

$\simeq 2$, in contrast to the hyperfine lines for smaller Mn contents. As a result, the hyperfine line is not broadened by the dipolar broadening in usual paramagnetic materials, but rather narrowed to couple to each others by the dipolar interaction and the isotropic exchange of s-d interaction (or RKKY interaction via s-d interaction), and thus the wings of each lines are superposed like a base line which is going to be homogenous by mixing different spin states (spin flip-flop process) with increasing Mn contents.

(b-i).2 0.6 at.% $< x <$ 1.2 at.%

In this region, Mn spins are not localized perfectly but rather interact each others as a long-range indirect exchange. Figure 30 shows the observed ESR spectra at 4.2 K for $Pb_{1-x}Mn_xTe$ with various Mn contents x in at.% units. As the sample has a rather high electrical conductivity, the signals consist of the dispersion part as well as the absorption part. The correct linewidth ΔH was derived from the observed peak-to-peak width ΔH_{pp} according to the procedure developed by Nakamura and Kinoshita.[72] For the sample with x = 0.6 at.%, the HFS-resolved lines converge to almost a single broad line with slightly overlapping of the HFS lines, and the signal lines are Gaussian type whose linewidth is mainly decided by hyperfine width. While, for the sample with x = 0.6 $\sim$ 1.2 at.%, the line shape of spectra vary gradually from Gaussian type to Rorentzian one with increasing Mn content.

The linewidth narrowing with increasing Mn content at this region (shown in Figs. 26, 27 and 28) is attributed to the exchange narrowing accoding to the isotropic exchange interaction. The problem of the shape of an exchange-narrowed line has been studied in more details by Anderson, using a mathematical model in which the dipolar interaction is assumed to produce a Gaussian distribution of internal fields and, in addition, this field is time-modulated in a random way.

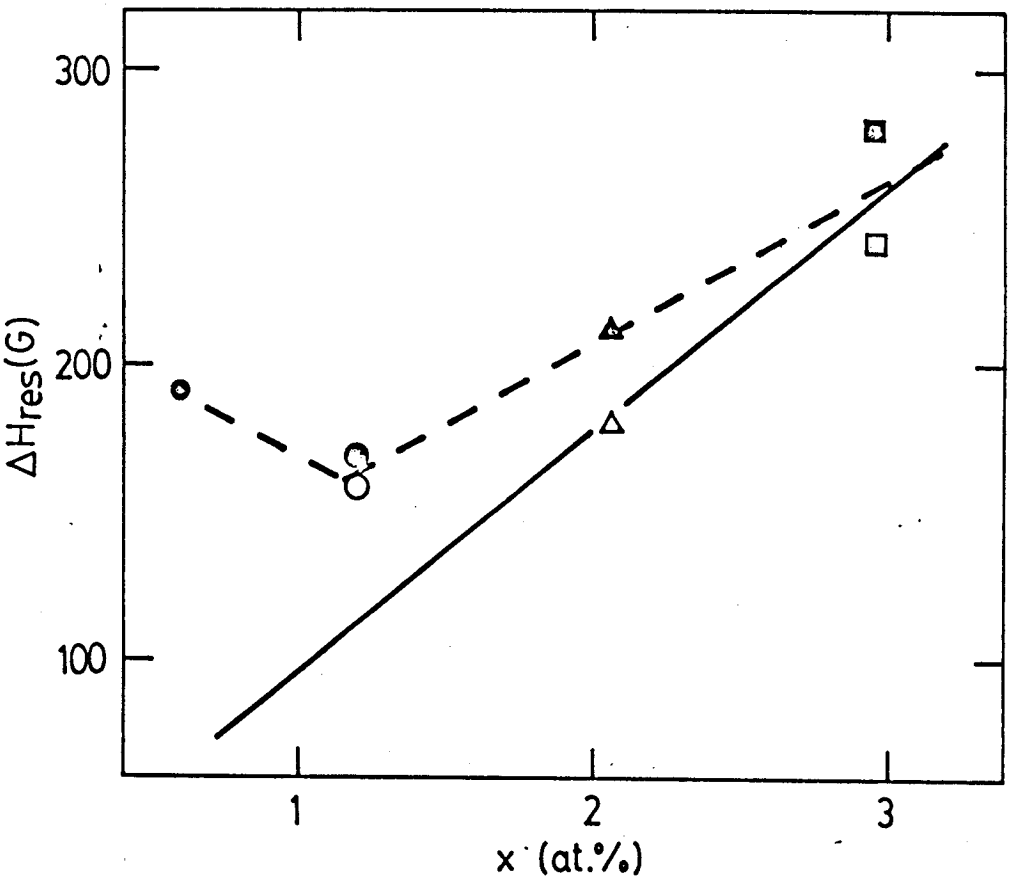

Fig. 26. Mn content dependence of the residual linewidth for $Pb_{1-x}Mn_xTe$. The solid line is caculated by eq.(11) according to the simplified dipole-dipole broadening method.

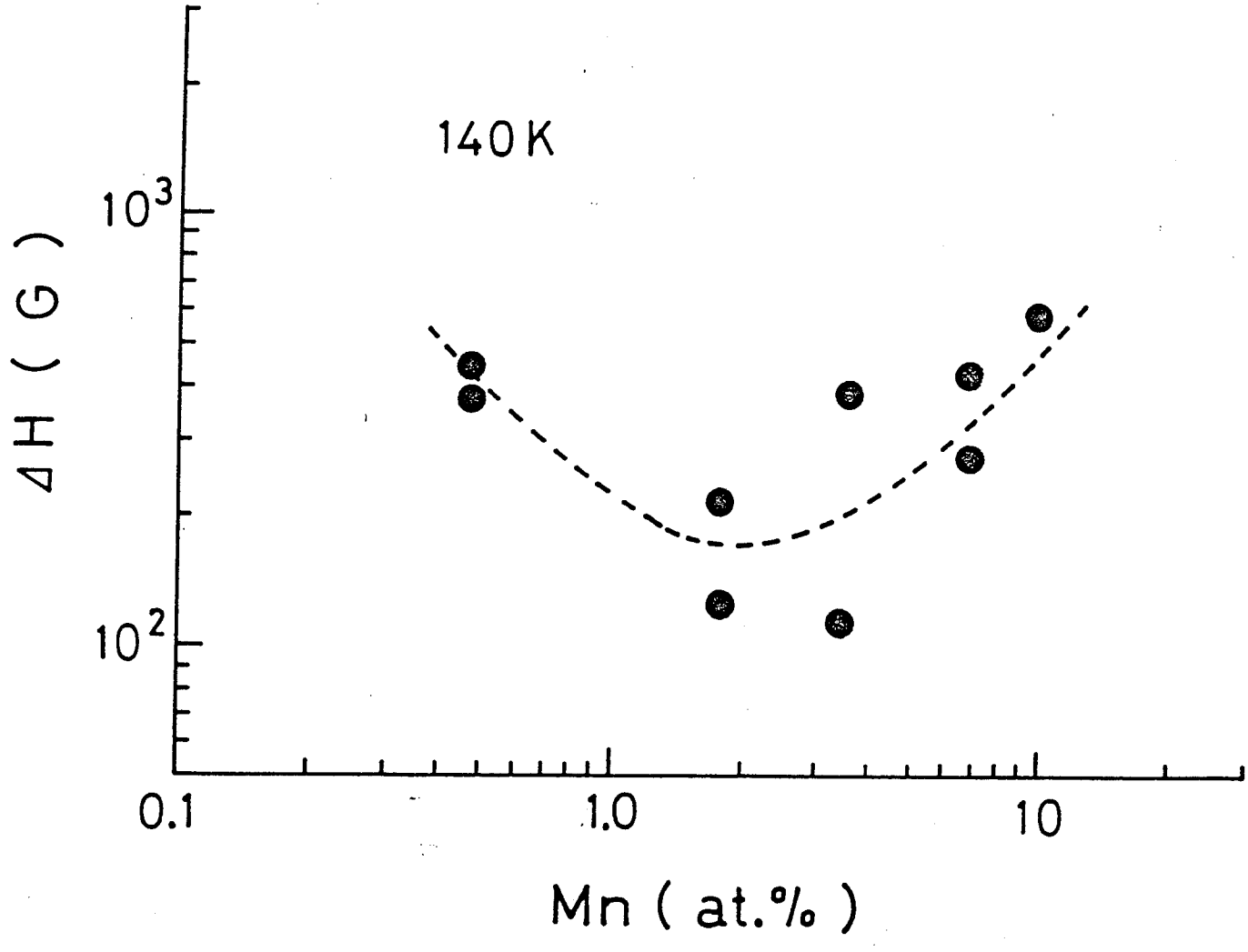

Fig. 27. ESR linewidth ΔH at 140 K vs nominal Mn content in GeTe.

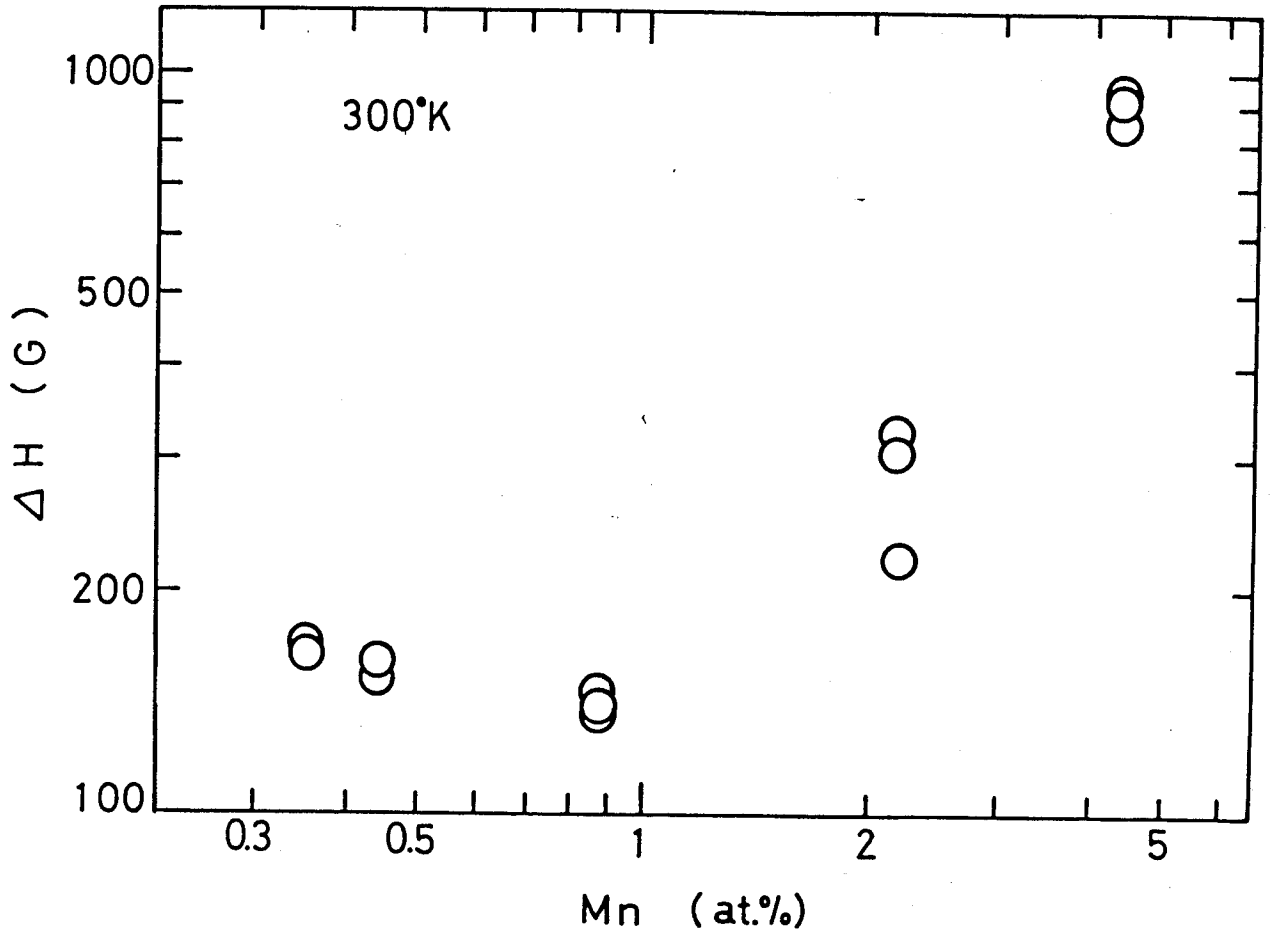

Fig. 28. ESR linewidth ΔH of SnTe at room temperature against the nominal Mn content.

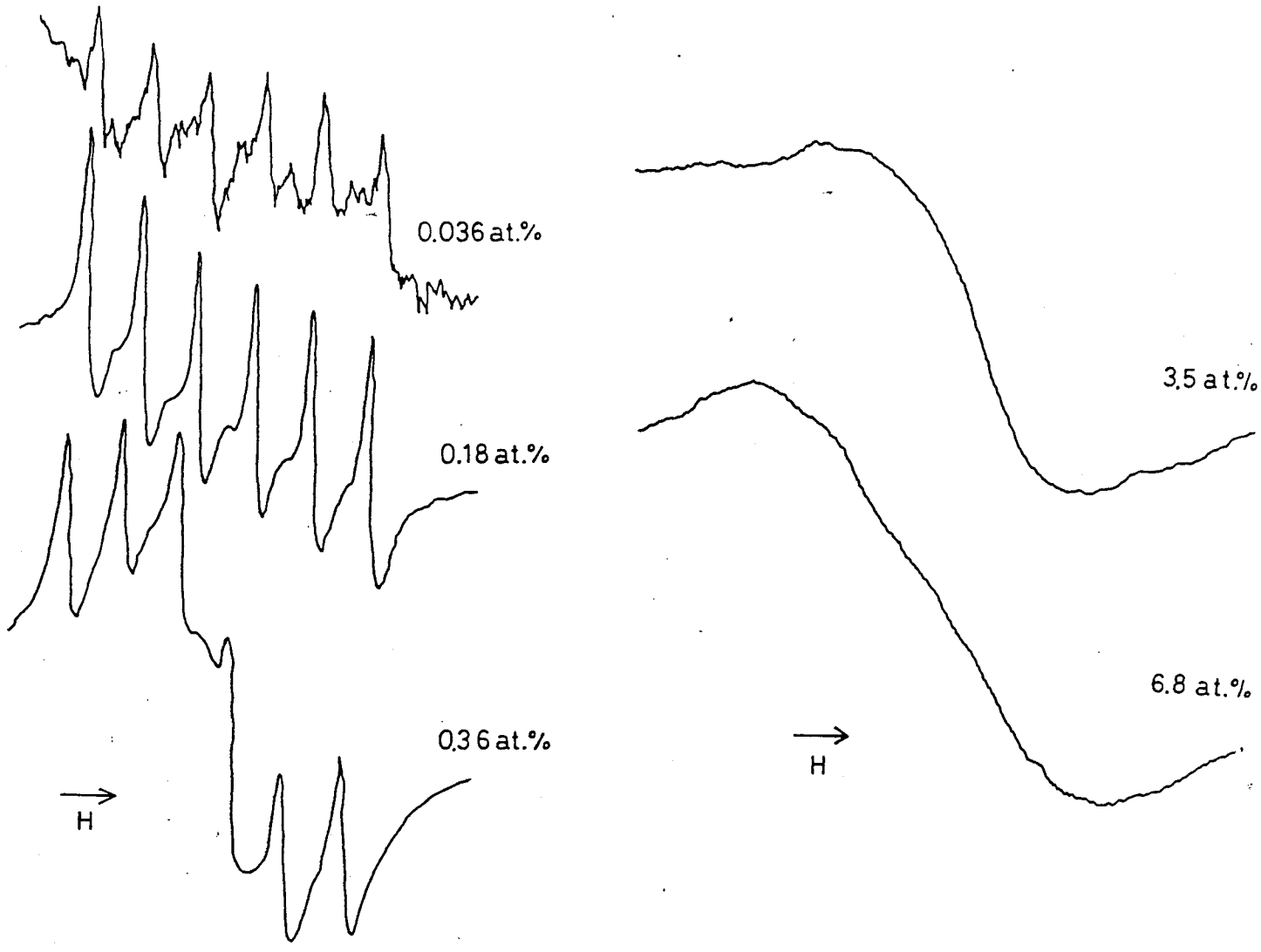

Fig. 29. ESR signals at 140 K for GeTe with various Mn contents.

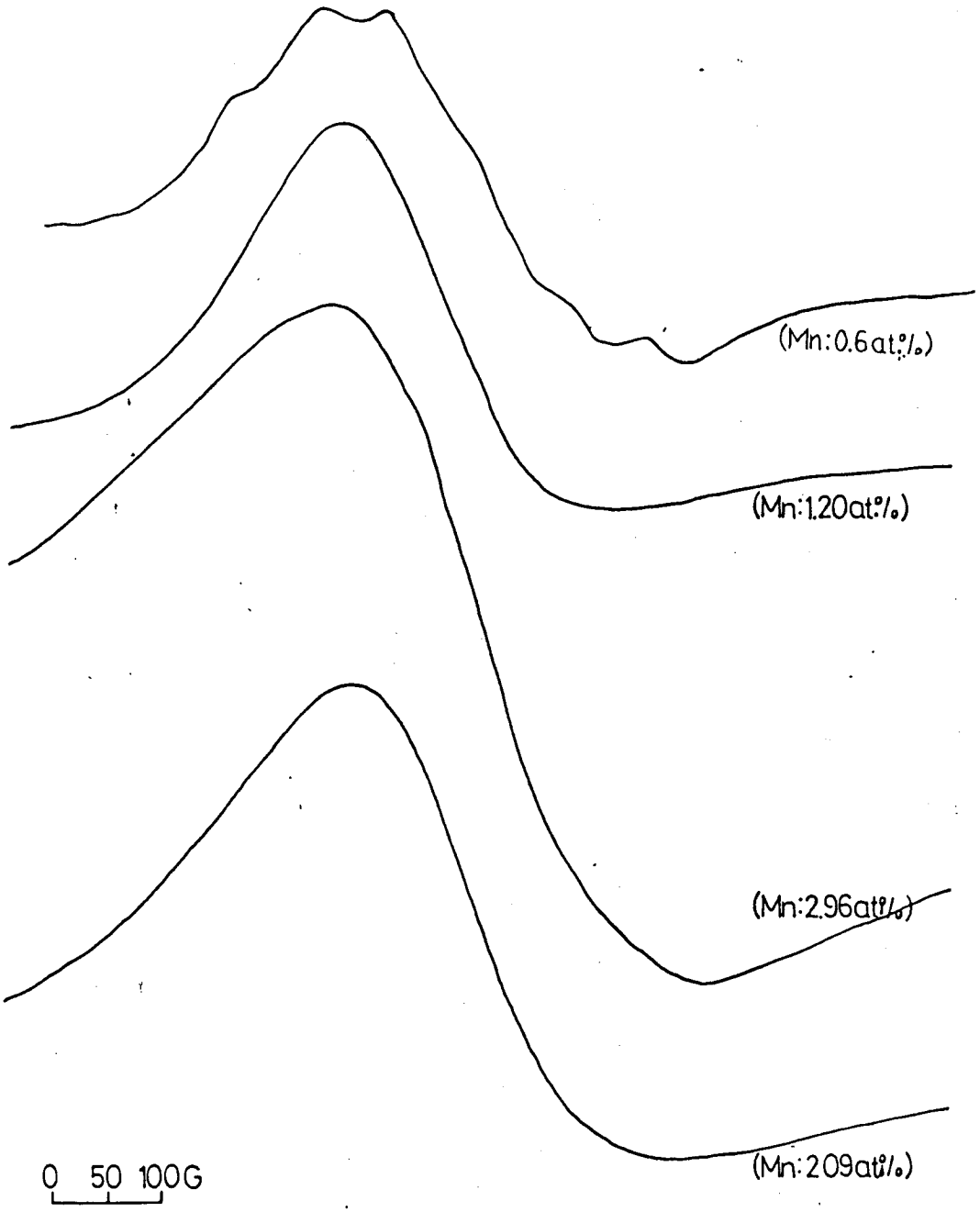

Fig. 30. ESR signal spectra at 4.2 K for $Pb_{1-x}Mn_xTe$ with variuos values of x.

In the case of a pair of dissimilar ions which have a different g-values or different hyperfine field, the spectral intensity for a pair of lines is expressed as a function of the ratio of exchange frequency ω_e to splitting frequency ω_0 between different resonances.

$$I(\omega) = \frac{8\,\omega_e^3\,x^2}{\omega^4 + 2\,\omega^2\omega_e^2\cdot(2 - x^2) + \omega_e^4\cdot x^2} \quad , \tag{10}$$

and $\quad x = \omega_e/\omega_0$,

where $I(\omega)$ is the spectral intensity at frequency ω. According to eq. (10), the spectral line is two different functions at $x = 0$, and these lines merge into a single line through the exchange interaction with increasing x, as shown in Fig. 31.

Applying the relation between hyperfine field and exchange interaction to eq. (10) for 1 at.% of Mn content, the effective exchange interaction between two spins through s-d interaction J_{eff} is given by about 0.06 eV, which may be reasonable value for these samples. In practice, for $Sn_{1-x}Mn_nTe$ and $Ge_{1-x}Mn_xTe$, J_{sd} was obtained from magnetization measurements by Cochrane et al.[24] and its values are about 1 eV which is very close to the values for dilute alloys such as Cu;Mn[74,75] and Cu;Cr.[76]

However, the other results from temperature dependent linewidth of ESR for $Pb_{1-x}Mn_xTe$ and $Sn_{1-x}Mn_xTe$ have shown that the J_{sd} is the order of 0.07 and 0.1 eV,[22,25] respectively as will be described in details later. Moreover, J_{sd} expected from transport results by Cochrane is about 0.01 eV. For this disagreement between the transport and the other measurements Cochrane[25] suggested that the transport measurements are more sensitive to the combination of the potential scattering with the spin one than other measurements. While, the difference between magnetization results and the temperature dependent ESR linewidth results may be arised from the symmetric properties of the carrier interaction with Mn spin through the exchange interaction. The

mobile carriers in the degenerate magnetic semiconductors exist in mixed state of s-state and non-s-state (mainly p-state) due to the same reason as discussed in AHE previously.

Since the temperature-dependent ESR linewidth is mainly due to the spin-lattice relaxation coupled with phonon, this relaxation effect depends tightly on the spin-orbit interaction. As a result, J_{sd} obtained from the temperature dependent ESR seems to express the exchange interaction Mn spins and non-s-state carriers which have orbital momentum. While, J_{sd} estimated from Curie-temperature of magnetization measurements, can be attributed not only to the non-s-state carriers but also to-the s-state carriers, for which J_{sd} may be obtained as rather larger value even for the small probability of s-state because of its symmetry.

In conclusion, the various experimental J_{sd} values are attributed to the different parts of s-d interaction concerned with experimental method.

(b-i).3 Mn > 1.5 at.%

In this Mn content region, the direct interaction between two spins becomes considerable strong and especially, for more than 2 at.%, various types of clusters seem to exist. In practice, for degenerate magnetic semiconductor, our various transport results show the existence of spin-dependent scattering such as Kondo effect, in wide ranges of Mn contents 0.02 $\sim$ 10 at.%. Moreover, for the degenerate magnetic semiconductors at this region of Mn contents, various types of magnetism exist at the same time, though the ESR results are relatively simple.

As shown in Figs. 26, 27 and 28, for all the samples with Mn contents of this ranges, ESR linewidth increases linearly with increasing the Mn content. ESR line shape is going to be Gaussian type from Lorentzian type. The line broadening is attributed to the off diagonal terms of non-isotropic interactions such as dipole-dipole or other anisotropic interactios of paired spins.[77]

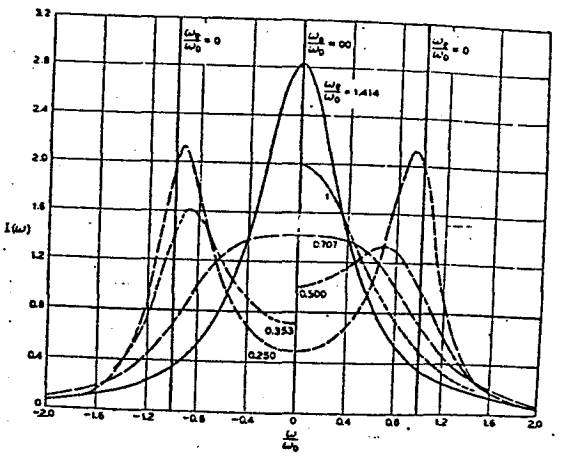

Fig. 31. Spectral intencity for a pair of lines with the ratio ω / ω_0 of jump-rate to splitting as parameter [from P. W. Anderson ,J. Phys. Soc. Jpn. 9 (1954) 316].

According to the second moment method developed by Van Vleck, the dipole-dipole linewidth[78] is expressed by

$$\Delta H = 2.35 / g\beta \{ 1/3\ S(S+1)\Sigma\ B_{jk}^2 \}^{1/2}, \qquad (11)$$

$$\text{with} \quad B_{jk} = (3/2)\ g^2\ \beta^2\ r_{jk}^{-3}\ (\ 3\cos^2\theta_{jk} - 1\ ),$$

where β is the Bohr magneton, S the spin quantum number, r_{ik} the distance between the two spins at the j-th and k-th sites and θ_{jk} their angle. The experimental values are in good agreements with those calculated, where the Mn impurity distribution is assumed to be in the cubic PbTe host lattice with $\Sigma\ 1/r_{jk}^6 = 8.5/d^6$ (d = average distance between Mn atoms) and with the angular average $\langle(3\cos^2\theta_{jk} - 1)^2\rangle = 4/5$ for powdered samples (see Fig. 26).

However, for the experimental values, there are contributions of other anisotropic interactions as well as dipolar interactions such as pseudodipolar exchanges,[79] or more higher order terms of virtual phonon exchanges,[80] anti-symmetric exchanges,[81] and electric quadrupole-quadrupole interactions.[82] The total Hamiltonian $\mathcal{H}$ (included dipolar interaction) is expressed by the following form[77] similar to the dipolar Hamiltonian.

$$\mathcal{H} = D_e\ (3S_{1z}S_{2z} - S_1S_2), \qquad (12)$$

$$\text{with} \quad D_e = D_d(\text{dipolar}) + D_p(\text{pseudodipolar})$$

$$+ D_{other}(\text{effect of higher degree terms}).$$

Here the interactions in eq. (12) show characteristic angular dependent term of two spins and D_d, D_p, D_{other} are shown by the bracket terms. In our experiment, the linewidth from the calculation is about 50 Gauss for the linewidth caused by the higher order terms ($D_p + D_{other}$) for the samples with $x = 2 \sim 3$ at.%.

(b-ii) Temperature dependence of linewidth

Figure 32 shows the temperature dependence of the linewidth ΔH for $Pb_{1-x}Mn_xTe$ with different values of x. For $x < 1.2$ at.%, ΔH first deceases with decreasing temperature and then becomes constant at the low temperature side. On the contrary, ΔH for $x > 2$ at.% is almost constant in the high temperature region down to 77 K and then increases with further decreasing temperature. The increase of ΔH at the low temperature side is attributed to a magnetic ordering effect, similar to the cases for $Sn_{1-x}Mn_xTe$ and $Ge_{1-x}Mn_xTe$.[24,25]

Now let us consider the case of a set of impurities interacting with the conduction electrons in the metallic material through the s-d interaction. The s-d interaction Hamiltonian can be written as[26]

$$\mathcal{H}_{sd} = -\sum_{kk'n} J\{\exp i(k-k')R_n\}\cdot\{(c^+_{k\uparrow}c_{k'\downarrow} - c^+_{k\uparrow}c_{k'\downarrow}) S_{nz} + c^+_{k\uparrow} c_{k'\downarrow}S_{n-} + c^+_{k\downarrow}c_{k'\uparrow}S_{n+}\} , \quad (13)$$

where c^+_{ks} and c_{ks} are the creation and annihilation operators of the electron with the wave vector k and the spin s, and R_n represents the location of the n-th impurity atom with the spin of S_n. In this case, J denotes average of various exchange integrals. Equation (13) is of the same form as the Fermi interaction among the nucleus in a metal with degenerated electrons.[83] The analogy of the present case with the NMR one is exact by replacing S by I and J by A, so that the following form for the Knight shift proportional to $J\cdot N(0)$ and the Korringa relaxation of the form[84] can be applied to the present case;

$$\Delta H \propto 1/T_1 = (4\pi/\hbar)\, J^2\cdot N^2(0)\, kT , \quad (14)$$

where N(0) is the state density of the Fermi level at absolute zero temperature.

For degenerate magnetic semiconductors, Toth et al.[22] and Cochrane et al.[25] have shown that the temperature dependence of ESR linewidth agrees with the expression of eq. (14). They obtained the conclusion from their ESR

results in which the s-d interactions J_{sd} are the order of 0.1 eV, previously. Our results for lower Mn content similrarly show the temperature dependence obeying the Korringa type relaxation of eq. (14).

In addition, it is interesting to note that the temperature dependence of ΔH for low Mn density resembles very closely to the temperature variations of the PbTe band-gap, E_g, which is effectively constant ($\sim$0.18 eV) up to 50 K, beyond which the gap increases with temperature.[23] This effect shows that a Korringa relaxation arises from a ℓ-s coupling related to the band gap.

In our system of $Pb_{1-x}Mn_xTe$, the g-value of Mn d spins, g_d, was found to be 2.00 ± 0.03 in the temperature range of the measurements and for the Mn contents studied, while the g-value of carrier, g_c, is known to be larger (= $7 \sim 57$) because of the spin-orbit interaction.[1] Thus, as pointed out by Toth et al.,[22] these two systems of spins with quite different g-values can not give rise to the bottleneck effect, because the two different momentum suppress spin flip terms such as $c^+_{k\downarrow}c_{k'\uparrow}S_{n+}$ and $c^+_{k\uparrow}c_{k'\downarrow}S_{n-}$ in eq.(13); these different two systems at the individual Lamor frequencies in an applied magnetic field. Cosequently, the spin-lattice relaxation arising from scalar interaction (spin-flip type) causes a phonon absorbtion with the energy of $\hbar(\omega_d - \omega_c)$, where ω_d and ω_c are the Lamor angular frequency of the magnetic d spin and carrier spin, respectively. This phonon absorbtion together with an energy transfer to phonon from spin system is mainly attributed to spin-lattice interaction through an ℓ-s coupling.

In general, for any narrow gap semiconductors, it may be expected a strong temperature-dependent linewidth since the mobile carriers stay in the orbital state (mainly the p-state) as well as the s-like state.

However, in our results as shown in Fig. 32, ΔH shows scarcely temperature dependence and thus is little attributed to the Korringa relaxation for high Mn contents.

In addition, from the magnetic susceptibility measurement by Cochrane et al., J_{sd} is the order of 1 eV for $Ge_{1-x}Mn_xTe$ or $Sn_{1-x}Mn_xTe$, and the value disagrees with that obtained from the temperature dependence of ESR. Moreover, the temperature (or relaxation) coefficient B {= d(ΔH)/dT} for $Pb_{1-x}Mn_xTe$ varies with the Mn content as shown in Fig. 33.

The relaxation coefficient first decreases with increasing Mn content up to about x = 1.5 at.% and then becomes vanishingly smaller at higher contents. Such a tendency of the relaxation coefficient is in a good agreement with those found in the dilute alloy system of Cu;Mn[85] and can be attributed to the bottleneck effect . The spin-lattice relaxation time T_1 and thus ΔH due to the bottleneck effect can be written as[86]

$$\Delta H \propto T_1^{-1} = 3/2 \{ N(0) \cdot kT / S(S+1) \cdot C \} T_{sl}^{-1} , \qquad (15)$$

where C is the magnetic impurity density, S the impurity spin, T_{sl} the spin-lattice relaxation time of the conduction electrons and N(0) the carrier concentration per atom at absolute zero degree. According to eq. (15), the relaxation coefficient is proportional to 1/C. The present result shown in Fig. 33 well follows the theoretical consideration.

In general, when the bottleneck effect is effective,[86] the g-value of the impurity spins g_d is nearly equal to that of the carriers spins g_c where both spins couple and move together in the applied magnetic field, because of the existence of the first order spin flip-flop interaction $S^{\pm}s^{\mp}$, here $s^{\pm}$ is the up or down operator of the carrier spin; in this case the temperature and spin density dependence of the g_d values are small, in an agreement with our observation as shown in Figs. 21 and 22.

For the predominance of the bottleneck effect in our system, the following are to be noted. 1) As has been shown in Figs. 26, 27, and 28, the linewidth ΔH in degenerate magnetic semiconductors has a contribution

from exchange narrowings in the Mn content ranging from 0.5 to 1.5 at.%. The presence of the exchange narrowing indicates that there is an isotropic exchange coupling between the localized and itinerant carriers with nearly equal g-values. 2) The magnitude of the spin-orbit interaction for the L_6^- band (conduction) or L_6^+ band (valence) of PbTe is in the range 0.1 ∿ 1 eV,[1,2] which is of the same order of magnitude as the s-d exchange interaction $J_{sd} \simeq 1$ eV or smaller. 3) The s-d exchange interaction is proportional to the overlapping between a localized d-state of the Mn ion (^6S) and an s-state of the itinerant carriers and it should become large for those carriers that have zero orbital angular momentum, although there are carriers with differrent orbital states (p-, d-, ···) arising from the spin-orbit mixing as described above. Thus the carriers with $g_c \simeq 2$ existing near the Mn ions contribute to the ESR linewidth. 4) For example, L_6^+ band is intrinsically s-like around cation Pb site, even if L_6 bands are formed by a linear combination of atomic p-states. Thus the holes in L_6^+ band with the compensatory concentration of the same order as that of the electron in L_6^- for PbTe, have a small ℓ-s coupling and a small g-shift. 5) As shown in a previous section, such a proximity effect is known in the theory of the anomalous Hall effect for magnetic metals and alloys, in which itinerant carriers are imagined to have an orbit around the magnetic ion concerned with the mixed spin-orbit coupling effect.

Therefore, it is expected that the spin coupling between the Mn spins of carriers that come close to the Mn ions is strong enough to produce the bottleneck effect: This coupling may be the same type as that in the Anderson mixing system[87] in dilute alloy.

On the other hand, from the view-point of the spin relaxation mechanism for the bottleneck system, a spin-lattice relaxation through carrier spins is attributed to the off-diagonal terms of the spin-spin interaction matrix

Hamiltonian such as $S^- s_z$ and $S^- s^-$ because of $\omega_d = \omega_c$. However, in these cases of the predominant scalar type s-d interaction, the spin-lattice relaxation through the carriers is very small, because these off-diagnal terms do not exist in the first order approximation. The above effect appears in the temperature-independent linewidth for Mn > 2 at.%, in which ΔH is attributed to a direct anisotropic interaction as expressed in eq. (12).

As a result of the Mn content dependence, the ESR linewidth in these crystals with x < 2 at.% is mainly attributed to the s-d interaction and for x > 2 at.% a direct exchange is assumed, thus we arrived at the same conclusion as in the transport measurement.

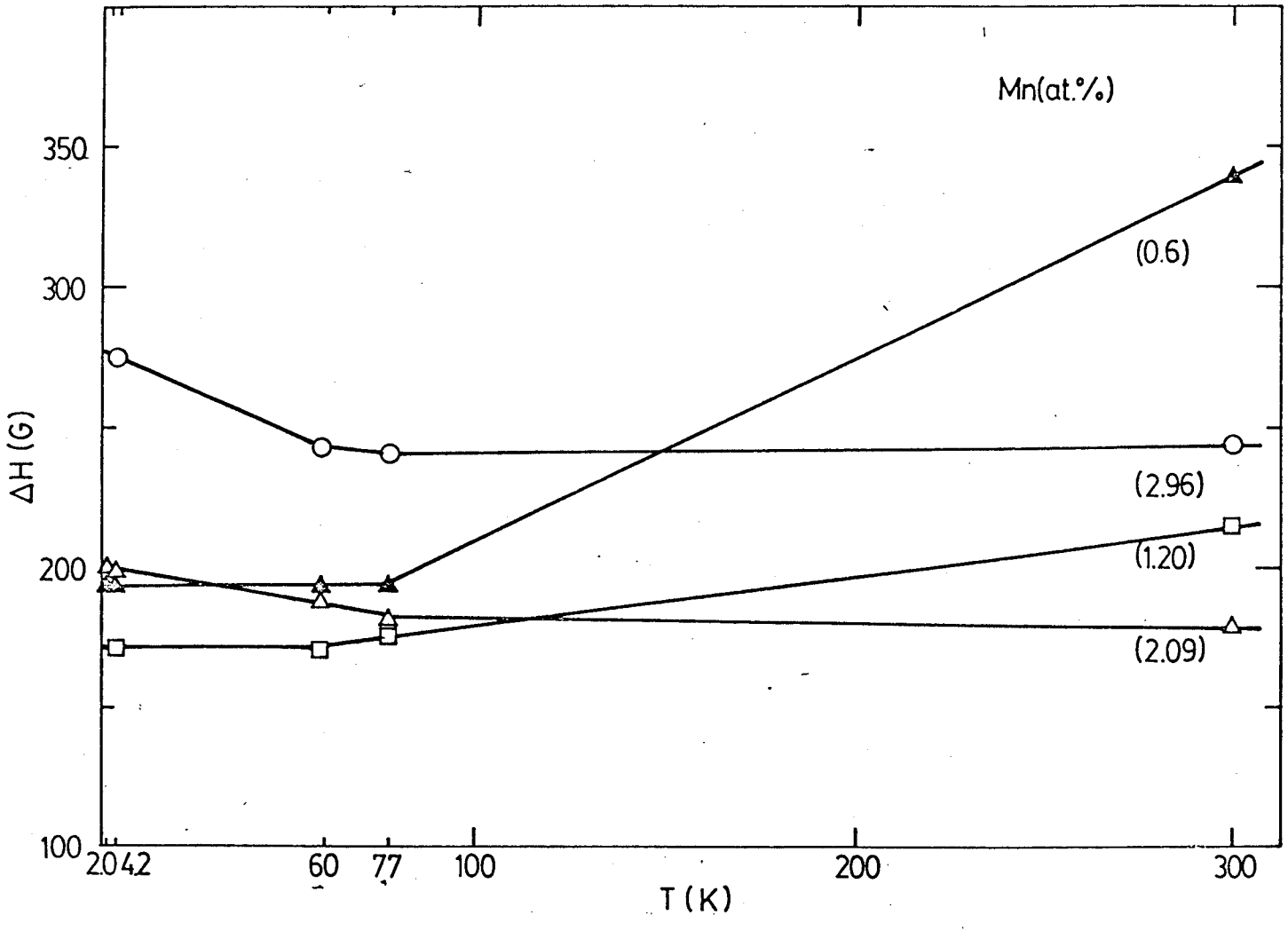

Fig. 32. Temperature dependence of the linewidth for $Pb_{1-x}Mn_xTe$ with various values of x.

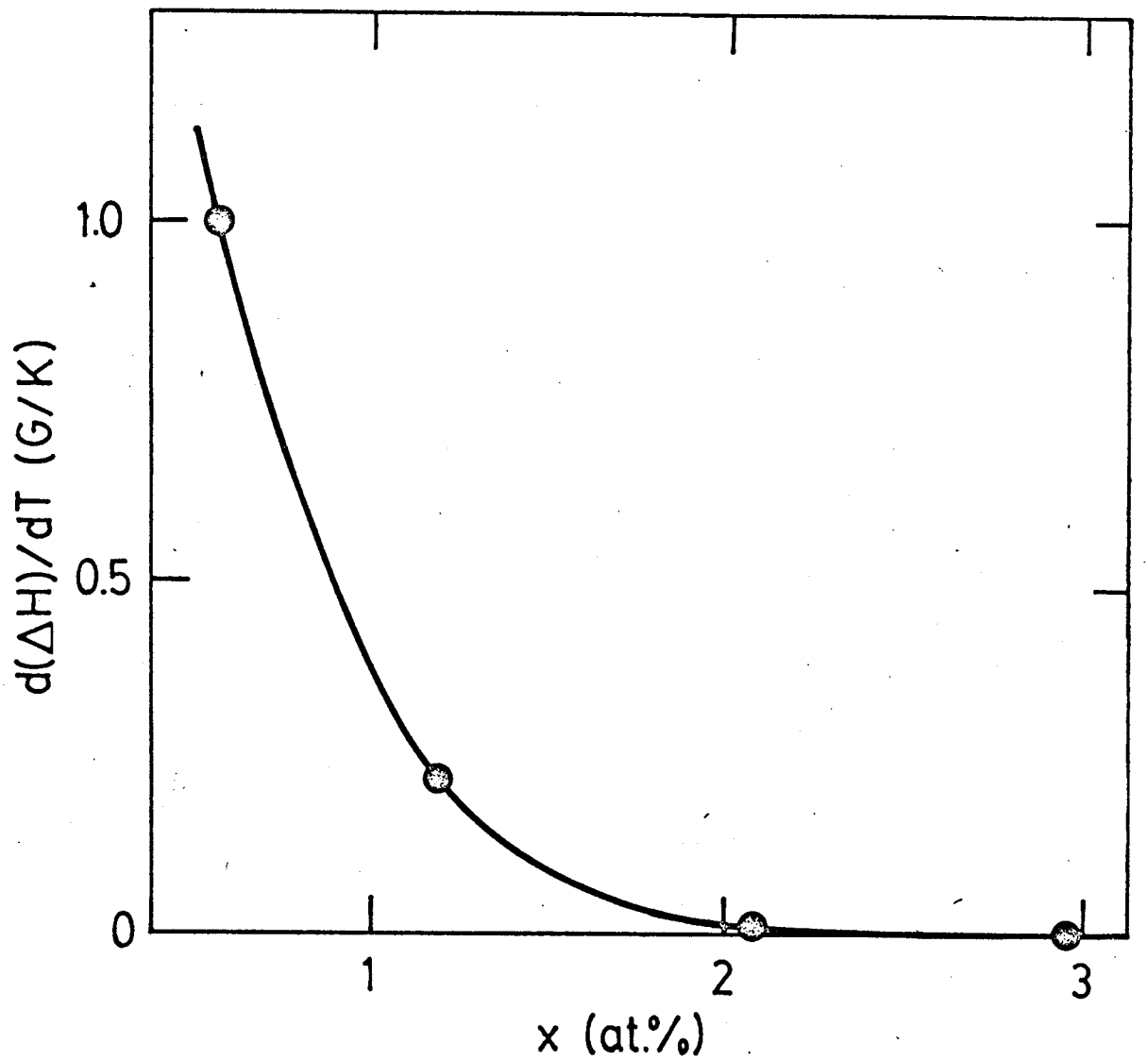

Fig. 33. Korringa-type relaxation coefficient of $Pb_{1-x}Mn_xTe$ against Mn content.

(b-iii) The other results of ESR linewidth

The temperature dependeces of the ESR linewidths for degenerate semiconductors also given us another information concerned with the phase transition. For examples, a ferroelectric phase transition and a magnetic order-disorder transition can be studied by the ESR measurements. In these cases, ΔH is often going to broaden near the critical temperature T_c because of the fluctuations of the order parameter which affects the spin relaxation. If the origin of the manifested in the linewidth of the ESR spectrum is the same as that of the fluctuation in the lattice polarization, then the linewidth variation can be related to the fluctuation of the polarization and then the linewidth will be generally given by

$$\Delta H \propto (T - T_c)^{-p} , \qquad (16)$$

where the exponent p determined experimentally shows a good agreement with theoretical one suggested as various values by many investigators.[88-90]

On the other hand, it has been shown that the degenerate semiconductor SnTe is a "near ferroelectric" material and there is an analogy between SnTe and a perovskite ferroelectric insulator, such as $SrTiO_3$, $BaTiO_3$,[91] etc. Both of them show the ferroelectric phase transition[92,93] at an well each defined critical temperature T_c. The mechanism governing the ferroelectric phase transition of SnTe is the electron-transverse optical phonon interaction, as was first proposed by Kristoffel and Konsin.[94] Because of this unusual characteristic, SnTe has been of current interest both theoretically[95] and experimentally.[11,92] The ferroelectric phase transition has been investigated by means of the neutron scattering,[93] the Raman scattering,[92] the X-ray diffraction,[96] the Hall mobility,[97] the de Hass-van Alphen effct,[98] and the resistivity measurements.[11]

Now, we report the first ESR study of SnTe doped with Mn and Cr which

serves as a probe for the ferroelectric phase transition study. Figures 34 and 35 show the temperature dependences of ΔH for ESR of $Sn_{1-x}Cr_xTe$ and $Sn_{1-x}Mn_xTe$, respectively. For both the samples, ΔH or Δg show anomalous changes caused by lattice-instability at displacive structural phase transition temperature T_s,[99] $70 \sim 80$ K.

Near the phase transition temperature T_s the linewidth increases in proportion to $(T_s - T)^{-1/2}$, in agreement with the Landau theory[100] of a second-order phase transition with $p = 1/2$ in eq.(16); in this theory the fluctuations in the lattices around the ions give rise to the fluctuations in the resonant magnetic field. Also the changes in the linewidth are associated with those in the spin-lattice relaxation time near T_s, since the magnitude of the relaxation time is essentially dependent on the strength of the coupling of the spin system to the crystal lattices. Moreover, through the changes in the effective distance between the ions (and thus exchange interactions) as well as in the crystal symmetry, the ℓ-s coupling changes; in other word, the change of the orbital momentum caused by the lattice-instability take place a g-factor shift.

In addition, our $Sn_{1-x}Cr_xTe$ is a ferromagnetic material with the Curie temperature $T_c \simeq 297$ K, as mentioned previously. Thus under the condition of the present experiments at $T < T_c$ we essentially observe the ferromagnetic resonance of the Cr contents. The resonant signal should be a good microscopic probe for identification of the structural phase transition, since the ground state of localized Cr ion is orbital configuration (Cr^{2+}; ^5D at the ionic state) which is affected more strongly by environment than ^6S state configuration such as Mn^{2+}. Thus, the g-value as well as linewidth ΔH for $Sn_{1-x}Cr_xTe$ are very sensitive to structural phase transitions.

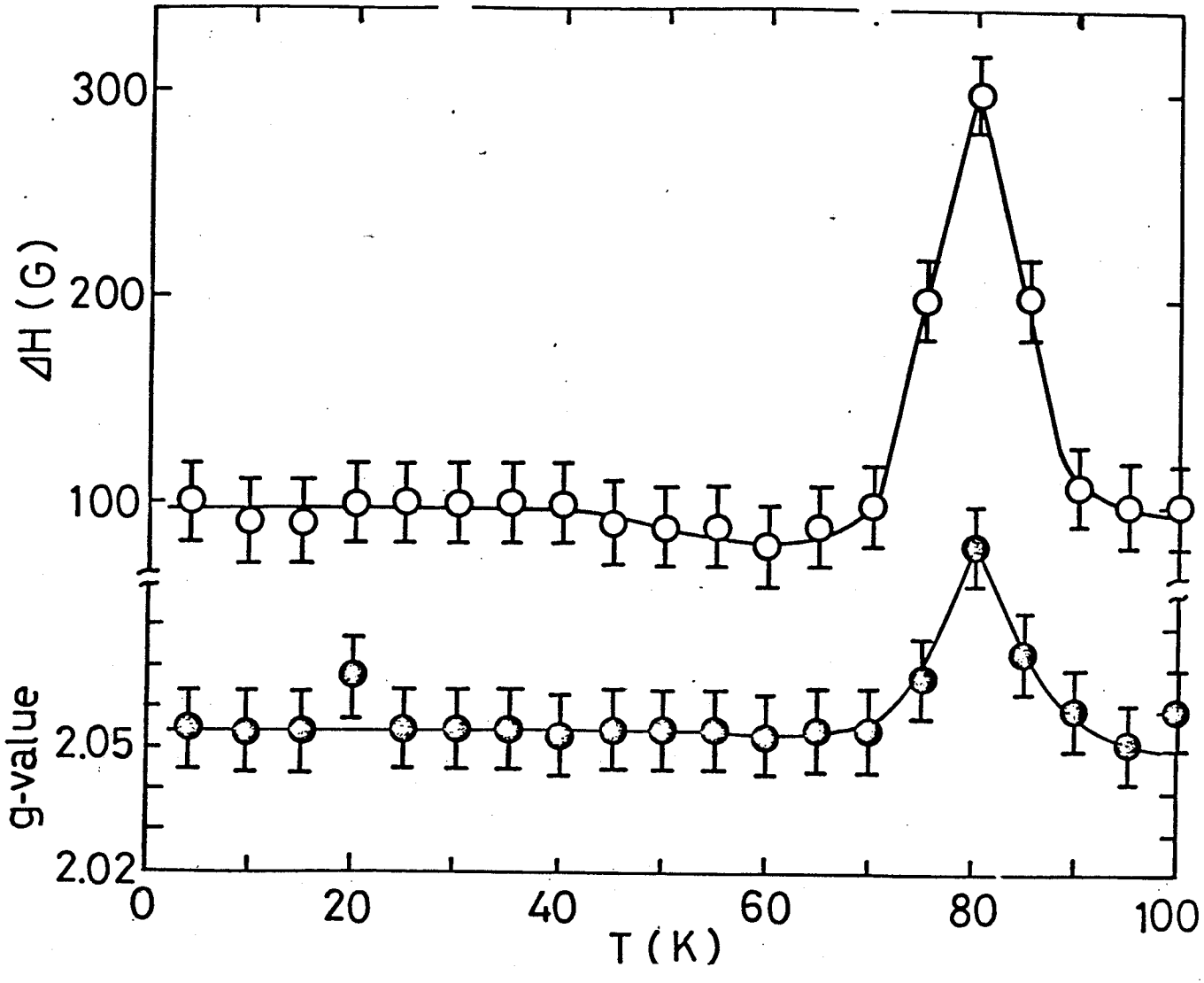

Fig. 34. Temperature dependence of the g-value (solid circles) and the linewidth ΔH (open circles) for $Sn_{1-x}Cr_xTe$ (x=1 at.%) with $p=3.5\times10^{20}$ cm^{-3}.

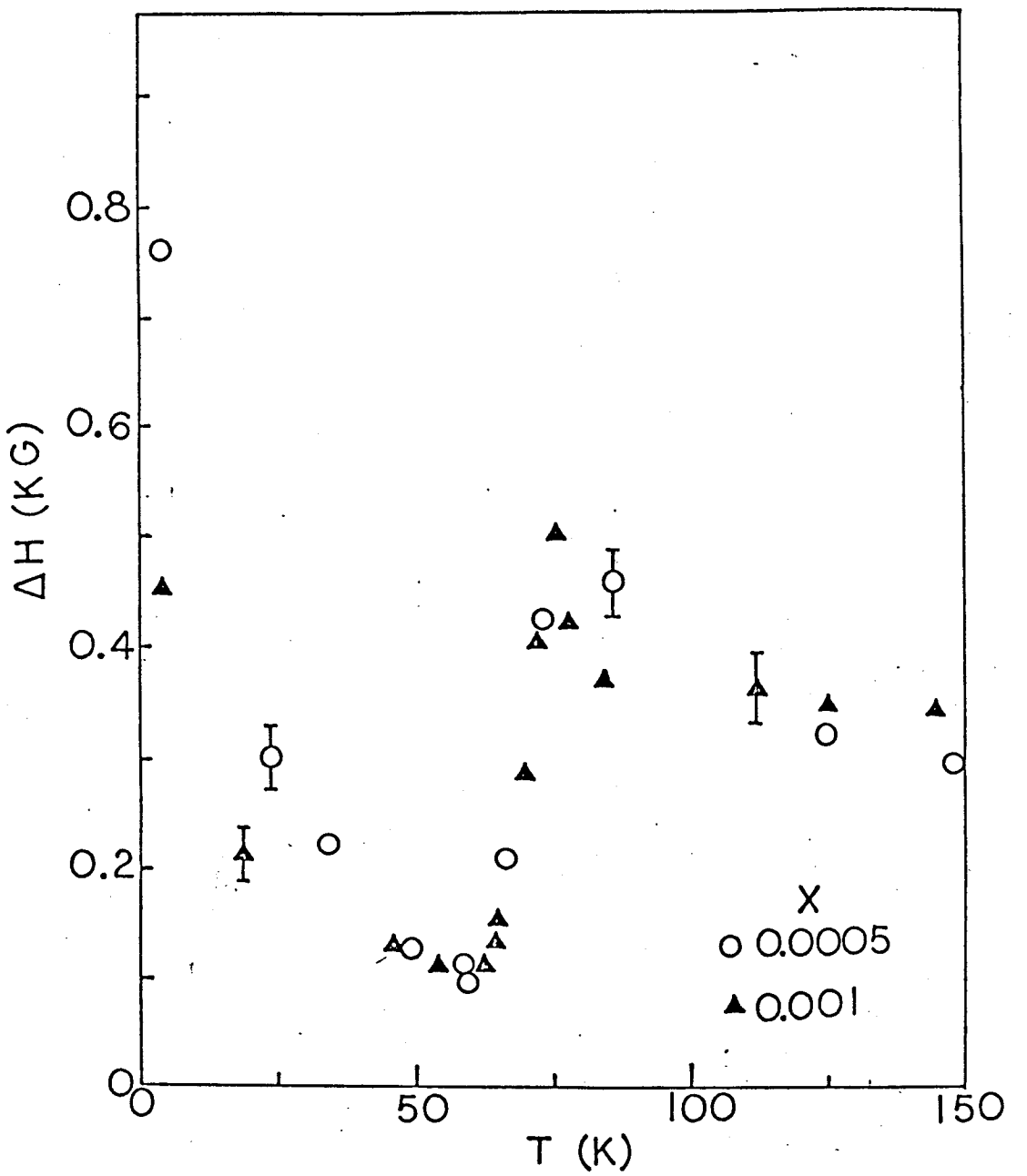

Fig. 35. Temperature dependence of ESR linewidth ΔH of Mn^{2+} in $Sn_{1-x}Mn_xTe$ (x = 0.0005 and 0.001).

Figure 36 shows the plot of T_s vs carrier concentration p and in the figure theoretical result by Kobayashi et al.[11] are also drawn for comparison. The values in our measurement is generally in a good agreement with their result except for the tendency of T_s independent of carrier concentration in our data and the difference between theirs and ones is ascribed to that of the crystal samples.

While, for the degenerate magnetic semiconductors, there is a phase transition concerned with the magnetic ordering effect. As previously mentioned for the ESR of $Pb_{1-x}Mn_xTe$($x > 2$ at.%), the increases of linewidth with decreasing temperature at less than 4.2 K is attributed to the existence of the magnetic ordering effect which are also observed for $Sn_{1-x}Mn_xTe$ by Cochrane in an agreement with other measurements in a previous section. In addition, for $Sn_{1-x}Cr_xTe$, the anomalies in ΔH or g-shift are observed at 150 K or 300 K as well as the structural phase transition.

Figure 37 shows typical results of the temperature dependence of g-value for the crystals with $x = 1$ at.% (as-grown and annealed samples). It should be noted that in both samples the anomalies in the g-value and the linewidth ΔH are clearly seen around the ferromagnetic Curie temperature T_s. The anomalies are of a critical divergence or a dispersive form, which may depend on the crystal orientaion with respect to the static magnetic field.

Figure 38 shows the Cr concentration dependence of the Curie temperature determined from the anomalies of the g-value and of ΔH for both as-grown and annealed crystals, together with those determined from magnetization measurements for comparison. We note that both values of T_c determined from the g-value and ΔH well agree with the curve determined from magnetization measurements (chain lines). For $x < 2$ at.% the difference in T_c is remarkable between the as-grown and the annealed crystals. For the above problem we can postulate a few possible reasons; instabilty of Cr center, position of Cr impurity in the lattice (substitutional and intersti-

tial) and the presence of any magnetic substances or clusters. A small difference between the values from ΔH and the g-value may arise because the linewidth is rather sensitive to the crystal orientation than g-value. For crystals with $x < 0.3$ at.% the signals were too small to be detectable.

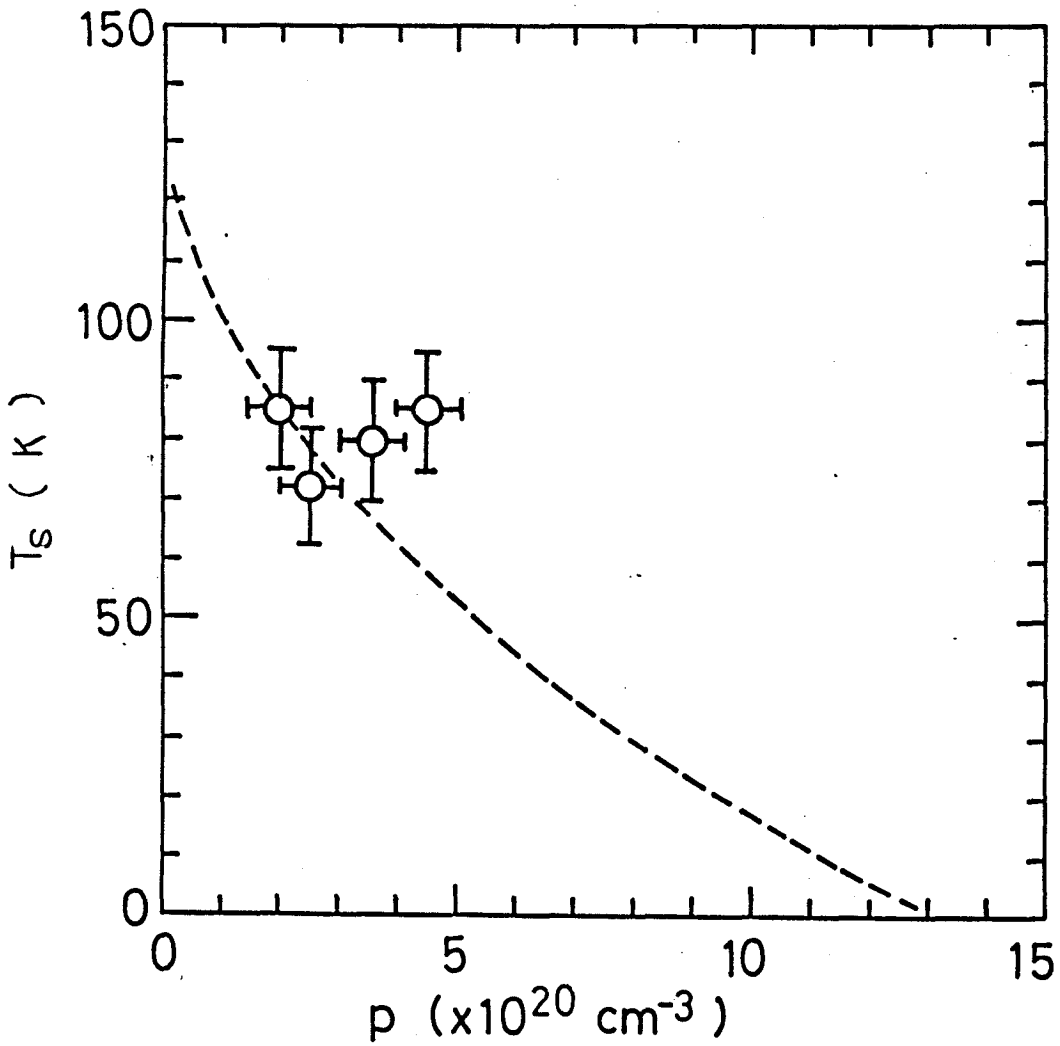

Fig. 36. Structural phase transition temperature T_s of SnTe vs carrier concentration p. The dotted line is the theoretical curve by Kobayashi et al..

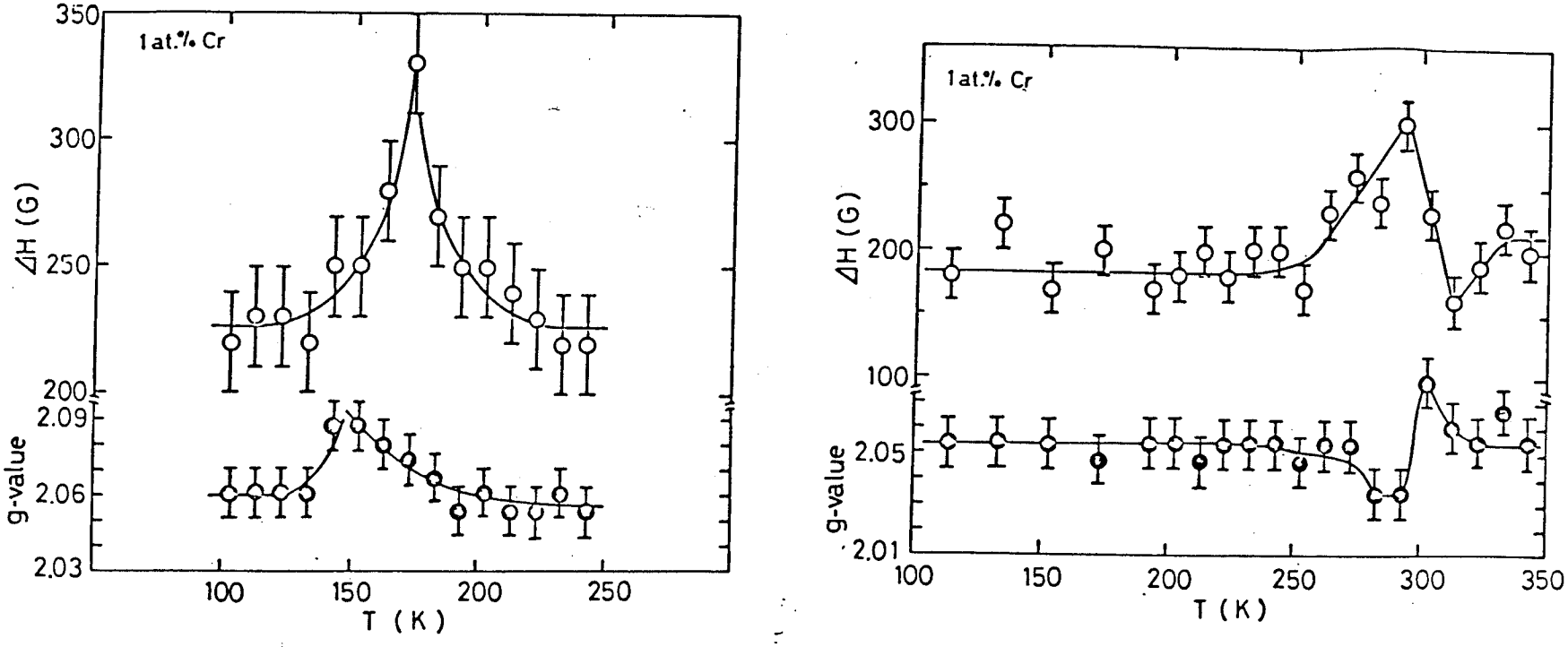

Fig. 37. Temperature variations of g-value and linewidth ΔH for $Sn_{1-x}Cr_xTe$ with x=1 at.%; (a) as-grown and (b) annealed crystals.

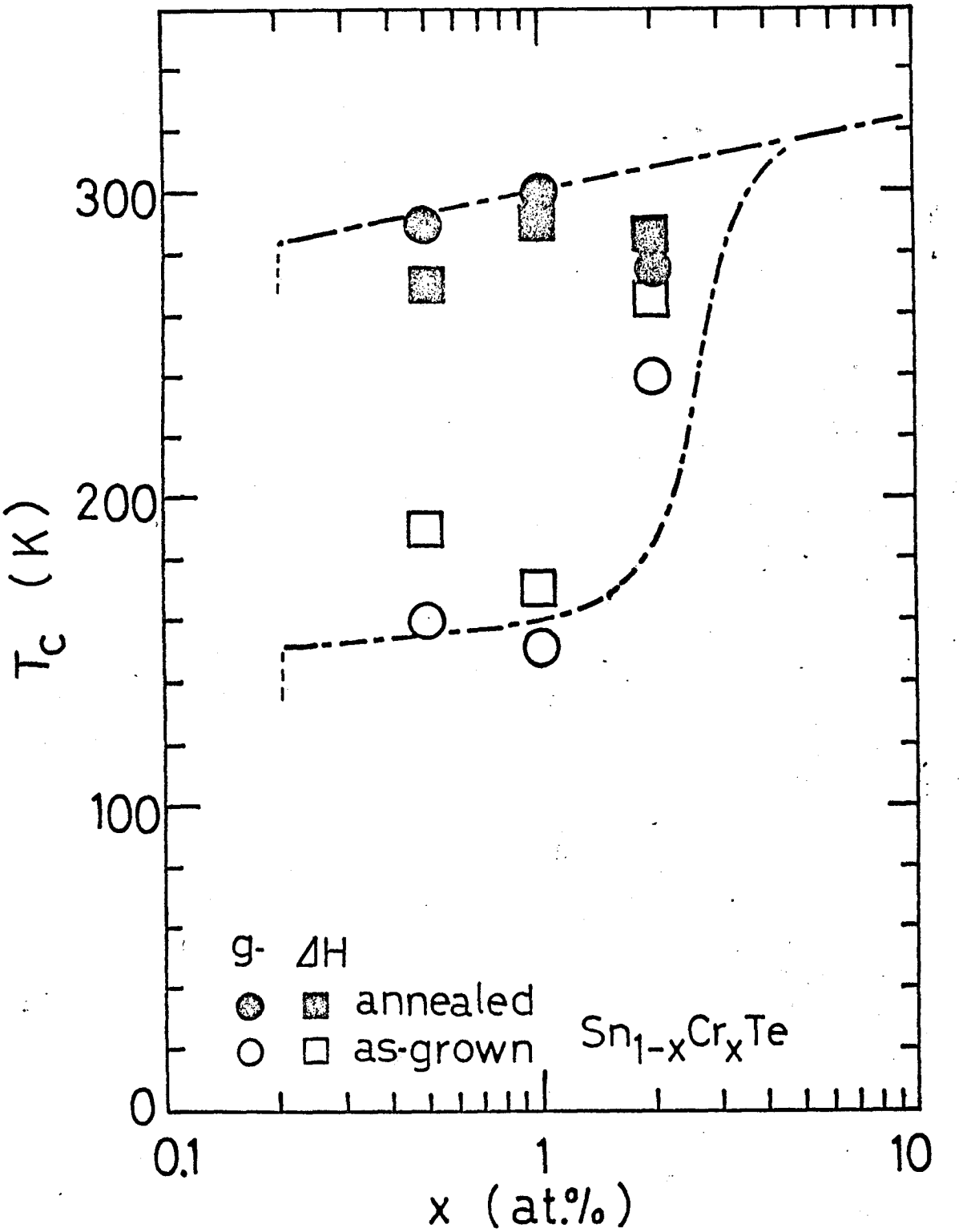

Fig. 38. Ferromagnetic Curie temperatures obtained from anomalies in the g-value and ΔH for as-grown and annealed $Sn_{1-x}Cr_xTe$ plotted against x. The chain lines are determined from the magnetization measurements.

IV Conclusion

ESR, transport, and magnetic measurements have been carried out in the temperature range of 1.8∿350 K on degenerate magnetic semiconductor systems of $Pb_{1-x}Mn_xTe$, $Sn_{1-x}Mn_xTe$, $Ge_{1-x}Mn_xTe$, and $Sn_{1-x}Cr_xTe$ — mixed crystals of group IV-Te compounds with magnetic materials of MnTe and CrTe. In these systems the magnetic impurities play two different kinds of role. First, they serve as a microscopic probe to obtain information on the local crystalline environment in the host crystals. Second, these impurities interact with conduction carrier spins or another magnetic spins giving rise to different types of magnetism. Thus these crystals constitute a new type of material system of "degenerate magnetic semiconductor". Experimental results are summerized as follows.

1. Magnetic Impurities as Microscopic Probe

In order to obtain the information about the crystalline environment of the host crystals, we have performed the ESR measurements of magnetic impurities doped in the host crystals. From the measurements we have studied the bonding state of the crystals, their variation with x in $Pb_{1-x}Sn_xTe$, and structural phase transition in SnTe. Some of our results are in good agreements with those reported by other researchers.

i) Various tellurides with well diluted Mn impurities less than 0.3 at.% show typical hyperfine structure, whose magnitude (or the hyperfine structure constant) gives a degree of covalency (or ionicity) in the chemical bonding of the host crystals. In general group IV-Te compounds possess considerably strong covalency and their temperature variation is larger than ionic crystals, in agreement with the results of general tellurides. SnTe and GeTe possess nearly the same order of magnitude of covalency, while PbTe has a rather stronger ionicity which is not due to the spreading of the outer electron of the cation but rather due to the variation of the Phillips ionicity.[8)]

ii) ESR experiments on Mn^{2+}- doped $Pb_{1-x}Sn_xTe$ crystals show that the hyperfine constant decreases drastically with increasing x up to 0.3 at.%, and becomes constant for x > 0.3 at.%. This result indicates that the chemical affinity of the crystals for x > 0.3 at.% is nearly the same as those of the host SnTe, which varies considerably from that of PbTe (x =0) to the gapless state (x ≃ 0.3 at.%), which is in contrast to the linear dependence of the band gap on x. This result corresponds to the fact that the density of the cation vacancies in SnTe is higher than in PbTe, and thus the type of the conduction exhibits p-type with higher carrier concentrations for x > 0.3 at.%.

iii) ESR measurements on Mn and Cr in SnTe show that the signals near 70 ∿ 80 K are anomalous associated with the structural phase transition. Around the critical temperature the linewidth ΔH for Mn and Cr doped SnTe crystals shows an anomalous increase and for Cr-doped crystals even the g-shift is observed. These results indicate that the ESR technique is a powerful tool to study such structural phase transition. In particular, in the case of Cr impurities a critical divergent behavior of the ESR signals is found, which suggests that the Cr impurities are sensitive to the lattice instability near the phase transition and are in the orbital angular momentum state.

2. Degenerate Magnetic Semiconductor

The study of various types of magnetism in degenerate semiconductor is our main theme for which we have employed different types of measuring techniques.

i) Magnetic susceptibility measurements reveal that different magnetisms in these magnetic semiconductors are observed depending on the kind of dissolved magnetic impurities and for $Sn_{1-x}Mn_xTe$(x = 0.2 ∿ 2.0 at.%) it is paramagnetic followed by the Curie-Weiss law above liquid N_2 temperature, and for

$Sn_{1-x}Cr_xTe$($x = 0.3 \sim 2$ at.%) it is ferromagnetic having a transition temperature T_c of $150 \sim 300$ K that depends on the impurities concentration and the heat-treatment (as-grown or annealed crystals). The anomalous behavior observed in $Sn_{1-x}Cr_xTe$ is attributed to an inhomogeneous distribution of the doped Cr impurities, forming some sort of clusters with a certain order of magnitude in size which increases by the isothermal annealing.[101]

ii) Resistivity, AHE, and ESR measurements on $Sn_{1-x}Mn_xTe$ show the presence of a magnetic transition near 6 K. The transition temperature is determined by these measurements almost independent of x, and especially it is shown in the x dependence of the transition temperature obtained from the resistivity anomaly which is proportional to $x^{1/5}$, in similar to the x dependence of the Kondo minimum temperature in dilute alloy systems. However, the transition temperature of $Ge_{1-x}Mn_xTe$ obtained from magnetic measurements by Cochrane et al.[24] depends linearly on x, for which they explained the results by their proposed model based on the RKKY interaction. The difference of x dependence of transition temperatures among these measurements is ascribed to that of the crystal samples, while unexplained less x dependent transition temperatures may be related to the full expression of RKKY interaction in which the influence of band structures with a narrow gap is considered explicity. (those effect is not included in Cochrane's RKKY model)

iii) Furthermore, as an interesting result of the s-d interaction we have found that in the temperature dependence of the ESR linewidth ΔH for $Pb_{1-x}Mn_xTe$, a bottleneck effect is observed, and from the AHE measurements on $Sn_{1-x}Mn_xTe$, the presence of the mixed spin-orbit interaction is confirmed. These results indicate that the interaction between Mn spins and carrier spins is attributed to the s-d interaction with both spins having nearly equal g-value ($\simeq 2$), which are in a great contrast with a known large g-value of carrier electrons in the host degenerate semiconductor. It means that the carrier near the Mn impurities are strongly bounded to them,[102] thus having

different symmetry (s-state) near the impurities compared with other carriers.

iv) Finally, one of the characteristic features of our material systems is that various properties are different between low and high impurity concentration at the critical boundary of $x \simeq 2$ at.%, as found in the x dependence of the Hall mobility $\mu(x)$, resistivity $\rho(x)$, ESR linewidth $\Delta H(x)$, and AHE coefficient $R_1(x)$. These results are attributable to the formation of clusters of magnetic impurities which distribute inhomogeneously in the lattices, giving rise to an anisotropic magnetic interactions.

In summarizing these present studies, the degenerate magnetic semiconductors show various types of magnetism as a result of the overlappings of s-d interaction, RKKY interaction and direct exchange interaction beween two magnetic impurity spins. The way in which spin alignments occur through these interactions is different for each type of interaction, and thus the resultant magnetism shows a complicated feature. Such magnetism is considered in a wide sense as one of the problem of random spin system,[103] including spin glass state for dilute alloy predicted by Cannella et al.[104] and Wenger,[105] and for semimagnetic semiconductor by Nagata.[106]

Another problem of the interaction associated with the carrier symmetry (s-d or p-d interactions) is also found in similar systems of semimagnetic semiconductors such as $Hg_{1-x}Mn_xTe$.[26,27] These problems are expected to be studied further.

References

1) D. L. Mitchell and R. F. Wallis : Phys. Rev. 151, 581 (1966).

2) S. Rabii : Phys. Rev. 167, 801 (1968).

3) Y. W. Tung and M. L. Cohen : Phys. Rev. 180, 823 (1969).
Phys. Lett. 29A, 236 (1969).

4) M. L. Cohen and Y. W. Tsang : Proc. Int. Conf. Phys. Semimetals and Narrow Gap Semicond., Dallas, (Pergamon Press, 1970) p. 303.

5) G. Martinez, M. Schluter and M. L. Cohen : Phys. Rev. B11, 651 (1975).

6) Y. Ota and S. Rabii : J. Nonmet. 1, 117 (1976).

7) G. M. T. Foley and D. N. Langenberg : Phys. Rev. B15, 651 (1975).

8) E. Burstein, A. Pinczuk and R. F. Wallis : Proc. Conf. Phys. Semimetals and Narrow Gap Semicond., Dallas, (Pergamon Press, 1970) p.251.

9) H. Kawamura, S. Nishikawa ana S. Nishi : Proc. 13th Int. Conf. Phys. Semicond., Rome, (1976) p. 310.

10) K. Shimizu, Y. Nishida and S. Narita : J. Phys. Soc. Jpn. 46, 1797 (1979).

11) K. L. I. Kobayashi, Y. Kato, Y. Katayama and K. F. Komatsubara : Solid State Commun. 17, 875 (1975).
Solid State Commun. 19, 381 (1976).
Phys. Rev. Lett. 20, 772 (1976).

12) K. M. Muller, N. S. Dalal and R. W. Berlinger : Phys. Rev. Lett. 36 1504 (1976).

13) H. Kawamura : Proc. Int. Conf. Phys. Narrow Gap Semicond., Warzawa, (1977) p. 7.

14) J. O. Dimmock : Proc. Int. Conf. Phys. Semimetals and Narrow Gap Semicond., Dallas, (Pergamon Press, 1970) p. 319.

15) S. Narita : Oyo Buturi 43, 601 (1974) [in Japanese].

16) K. W. Nill, J. N. Waispole, A. R. Calawa and T. C. Harman: Proc. Int. Cof. Phys. Semimetals and Narrow Gap Semicond., Dallas, (Pergamon Press, 1970) p. 383.

17) J. Melngailis, T. C. Harman, J. G. Mavroides and J. O. Dimmock : Phys. Rev. B3, 370 (1971).

18) S. Narita and Y. Takafuji : Solid State Commun. 20, 357 (1976).

19) M. Inoue and H. Yagi : Butsuri 31, 357 (1976) [in Japanese].

20) A. J. Heeger : Solid State Physics, ed. F. Seitz, D. Turnbull and H. Ehrenreich (Academic Press, New York - London 1969) Vol.23 p.283.

21) M. Peter, D. Shatiel, J. H. Wernick, J. B. Mock and R. C. Sherwood : Phys. Rev. 126, 1395 (1962).

22) G. Toth, J. Y. Leloup and H. Rodot : Phys. Rev. B1, 4573 (1970).

23) C. R. Hews, M. S. Alder and S. D. Senturia : Phys. Rev. B7, 5195 (1973).

24) R. W. Cochrane, F. T. Hedgcock and J. O. Ström-Olsen : Phys. Rev. B9, 3013 (1974).
AIP 20th Annual Conf. Mag. Mag. Materials, San Francisco, (1974) p. 71.

25) R. W. Cochrane, F. T. Hedgcock and A. W. Lingstone : 14th Int. Conf. Low Temp. Rhys., Otaniemi, (1975) p. 290.

26) G. Bàstard : Proc. Int. Conf. Phys. Narrow Gap Semicond., Warszawa, (1977) p. 63.

27) M. Jaczyński, J. Kossut, and R. R. Gałazka : Proc. Int. Conf. Phys. Narrow Gap Semicond., Warszawa, (1977) p. 325.

28) J. Kondo : Solid State Physics, ed. F. Seitz, D. Turnbull and H. Ehrenreich (Academic Press, New York - London 1969) Vol. 23 p. 183.

29) J. A. Gaj, R. Planel and G. Fishman : Solid State Commun., 29, 435 (1979).

30) S. Takeyama and S. Narita : Kotai Butsuri 15, 634 (1980).

31) M. Inoue, H. K. Fun, M. Fukuoka and H. Yagi : Proc. 15th Int. Conf. Phys Semicond., Kyoto, (1980), J. Phys. Soc. Jpn. 49 (1980) Suppl. A, p. 835.

32) J. F. Butler and T. C. Harman : J. Electro-chem. Soc. 116, 458 (1969).

33) K. Ishii, M. Inoue, H. Yagi and T. Tatsukawa : Memoirs Fac. Eng. Fukui Univ. 25, 51 (1977).

34) S. Hasegawa, M. Inoue, T. Tatsukawa, H. Takahashi and H. Yagi : Memoirs Fac. Eng. Fukui Univ. 24, 287 (1976) [in Japanese].

35) T. Tatsukawa, M. Inoue, H. Yagi and H. Takahashi : Memoirs Fac. Eng. Fukui Univ. 28, 225 (1978).

36) A. Ghazali, M. Escorne, H. Rodot and P. Leroux-Hugen : AIP Conf. Proc. 10(2) (1972) p. 1374.

37) J. Barden and W. Shockley : Phys. Rev. 80, 72 (1950).

38) E. Conwell and V. F. Weisskopf : Phys. Rev. 77, 388 (1950).

39) C. Erginsoy : Phys. Rev. 79, 1013 (1950).

40) J. Kondo : Prog. Theor. Phys. 32, 37 (1964).

41) R. P. Debye and E. M. Conwell : Phys. Rev. 93, 693 (1953).

42) E. J. Morin and J. P. Maita : Phys. Rev. 96, 28 (1954).

43) C. M. Hurd : The Hall Effect in Metals and Alloys (plenum Press, New York - London 1972) p. 153.

44) A. N. Voloshinskii : Phys. Met. Metal. 18, 13 (1964).

45) F. E. Maranzana : Phys. Rev. 160, 421 (1967).

46) Yu. P. Irkhin and Sh. Sh. Abel'skii : Soviet Phys. Solid State (Engl. Trans.) 6, 1283 (1964).

47) J. Cohen, A. Globa, P. Mollard, H. Rodot and M. Rodot : J. Phys. 29, C4-142 (1968).

48) M. Escorn, A. Ghazali and P. Leroux-Hugen : Proc. 12th Int. Conf. Phys. Semicond., Stuttgart (1974) p. 915.

49) U. Sondermann : J. Mag. Mag. Materials 2, 216 (1976).

50) M. P. Mathur, D. W. Deis, C. K. Jones, A. Patterson and W. J. Carr,Jr. : J. Appl. Phys. 42, 1693 (1971).

51) M. Inoue, M. Fukuoka and H. Yagi : J. Phys. Soc. Jpn. 47, 1836 (1979).

52) W. B. Person : Phil. Mag. 46, 920 (1955).

53) R. Dalven : Infrared Phys. 9, 141 (1969).

54) R. C. Wead, ed. : Handbook of Chemistry and Physics (Chemical Rubber Co., Cleveland 1970) 51st. ed.

55) M. Hansen and K. Andreko : Constitution of the Binary Alloys (McGraw-Hill, New York 1958).

56) A. J. Bevolo, H. R. Shanks and D. E. Eckels : Phys. Rev. B13, 3523 (1976).

57) D. E. Grad ed. : American Institute of Physics Handbook (McGraw-Hill, New York 1972) 3rd. ed.

58) E. Šimánek and K. A. Müller : J. Phys. Chem. Solid 1, 1027 (1970).

59) J. H. Pifer : Phys. Rev. 157, 727 (1967).

60) R. E. Watson and A. J. Freeman : Phys. Rev. 123, 2027 (1961).

61) J. S. Van Wieringen : Disc. Faraday Soc. 19, 118 (1955).

62) E. Šimáneck and R. Orbach : Phys. Rev. 145, 191 (1966).

63) C. Y. Huang : Phys. Rev. 158, 280 (1967).

64) W. M. Waish, J. Jeener and A. Bloembergen : Phys. Rev. 139, 1338 (1965).

65) J. O. Dimmock, I. Melngailis and A. J. Strauss : Phys. Rev. Lett. 16, 1193 (1966).

66) A. Abragam and B. Bleaney : Electron Paramagnetic Resonance of Transition Ions (Clarendon Press, Oxford 1970) p. 527.

67) M. F. Deigen, V. Ya. Zevin, V. M. Maeuskii, I. N. Geifman, V. I. Konovalov and N. I. Vitrinkhovskii : Soviet Physics-Semicond. 2, 923 (1969).

68) M. Inoue : J. Phys. Soc. Jpn. 33, 1024 (1972).

69) S. Asano, Y. Nakao and K. Omori : J. Phys. Soc. Jpn. 20, 1120 (1965).

70) M. Inoue and C. Y. Huang : J. Phys. Soc. Jpn. 32, 763 (1972).

71) H. Watanabe : Phys. Chem. Solids 25, 1471 (1964).

72) A. Nakamura and N. Kinoshita : Bull. Electrotech. Lab. 30, 19 (1966) [in Japanese].

73) P. W. Anderson : J. Phys. Soc.Jpn. 9, 316 (1954).

74) C. Herring : Magnetism ed. G. T. Rado and H. Suhl (Academic Press, New York 1966) Vol. IV

75) A. Nakamura and N. Kinoshita : J. Phys. Soc. Jpn. 26, 48 (1969).

76) R. E. Watson : Phys. Rev. 118, 1036 (1960).

77) J. Owen and E. A. Harris : Electron paramagnetic Resonance ed. S. Geshwind (Plenum Press, New York 1972) p. 427.

78) A. Abragam : The Priciples of Nuclear Magnetism (Clarendon Press, Oxford 1961) p. 111.

79) J. Kanamori : Magnetism ed. G. T. Rado and H. Shul (Academic Press, New York 1963) Vol. I, p. 161.

80) S. R. Smith and J. Owen : J. Phys. C4, 1399 (1971).

81) K. Sugihara : J. Phys. Soc. Jpn. 14, 1231 (1959).

82) T. Moriya : Phys. Rev. 120, 91 (1960).

83) C. P. Slichter : Principles of Magnetic Resonance (Harper & Row, New York - London 1963) p. 64.

84) J. Korringa : Physica 16, 601 (1950).

85) A. Nakamura and N. Kinoshita : J. Phys. Soc. Jpn. 22, 449 (1967).
J. Phys. Soc. Jpn. 22, 335 (1967).

86 H. Hasegawa : Prog. Theor. Phys. (Kyoto) 21, 483 (1959).

87) P. W. Anderson : Phys. Rev. 124, 41 (1961).

88) H. Mori and K. Kawasaki : Prog. Theor. Phys. 28, 971 (1962).

89) H. Mori : Prog. Theor. Phys. 39, 478 (1963).

90) K. Kawasaki : Prog. Theor. Phys. 39, 285 (1968).

91) K. A. Muller : Phase Transitions and soft Modes ed. E. J. Samuelsen, E. Anderson and J. Feder (Univ. Forlaget, Oslo 1971).

92) L. J. Brillson, E. Burstein and L. Muldawer : Phys. Rev. B9, 1547 (1974).

93) G. S. Pawley, W. Cochran, R. A. Cowley and G. Dolling : Phys. Rev. Lett. 17, 753 (1966).

94) N. Kristoffel and P. Konsin : Ferroelectrics 6, 3 (1973).

95) S. Watarai and T. Matsubara : Prog. Theor. Phys. 53, 1214 (1975).

96) L. Muldawer : J. Nonmetals 1, 177 (1973).

97) R. S. Allgaier and B. Houston : Phys. Rev. B5, 2186 (1972).

98) H. T. Savage, B. Houston and J. R. Burke Jr. : Phys. Rev. B6, 2292 (1972).

99) F. J. Owens : Magnetic Resonance of Phase Transitions ed. F. J. Owens, C. P. Poole and H. A. Farach (Academic Press, 1979) p. 291.

100) L. D. Landau : Phys. Z. Sowjet, Un. 11, 26 (1937).

101) A. Katty et O. Gorochov : C. R. Acad. Sci. Ser.C 279, 26 (1974).

102) K. Yoshida : Magnetism (Kyoritu Press, Tokyo 1972) Vol. II p. 223 [in Japanese].

103) M. Inoue and H. Yagi : Butsuri 36, 733 (1981) [in Japanese].

104) V. Cannella and J. A. Mydosh : Phys. Rev. B6, 4220 (1972).

105) Y. Miyako : Butsuri 32, 463 (1977).

106) S. Nagata, R. R. Galazka, D. P. Mullin, H. Akbarzadeh, G. D. Khattak, J. K. Furdyna and P. H. Keeson : Phys. Rev. B22, 3331 (1980).